BIOPHYSICAL MODELING TO REVERSE ENGINEER TWO MAMMALIAN NEURAL CIRCUITS – LOWER URINARY TRACT AND HIPPOCAMPUS

A Dissertation presented to

The Faculty of the Graduate School

University of Missouri – Columbia

In Partial Fulfillment

of the Requirement for the Degree

Doctor of Philosophy

---

by

VINAY SANDEEP KUMAR GUNTU

Dr. Satish S. Nair, Dissertation Supervisor

DECEMBER 2020

The undersigned, appointed by the dean of the Graduate School, have examined the

Dissertation entitled

BIOPHYSICAL MODELING TO REVERSE ENGINEER TWO MAMMALIAN NEURAL CIRCUITS – LOWER URINARY TRACT AND HIPPOCAMPUS

Presented by

Vinay Sandeep Kumar Guntu

A candidate for the degree of Doctor of Philosophy in

Electrical and Computer Engineering

And hereby certify that, in their opinion, it is worthy of acceptance.

Dr. Satish S. Nair

Dr. Guilherme DeSouza

Dr. Justin Legarsky

Dr. David J. Schulz

ACKNOWLEDGEMENTS

I would like to express my sincere gratitude to my advisor, Dr. Satish S. Nair for his immense support and guidance through his mentorship. Dr. Nair has helped me above and beyond in this journey, he is compassionate and a great mentor. I would also like to extend my sincere gratitude to my committee members Dr. Guilherme DeSouza, Dr. Justin Legarsky and Dr. David J. Schulz for serving on my committee. I would like to specially thank Dr. DeSouza for being there, guiding me and always encouraging. I would like to greatly thank Dr. Schulz for his collaboration on various projects, help with computational neuroscience labs and providing valuable insights.

I received great support from my lab mates and would like to thank each and every one of them. I would like to thank Dr. Robert McLaren for his guidance and advice. I would also like to acknowledge the support provided by the administrative staff from EECS department. Also, members of Mizzou Badminton Club for social and emotional support.

Special thanks to my parents and sister for their unconditional love and support. Thank you for never losing faith in me. Finally. I am particularly grateful to my very kind and wonderful wife Dr. Lu Tian whose support I cannot express in words. I am grateful to have your love and patience.

TABLE OF CONTENTS

LIST OF FIGURES

LIST OF TABLES

ABSTRACT

Computational neuroscience provides tools to abstract and generalize principles of neuronal function using mathematics and computers. This dissertation reports biophysical modeling approaches to facilitate reverse engineering of two mammalian neural circuits - the lower urinary tract for the development of stimulation techniques, and the rodent hippocampus to understand mechanisms involved in theta rhythms.

The LUT in mammals consists of the urinary bladder, external urethral sphincter (EUS) and the urethra. Control of the LUT is achieved via a neural circuit which integrates distinct components. Dysfunctions of the lower urinary tract (LUT) are caused by a variety of factors including spinal cord injury and diabetes. Our model builds on previous models by using biologically realistic spiking neurons to reproduce neural control of the LUT in both normal function and dysfunction cases.

The hippocampus has long been implicated in memory storage and retrieval. Also, hippocampal theta oscillations (4-12 Hz) are consistently recorded during memory tasks and spatial navigation. Previous model revealed five distinct theta generators. The present study extends the work by probing deeper into the intrinsic theta mechanisms via characterizing the mechanisms as being resonant, i.e., inherently produce theta, or synchronizing, i.e., promote coordinated activity, or possibly both. The role of the neuromodulatory state is also investigated.

CHAPTER 1: INTRODUCTION AND OBJECTIVES

BACKGROUND AND MOTIVATION

The human brain has billions of neurons which produce complex electrical activity. These individual neurons communicate via synapses mostly by chemical interactions and are networked into complex local and inter-region circuits that are thought to implement various biological functions which give rise to physical and mental faculties of life. Computational models are becoming increasingly invaluable tools to neuroscientists to test various hypothesis before venturing into actual experimentation. At the cellular level, the Hodgkin-Huxley formulation is the most popular method used to model single cells because it can incorporate different current channels and their dynamics. Networks of neurons are then built on using these single cell models with connectivity estimates from appropriate brain regions. The models are them tuned to match data from in vitro and in vivo experiments, typically in rodents.

This dissertation uses computational modeling techniques to investigate two different biological functions involving different brain regions, as described in chapter overviews below for chapters 2-4. Chapter 5 provides a summary of the work, together with topics for future research. An appendix lists a primer developed as a chapter, to illustrate the development of computational model using the Hodgkin-Huxley, Izhikevich and integrate & fire formulations.

CHAPTER OVERVIEW AND OBJECTIVES

Chapter 2 – This chapter focuses primarily on outlining the challenges in the development of computational model of the neural circuit that controls the lower urinary

tract (LUT) of mammals. The LUT in mammals consists of the urinary bladder, external urethral sphincter (EUS) and the urethra. Control of the LUT is achieved via a neural circuit which integrates two distinct components. We describe the anatomy of the LUT with primary focus on the neural anatomy, then the overall efferent and afferent neural pathways of LUT and briefly discuss the neurotransmitters involved and known details related to species/sex differences and developmental changes. The challenges in modeling the control of LUT at cellular and network levels are then listed.

Chapter 3 – Dysfunctions of the lower urinary tract (LUT) are caused by a variety of factors including spinal cord injury and diabetes. This has resulted in increased focus on both understanding LUT function and in trying to alleviate dysfunction via stimulation techniques. Computational modeling, the focus of our research, is a powerful tool that can complement experimental investigations in such cases and are beginning to be developed for micturition loops. Models to date of the LUT have focused on mechanical properties of the LUT (Duin et al., 1998, Bastiaanssen et al., 1996). The models consider various neural feedback mechanisms (Duin et al., 2000) but biophysical ones incorporating spiking dynamics and neurophysiology have not been reported. Animal models have considerably enhanced our understanding of the LUT, although there are known physiological discrepancies between human and animal models (Birder et al. 2010). The pressure and flow characteristics have been well reproduced with appropriate, albeit reduced, neural infrastructure (Duin et al., 1998). Our model builds on this previous work by using biologically realistic spiking neurons to reproduce neural control of the LUT in both normal function and dysfunction cases.

Chapter 4 – The hippocampus has long been implicated in memory storage and retrieval. Also, hippocampal theta oscillations (4-12 Hz) are consistently recorded during memory tasks and spatial navigation. Our recent work used a biophysical spiking network model of the CA3 region of the hippocampus that included an interconnected network of pyramidal cells, inhibitory basket cells (BC) and oriens-lacunosum moleculare (OLM) cells to investigate the role of intrinsic mechanisms in the generation of theta. The model revealed five cooperating theta generators: spiking oscillations of pyramidal cells, recurrent connections between them, slow-firing interneurons and pyramidal cells subnetwork, the fast-spiking interneurons and pyramidal cells subnetwork, and non-rhythmic structured external input from entorhinal cortex to CA3. The present study extends the work by probing deeper into the intrinsic theta mechanisms via characterizing the mechanisms as being resonant, i.e., inherently produce theta, or synchronizing, i.e., promote coordinated activity, or possibly both. The role of the neuromodulatory state is also investigated.

Chapter 5 – This chapter provides a summary of the work, together with a listing of ideas for future research.

Appendix – We provide a tutorial illustration of how biophysical models can be developed systematically starting with models for single cells, using the example of amygdala nuclei that is one of the focus of our Lab. A step-by-step introduction to creating computational models using Hodgkin-Huxley, Izhikevich and integrate & fire formulations.

CHAPTER 2

CHALLENGES IN MODELING THE NEURAL CONTROL OF LUT

1. OVERVIEW

The lower urinary tract (LUT) in mammals consists of the urinary bladder, external urethral sphincter (EUS) and the urethra. Control of the LUT is achieved via a neural circuit which integrates two distinct components. One component of the neural circuit is 'reflexive' in that it relies solely on input from sensory neurons in the bladder and urethra that is fed back via spinal neurons to the LUT. The second neural component is termed 'top-down' and is a conditioned input that comes from structures such as Pontine Micturition center (PMC), and Pontine storage center (PSC), that also receive the afferent sensory input from the LUT relayed through periaqueductal gray (PAG). The reader is referred to excellent references such as [1-3] from de Groat's group for the top down control, which is not discussed here. This chapter focuses primarily on outlining the challenges in the development of computational model of the neural circuit that controls the LUT. Section 2 describes the anatomy of the LUT with primary focus on the neural anatomy. We describe the overall efferent and afferent neural pathways of LUT and briefly discuss the neurotransmitters involved and known details related to species/sex differences and developmental changes. Section 3 provides a brief summary of efforts to model the various neural components of the LUT for the purpose of understanding how they might participate in control. We list challenges in modeling the control of LUT at cellular and network levels and finally provide a brief description of an on-going effort to develop a biophysical model of the system.

2. NEUROBIOLOGY OF THE MAMMALIAN LOWER URINARY TRACT

2.1.General anatomy of LUT

The urinary bladder is a sphere-like hollow muscle that collects and stores urine from the ureters until it is stimulated to contract and evacuate the urine through the urethra – a process termed as micturition. The bladder is composed of a smooth muscle chamber, denoted the body, and a neck or posterior urethra, which serves to funnel urine into the urethra. At the base of the neck, a smooth muscle sphincter, the internal sphincter (IUS), prevents outflow to the urethra until a certain pressure is achieved. The urethra is a tube by which urine exits the bladder and flows to the exterior of the body. At the other end of the urethra is the EUS, which is a skeletal muscle sphincter, and the only voluntary component within the LUT. The main mechanical functions of sphincter muscles are controlled constrictions and relaxations. EUS allows conscious control over micturition and can be closed against fluid pressure by top-down signals from PSC. The coordination between EUS and bladder is mediated by complex neural circuits at the brain, spinal cord and ganglionic levels, and is crucial for proper functioning of the LUT. From a control point of view, internal changes such as convulsions, dysfunctions and infections, and external factors such as coughing, sneezing, cold, and fear, impact functioning of the EUS [4][5].

2.2.Neural Anatomy of LUT

The neural anatomy of the LUT can be viewed as having three main pathways labeled sympathetic, parasympathetic and somatic pathways. Although the functions of these pathways are similar in most species, differences exist between rat, mouse, cats and humans. The sympathetic pathway is responsible for relaxation of the bladder and

contraction of the IUS. the parasympathetic pathway does the opposite by relaxing the IUS and contracting the bladder. These bladder contractions can be periodic non-voiding or voiding contractions. The somatic pathway implements the conscious control of micturition via the EUS.

The sympathetic, parasympathetic and somatic pathways carry sensory information from LUT to the spinal cord (hypogastric nerve) and efferent signals from the spinal cord to LUT (pelvic and pudendal peripheral nerves). Primary sensory afferents of the LUT project to spinal interneurons and can initiate and modulate several spinal level reflexes. These afferents may be involved in reflex integration at local ganglionic levels, and/or project to higher order centers to convey bladder fullness sensation to facilitate voluntary voiding. Pressure, stress, or toxins can also activate these afferents [6]. Efferents control the functional output of bladder by timed contraction or relaxation of the bladder, IUS and EUS. Summary of the neural anatomy can be found in (Fig 1) below adapted from Inskip et al.[7]

Sympathetic:

Ganglia. It is estimated that in each hypogastric nerve about 1,300 afferent neurons, about 1,700 preganglionic neurons, and about 17,000 postganglionic neurons project their axons [8]. In Rats, Hypogastric ganglion contains around 3078 ± 193 (mean ± SEM) neurons and are known to exhibit both tonic and phasic firing patterns (Table1)[9]. However, several of these neurons innervate different visceral organs. So, it is difficult to isolate and obtain data from the ones innervating only the LUT.

Hypogastric efferents. Sympathetic efferent innervation of LUT arise from preganglionic neurons located between thoraco-lumbar (T10-L2) spinal segments in humans and lumbar (L1-L2) spinal segments in rats which project to postganglionic neurons in inferior mesenteric ganglion (IMG) and pelvic plexus (Fig 1). Axons from these postganglionic neurons innervate the body and neck of the bladder, and the urethra. These sympathetic postganglionic nerves release norepinephrine (NE) and contribute to storage mechanisms by contracting IUS (mediated by α-AR expressed in trigone, bladder neck and urethra) and relax the detrusor muscle (mediated by β-AR). [7]

*Hypogastric afferents***.** Hypogastric afferents are sensitive to small changes in bladder pressure caused by intrinsic detrusor contractions, across a wide range of pressures and tension [10]. The afferent signals in the pelvic and hypogastric nerves qualitatively appear to carry similar information and no functional classification can be made based on just afferent activity; the difference seems to be primarily related to the neurons they interact with at spinal level. Most of these afferents to the rostral lumbar segments terminate in laminae I, V–VII, and X [11]. Urethral afferents in hypogastric nerve can be both myelinated and unmyelinated and respond to urine flow and urethral distention. These urethral afferents exhibit rapidly adapting responses [12]. Hypogastric afferents are often active with bladder empty [13] and transection or pharmacological blockade of the sympathetic nerves can reduce urethral outflow resistance, reduce bladder capacity, and increase the frequency and amplitude of bladder contractions recorded under isovolumetric conditions, thus reinforcing their functional significance during storage

mode [14]. Hypogastric nerve also contains nociceptive afferents which are activated by chemicals and irritants.

Parasympathetic:

Ganglia. In rats, the number of labelled neurons in MPG that connect to bladder are 715 ± 126 neurons in 6 ganglia [15]. However, these labelled neurons are seen in penile, hypogastric, pelvic and accessory nerves. These neurons lacked dendrites and have soma cross section area of 309±7 μm^2 and are known to exhibit both tonic and phasic firing patterns [16].

Pelvic efferents. Parasympathetic inputs to LUT originate at the sacral level in humans (S2-S4) and at the lumbosacral level in rats (L6-S1). These inputs synapse onto neurons in the major pelvic ganglion (MPG) at the post ganglionic level. Axons from MPG innervate the body and neck of the bladder and the urethra; they excite the bladder and inhibit the IUS. Inhibition of IUS is mediated by nitric oxide (NO) (Fig 1). Parasympathetic excitatory transmission is mediated by ACh acting on muscarinic receptors (mAChR) especially the M3 subtype; when activated triggers extracellular Ca^{+2} release and results in contraction of detrusor smooth muscle (DSM). In some animals a noncholinergic contraction also occurs that is resistant to muscarinic receptor blocking agents. Adenosine triphosphate (ATP) is the excitatory transmitter mediating the noncholinergic contractions. Excitation of the bladder smooth muscle via ATP is also termed purinergic transmission [17], occurs via the action of ATP on P2X receptors (P2X1 in humans and rats) which are ligand gated ion channels. Purinergic transmission

has an important excitatory role in animal bladders but is not important in the normal human bladder, except in patients with pathological conditions [18].

*Pelvic afferents***.** Pelvic afferents have cell-bodies in the dorsal root ganglion (DRG) and innervate the bladder as well as urethra and transmit afferent signals to the spinal cord at the lumbosacral level, into laminae V–VII and X at the base of the dorsal horn. They are broadly classified into mechanosensitive Aδ and C-fibers (Fig 1). The pelvic nerve carries "pressure-related" sensory information from the bladder to the spinal centers. Aδ mechanoreceptor afferents are myelinated and respond to both passive distention and active bladder contractions. Unmyelinated C-fibers that are not mechanosensitive respond to chemical irritants such as capsaicin and turpentine oil or cold. C-fibers are not active during normal physiological conditions of continence or micturition but are selectively active at high bladder pressures [10]. Some C-fibers are mechanosensitive and are less excitable than Aδ fibers. Some small number of pelvic afferents (both Aδ and C) track bladder pressure in exclusively high-pressure conditions and are quiescent at low pressures. This is most likely due to hyperdistention of DSM and the information conveyed is a sensation of pain.

Aδ mechanoreceptor afferents have conduction velocities in the range of (2.5 -15 m/s) [19] and are typically silent when the bladder is empty but display a graded increase in firing rate during slow filling, at pressures below 25 mmHg [20]. Basal firing rate of pelvic afferent neurons is ~1Hz when bladder volume is low [21] ; the maximal firing rates range from 15 to 30 Hz in cats. Four types of mechanosensitive fibers were identified

by stretch, stroke and probe – Muscle (63%), muscle-urothelial (14%), serosal (14%) and urothelial (9%). Pelvic afferents can also be classified, based on pressure thresholds, into low threshold (LT) (65%-80%) and high threshold (HT) (20%-35%) categories [22]; for rats, these thresholds (mmHg; mean± std dev) are reported as 5.7 ± 1.0 for LT and 34.0 ± 2.5 for HT [23].

In awake behaving cats, low voiding efficiency and improper micturition are observed with chronic pelvic transection; no effect was observed with hypogastric nerve transection[24]. The normal micturition reflex is triggered by myelinated Aδ-fiber afferents [25, 26].The C-fiber afferent neurotoxin (capsaicin), does not block normal micturition reflexes in cats and rats, and are believed to not be essential for normal voiding [27]. Stimulation studies in rats revealed that C-fiber afferent neurons (24 μm diameter) have an inward current which is capsaicin sensitive and produce a TTX resistant spike with phasic firing and Aδ afferent neurons (33μm diameter) have an inward current which is insensitivity to capsaicin and is not TTX resistant and exhibit tonic firing [28].

Somatic:

Ganglia. There is no postganglionic stage in the somatic pathway. In the cat pre-ganglion, 45% of EUS motoneurons fired spontaneously with frequencies ranging from 12-27Hz [29]. Also, it has been demonstrated in the cat that during micturition, the urethral sphincter motoneurons hyperpolarize and hence slow down their firing or become quiescent [30].

Pudendal efferents. The only somatic-LUT connection is to the striated muscle of external urethral sphincter. Motor neurons in Onuf's nucleus located in the anterior horn of sacral S2-S4 segments in humans and lumbosacral L6-S1 segments in rats have long axons which directly innervate EUS via the pudendal nerve without any postganglionic targets in between. Their axons release ACh that act on nicotinic receptors (nAChR). (Fig 1)

During bladder filling pudendal motoneurons are activated by low level afferent input, whereas during micturition the motoneurons are inhibited by inhibitory input from supraspinal centers. This inhibition is dependent on supraspinal mechanisms and so is weak or absent in chronic spinal animals and in paraplegic patients. During filling, in spinal injured patients, the inhibition to motoneurons during micturition is lost and excitatory sphincter reflex pathway commonly initiates a striated sphincter contraction the same time as contraction of the bladder causing dyssynergia between bladder and sphincter, and interferes with bladder emptying; this phenomenon is termed detrusor-sphincter dyssynergia (DSD) [31].

*Pudendal afferents***.** Pudendal afferents have cell bodies in the dorsal root ganglia and enter the dorsal horn at the sacral or lumbosacral level (L6-S1 in rats, S1-S3 in cats, and S2-S4 in humans. Pudendal nerve afferent pathways of the cat, rat and monkey terminate in lateral laminae I, V–VII, and in lamina X [32, 33]. Pudendal afferents carry information related to pressure and flow rate from the urethra and coordinate urinary continence and micturition across many species.

Passing fluid through the urethra, irrespective of direction, causes pudendal nerve afferents activation at a much lower pressure compared to pelvic and hypogastric nerve afferents, which are activated by high-pressure flow that caused a distension of the urethra. Pudendal afferents are known to exhibit a slowly adapting tonic discharge that increases with bladder filling [34, 35]. Conduction velocities of pudendal nerve afferent fibers were found to communicate twice as fast (45 m/sec) as the pelvic nerve afferent fibers (20 m/sec) when responding to electrical stimulation of the urethra in cats [36].

At low bladder pressures, fluid entering the urethra can trigger an EUS contraction to maintain continence [37]. Studies in cats have also suggested that neurons in PSC provide a tonic excitatory input to the EUS motoneurons [38]. Electrical stimulation in PSC excites the EUS motoneurons and induces contractions of the EUS [39]. EUS also promotes continence via a feedback mechanism; contraction of the EUS induces firing in pudendal afferent fibers, which activate spinal inhibitory interneurons involved in the micturition reflex to inhibit parasympathetic preganglionic neurons (PGN) to suppress reflex bladder activity [40]. In animal nerve transection experiments; by eliminating pudendal sensory feedback, voiding efficiency is reduced, suggesting that this sensory feedback critically interacts with the network that produces normal voiding behavior [41].

2.3. Neurotransmitters and receptors

Synaptic transmission in all ganglia (e.g., IMG, MPG) is mediated by ACh acting on different nicotinic receptors. However, there is neuromodulation at both pre and post synaptic receptor sites. Parasympathetic postganglionic neurons (MPG) release the

excitatory neurotransmitter ACh / ATP, which contracts bladder smooth muscle, and nitric oxide (NO), which relaxes urethral smooth muscle [42,43]. Sympathetic postganglionic neurons (IMG) release NA (Noradrenaline) which relaxes DSM and contracts the urethral smooth muscle [44]. Somatic axons (motor neurons in Onuf's nucleus) release ACh and activate nicotinic cholinergic receptors on EUS that results in contraction.

Muscarinic receptors. Axons from MPG innervate DSM and release ACh which stimulates M3 muscarinic receptors that in turn triggers intracellular Ca+2 release that results in contraction of bladder. M3 receptors are the primary receptors in DSM, but M2 receptors are also expressed in large numbers, as much as 3-fold [45]. M2 receptors appear to play a functional role in 'recontracting' DSM after relaxation [46]. M2 receptors when activated can suppress the inhibitory mechanisms mediated by β3 receptors and contribute to bladder contractions [44]. In the normal bladder, muscarinic receptors are the primary effector of contractility in DSM, and these receptors are the main target for therapies aimed at symptoms of overactive bladder (OAB).

Purinergic receptors. Purinergic receptors respond to ATP, ADP, and adenosine. These receptors produce non-cholinergic contraction of DSM. The primary purinergic receptor present in DSM is P2X which are ligand-gated ion channels (Fig 1). Purinergic transmission doesn't seem to be playing an important role in normal human bladders but are important in animal bladders. However, purinergic signaling emerges as more prominent role in disease (Detrusor overactivity (DO), partial/chronic outlet obstruction

and interstitial cystitis) and with aging [47]; potentially accounting for up to 65% of the total contraction force [44].

Adrenergic receptors (ARs). ARs expressed in the bladder mediate relaxation and the ARs expressed in urethral outlet mediate contraction in response to sympathetic innervation (Fig 1). The major receptor subtypes present in the human bladder are α1 and β3; however, β-receptors are expressed more compared to α-receptors [48]. The effects of α1-AR stimulation on smooth muscle contraction are rather weak, therefore, appear to play only a minor functional role in the detrusor, but play a prominent role near the bladder outlet in terms of maintaining outlet resistance [49]. The β3-receptor subtype is most expressed in human bladders and accounts for >95% of β-receptors. NE is released from the sympathetic efferents to activate β3-receptors and results in smooth muscle relaxation.

2.4.Differences in LUT circuit among species, sex and developmental changes

Species. Efferent innervation to LUT originates from different spinal sections among species: parasympathetic (pelvic nerves (S2-S4 in humans and L6-S1 in rats)), sympathetic (hypogastric nerves (T10-L2 in humans and L1-L2 in rats)), and somatic nerves (pudendal nerves (S2-S4 in humans and L6-S1 in rats)).

At the postganglionic level, morphology of the ganglion cells varies. In the rat MPG [50] and mouse IMG [51] the cells are (20-30 μm) in diameter and have no dendrites or only a few short dendrites. In cats, neurons in pelvic and bladder ganglia are larger (40–60 μm)

and have a few dendrites. Variations in conduction velocities, patterns of convergence and characteristics of transmitter release have been observed under different physiological conditions [52]. Preganglionic parasympathetic input to the bladder ganglia are carried by myelinated (B-fiber) axons in cats [53], unmyelinated C-fibers in rats and mouse [51,54] and a mixture of B- and C-fibers in guinea pigs [55].

Considerable differences have been noted in synaptic transmission regarding the properties of the preganglionic input, and facilitatory and inhibitory synaptic mechanisms. In the rat, single presynaptic stimuli in the pelvic nerve elicit large amplitude EPSPs in postganglionic neurons [50,54].These responses do not change in amplitude during repetitive stimulation with frequencies (0.25-20 Hz). However, the discharges decrease in amplitude at high frequencies (30–50 Hz). So, in mouse, rat, and guinea pig, parasympathetic ganglia may function as relay and not integration centers [50,55]. In cats, single or low frequency stimuli (<0.25 Hz) elicit small amplitude EPSPs which gradually increase in amplitude during continuous stimulation at frequencies of (1-20 Hz) and maximal facilitation requires 15 to 25 stimuli in a train and persists for 30 to 60 s after termination of high frequency stimulation [56, 57]. This facilitation, also observed in rabbits, can suppress low frequency efferent activity and amplify high efferent activity, thus acting like a high pass filter.

Sex. Apart from the obvious anatomical differences among sexes in different species, there are considerable differences in physiology, morphology and function. Anatomically, DSM is thicker in men than women, as greater voiding pressure is needed to empty the

bladder through the longer urethra of males [58]. Also, in male, the IUS is composed of smooth muscle that is arranged into long inner longitudinal and outer circular layers [59]. However, in women, the longitudinal cells do not form IUS, the bladder neck and proximal urethra form a functional rather than an anatomic internal sphincter. Contractility of DSM with cholinergic stimulation is found to be more sensitive in female rats than male [60]. Relaxation of bladder neck and urethra of male rabbits is more than in females with field stimulation [61] and gender doesn't seem to influence the contractility of the human bladder [62]. Regarding receptors, male rabbits have equivalent amounts of α1- and α2-ARs, whereas the females have a significantly denser population of α2-ARs [63] and cholinergic transmission was predominant in the male guinea pig bladder than the female bladder. And the opposite is true for purinergic transmission [64]. Differences also exist in voiding patterns between male and female rats. During voiding, maximum flow rate was lower and micturition time was shorter in female rats as compared to males. When we consider dysfunctions, it has been observed that overactive bladder (OAB) symptoms are more frequently observed and are significantly higher in women than in men but it is quite opposite in urinary urge incontinence (UUI) and DO symptoms [65 - 67].

Neonates vs adult. Voiding in neonates is dependent on pudendo-bladder reflex mechanism which is triggered when the mother licks the genital or perineal region of the young animal (e.g., rats and cats) [68, 69]. The pudendo-bladder reflex circuit is in the sacral spinal cord and has afferents coming in from the pudendal nerve and efferents transmitted in the pelvic nerve. In newborn kittens and rats, the pudendo-bladder reflex

is essential for survival because urinary retention could be fatal if the newborn is away from the mother [70, 71]. Upon maturation, reorganization of synaptic connections in bladder reflex pathways happens which downregulate neonatal spinal mechanisms and upregulates conscious voiding control via supraspinal mechanisms. Spinal cord injury in adult animals and humans which interrupts supraspinal-spinal cord connections causes the reemergence of the neonatal perineal/pudendal-to-bladder reflex. In neonates some supraspinal mechanisms may already be functioning to suppress the spinobulbospinal micturition reflex pathway allowing micturition to be controlled by primitive spinal reflex mechanisms [72].

3. PHYSIOLOGY OF NEURAL CONTROL OF LUT & COMPUTATIONAL MODELING

3.1. Filling vs Voiding

During filling, distension of bladder produces low-level afferent firing. At this stage parasympathetic efferents are quiescent and sympathetic and somatic efferents are active. Intravesical pressure measurements in both humans and animals reveal low and relatively constant bladder pressures when bladder volume is below the threshold for inducing voiding (Vol_{DEC}). Also, during filling, EUS electromyogram (EMG) show increases in the activity of the sphincter reflecting an increase in efferent firing in the pudendal nerve and an increase in outlet resistance that contributes to storage of urine [2].

Voiding can be triggered either voluntarily or involuntarily. In human infants, as the bladder fills, bladder afferent signals increase in strength until they exceed a certain

threshold in the brainstem, specifically the periaqueductal gray (PAG). In the absence of any controlling influences, the pontine micturition center (PMC) is activated, the urethral sphincter relaxes, the bladder contracts, and voiding occurs [73]. This mechanism constitutes the involuntary voiding. In adults, increased afferent firing from inline tension receptors in the bladder produces firing in the parasympathetic pathways, inhibits sympathetic pathways and somatic pathways. This phase consists of an initial relaxation of the urethral sphincter followed by a contraction of the bladder, an increase in bladder pressure, and the flow of urine. The generation of conscious bladder sensations and the mechanisms that underlie the switch from storage to voluntary voiding involve cerebral circuits above the PAG [2].

Stimulation based experimental data. Several stimulation experiments proposed solutions to different LUT dysfunctions. Here we discuss one such stimulation - Pudendal nerve (PN) stimulation which has been replicated in a computational model [74]. PN stimulation has been proposed as a method to restore continence and micturition. This is possible because pudendal afferent stimulation can differentially activate spinal circuits responsible for reflex inhibition or excitation of bladder [75,76]. Low frequencies for PN stimulation (2-15 Hz) inhibit bladder contractions and increase bladder capacity and thus helps with continence. GABAergic mechanism in lumbo-sacral spinal column is evoked by this low PN stimulation and inhibits the excitatory control of the bladder, rather than activation of a bladder relaxation pathway [77]. High frequency PN stimulation (25-50 Hz) evoked contractions in bladder but 33 Hz pudendal afferent stimulation caused sustained SEC (stimulation evoked contraction) for bladder volumes >70% Vol_{DEC}

(Volume threshold for distension evoked contractions) whereas 10 Hz caused SEI (stimulation evoked inhibition) [78, 79]. Pudendal afferent stimulation at 33 Hz failed to evoke robust bladder contractions (mean bladder pressure >10 cm-H_2O) below ~70 % of the volume necessary to evoke DECs showing volume dependence [80].

3.2. Brief history of modeling the LUT & challenges

The earliest reported computational model of the LUT was of a dog bladder. The authors assumed the bladder to be spherical with a structure that collapsed with increasing pressure. They used recordings from stimulations of female dog bladders to determine their feedback system with state space methods dependent on their measured motor neuron firing rates [81]. This general approach was followed throughout most of the later modeling attempts. Another group, Bastiaanssen et al. [82] developed a biomechanical model of LUT based on urine outflow data from patients, but further simplified their neural component to disregard firing rates, directly converting pressures to muscular contraction via empirically determined state variables. One of the earlier papers to attempt to model neural computation used a state-space formulation for each known neural ganglion. This group added levels of neural components incrementally and varied excitatory and inhibitory connectivity [83,84].

Since 2010, there has been a resurgence in modeling the neural circuit of micturition more realistically. Much of this has been devoted to determining the interactions between the supraspinal micturition centers (PMC/PAG, cortex, etc.) and the spinal ganglia or the interaction between the autonomic and somatic systems at the spinal level. De Groat's

group has focused on the former, while Grill's group focused on the latter. De Groat's group created a model with simple monosynaptic weighed integration of binary neurons in the spinal cord [3]. Their supraspinal neurons were based on recordings taken from the PMC and PAG, as their overall goal was to understand the role of the supraspinal switching circuitry in micturition. Grill et al. developed an integrate-and-fire model of the spinal circuit at lumbosacral level of cat [74]focusing on the afferent pudendal stimulation. They have the most detailed model of connectivity at the spinal level; however, they ignore the sympathetic nervous system in their model. Their results are centered on studying the spinal circuitry involved in pudendo-vesical reflex.

Challenges to modeling cellular network neurophysiology.

The role of computational modeling is to study complex functions with relatively simple principles while preserving the necessary realism in the model which can shed light on the inner working at different levels of organization. However, when trying to model a functional circuit such as the LUT, with gaps in data, several assumptions need to be made using informed judgement.

Ganglion level. There is much overlap in the neurons which project to visceral organs and it is hard to know LUT specific neurons because all the axons are bundled together in the efferent nerves. So, several aspects required to model such as interconnectivity if any, synaptic divergence and convergence are unknown. The functional role of most postganglionic neurons is predominantly spatial amplification and filtering of preganglionic inputs. It has been suggested that after spinal transection the firing patterns of these neurons can change (Ex: from tonic to Phasic). These postganglionic neurons are

subject to modulation from several neuromodulators at both pre and post synaptic sites. However, the implications of these changes are yet to be studied and models provide a great framework in that regard.

Cellular level. To model a biophysically constrained neuron, we match electrophysiological data such as passive properties (Resting membrane potential (V_{Rest}), input resistance (R_{IN}) and time constant (τ)) and active properties such as (firing patterns and FIR curve). To reproduce these electrophysiological characteristics, experimental data related to all the properties are typically obtained from intracellular current-clamp studies, if the channel types present in the neuron are known. These neurons come with markedly different morphology across species, some with no dendrites and other with few. In order to capture the necessary essentials, we need answers to questions such as: Can the properties of the neuron be explained by a single compartment or do we need more compartments? Are the location of synapses important? For a systematic review of the methodology to build single cell models please refer to Guntu et al. [85].

To model the LUT circuit a challenge was that single cell data had to be compiled and integrated across different species and even from neonates and adults. It is noted that this is typical in computational studies involving brain regions in general, with the assumption being that characteristics of channels and other neuronal properties are similar across brain regions. For instance, in the case of LUT, there are relatively few studies that thoroughly characterize the firing patterns innervating efferent neurons, with the primary focus of the literature being on neurons of the MPG (for example see references [16,86-

88]). There are even fewer studies that specifically characterize ionic conductances underlying those firing patterns. Finally, distinct cell types have been reported in the MPG, based on their outputs – at a minimum those that fire tonically as a result of depolarization, and those that show phasic output [86]. The existing literature on underlying membrane conductances is further limited by those that discriminate between these cell types in their analysis. Only a subset of membrane conductances of MPG neurons have been studied in voltage clamp, and many of these represent mixed currents. For example, sodium currents have only been measured in one study [89], and this same study separated at least three K+ current subtypes in dissociated cultured neurons [89]. Calcium channels have been fairly well documented, including voltage-clamp studies of both N- and T-type currents [90-92]. Finally, ATP-sensitive K+ conductance [93] and calcium-sensitive chloride currents [94] have been partially characterized. However, these studies have only begun to provide a comprehensive characterization of membrane currents of the pelvic ganglion neurons, and represent a diverse set of model organisms, pharmacological isolation, and cell-type specific localization.

Synaptic level. Synapses at all levels can be classified as excitatory and inhibitory and there is evidence of facilitating and depressing synapses as well. Neurotransmitters and receptors involved in the LUT circuit are highlighted above in section 2. Transmission through efferent nerves is either cholinergic or purinergic. A majority of transmission at postganglionic level is cholinergic and this transmission can be modulated at pre and postganglionic sites. Neuromodulation effects may be substantial on the computational

properties of a neuron, but concrete experimental data are not yet available to incorporate these effects into a model.

In addition to membrane conductances and properties, even fewer studies have characterized synaptic currents. It is known that the cholinergic synapses of the MPG are largely carried by α3β4 subunits [95], and some of the integrative properties of these synapses have been studied [88,96]. However, there is relatively little information about the full spectrum of synaptic properties in the ganglia of the LUT.

Network level. The afferent fibers consist of high-threshold and low-threshold types and functioning of LUT is state dependent i.e., depending on the state, several reflexes emerge and implement different functions in the LUT. Some reflexes are represented as mono synaptic while there is some evidence that they may be multisynaptic. Connectivity within ganglia is mostly unknown except we know that there is considerable divergence from preganglionic to postganglionic neurons e.g., PGN-MPG. While this brain stem switch itself is a complicated circuit, researchers have assumed the supraspinal input as a simple on-off switch. . While extracellular measures of LUT network activity have been made in conjunction with bladder output (for example see [26,97]), a comprehensive recording of simultaneous and coordinated efferent and afferent network activity during filling and voiding of the bladder has not yet been well reported.

Interface with bladder. The purpose of the neural circuit described so far is to control the urinary bladder. Specifically, to determine how efferents arising from the model result

in bladder contraction or relaxation and how bladder distention results in increased bladder afferent firing rate. Bladder stretch releases ATP and ACh which acts on P2X receptors or muscarinic receptors (M3) on the afferent nerve terminal as described above in section 2. The physiological details and complex interactions involved with bladder smooth muscles, urothelium, interstitial cells and afferent nerves is beyond the scope of this chapter and are reviewed in a hypothetical model of uroepithelial sensory web [98]. There have also been excellent efforts to model urinary bladder smooth muscle in the mouse [99]. The next logical step would be to incorporate the current model with bladder smooth muscle model [99] or even the mechanistic model of bladder [82]. To complete the picture incorporate model of supraspinal control by the higher order centers will need to be incorporated [3].

3.3. **Preliminary biophysical model of the neural LUT**.

We are currently developing and testing a biophysical model of the neural circuit of the LUT. The model contains EUS afferents, supraspinal PAG/PMC input and initial input for bladder afferents. At spinal level we modeled parasympathetic preganglionic neurons (PGN), sympathetic preganglionic neurons (Hypo), medial interneurons (IN_{M+}(excitatory) and IN_{M-}(inhibitory)), dorsal interneuron (IN_D), and Feedback interneuron (FB). At postganglionic level we have models for MPG and IMG neurons. We also modeled the somatic motorneuron (EUS_{MN}). All neurons are modeled using the Hodgkin-Huxley formulation with single compartments [100]. Single cells are matched to reproduce available electrophysiological data (Table 1). A consolidated figure of the LUT model is provided in (Fig 2) below.

There are 10 cells in each location and the connectivity between groups of cells is implemented using a Gaussian distribution as with our previous models [109-111] There is no interconnectivity between neurons within a ganglion. All synapses are modeled as double exponential functions with rise and decay times. Our spinal interneuron network uses a depressing synapse with the EUS afferent and an assumed excitatory synapse with the PAG/PMC input to model IN_{M+} as a low-pass filter for the EUS afferent. An excitatory synapse with the EUS afferent was used to model IN_{M-} as a high-pass filter for the EUS afferent. The bladder is filled at a constant rate. We use tuning curves from McGee et al., [74] to determine bladder pressure from PGN firing rate and we use this calculated pressure to then estimate bladder afferent firing rate. Once developed, a reliable model for bladder dynamics can replace this 'tuning curve' approximation that we use presently. . The model is implemented in NEURON [112] and uses the BMTK library to implement functions [113]. The feedback network uses the PGN firing rate to calculate bladder pressure, and then the bladder pressure and bladder volume to calculate bladder afferent firing rate at user-specified intervals during the simulation. This implementation permits implementation of closed-loop feedback given initial trends of bladder afferent firing rate.

Current model reproduces the observed trends of firing rates during a typical fill and void cycle with firing rates that match experimental observations (Fig 3). Further details related to the model can be found in Guntu et al. [114]

A key with such modeling efforts is to match preliminary trends with simple structures, e.g., 1 or 10 cells in each ganglion. Further refinements can be pursued once the model is able to reproduce key experimental findings. Challenges to improving the model are as follows: Biological data related to single cell characteristics are scarce and from different species. Once such data are available, the single cell models can be improved. The present model includes only tonic cells and so phasic and other cells types that may be discovered need to be incorporated. Both intra- and inter- connectivity are not known for the various ganglia, and so different parametric cases can be explored, ensuring all the while that firing rates are within the biological ranges. With increasing fidelity, such models can also help explore the various known 'reflexes' during both normal and abnormal (e.g., spinal cord injury) functioning of LUT networks. An important use of such models will be to provide or falsify testable hypotheses for understanding functioning as well as for the design of interventions such as electrical stimulation.

SUMMARY

This chapter focused on reviewing relevant literature with to the goal of highlighting the challenges in computational modeling of the neural control of the mammalian LUT. A brief overview of the anatomy, neurophysiology and neurotransmitters preceded the main focus on the neural components of the LUT. Differences among species, sex and developmental changes are also outlined to show the complexity in the underlying biology. To put the review in context, we provide a brief summary of ongoing modeling efforts related to the LUT circuit with 10-cells at each location. This preliminary model successfully simulated the firing pattern trends observed in experiments during the filling

and voiding cycle. Lack of experimental data necessitates thoughtful assumptions that are informed by an understanding of the neural fundamentals. As cited, an important use of such models will be to generate testable hypotheses for understanding normal and pathological functioning of the LUT, and to provide guidance for the design of interventions, e.g., electrical stimulation.

REFERENCES

[1] de Groat WC, Griffiths D, Yoshimura N (2015), Neural control of the lower urinary tract. Compr Physiol 5:327-396.

[2] Fowler CJ, Griffiths D, de Groat WC (2008), The neural control of micturition. Nat Rev Neurosci 9:453-466.

[3] de Groat WC, Wickens C (2013), Organization of the neural switching circuitry underlying reflex micturition. Acta physiologica (Oxford, England) 207:66-84.

[4] Wein AJ (1992). Neuromuscular dysfunction of the lower urinary tract. In Walsh PC, Retik AB, Stamey TA, Vaughan ED eds, Campbell's Urology, 6th edn., vol 2, WB Saunders Co, 573–642

[5] Hinman F Jr (1986). Non-neurogenic neurogenic bladder (the Hinman Syndrome) — 15 years later. J Urol; 136: 769–77

[6] Kanai A, Andersson K-E (2010), Bladder afferent signaling: recent findings. The Journal of urology 183:1288-1295.

[7] Inskip JA, Ramer LM, Ramer MS, Krassioukov AV (2009), Autonomic assessment of animals with spinal cord injury: tools, techniques and translation. Spinal Cord 47:2-35.

[8] Baron R, Janig W, McLachlan EM (1985), The afferent and sympathetic components of the lumbar spinal outflow to the colon and pelvic organs in the cat. I. The hypogastric nerve. J Comp Neurol 238:135-146.

[9] Melvin JE, McNeill TH, Hervonen A, Hamill RW (1989), Organizational role of testosterone on the biochemical and morphological development of the hypogastric ganglion. Brain Res 485:1-10.

[10] Danziger ZC, Grill WM (2016), Sensory and circuit mechanisms mediating lower urinary tract reflexes. Autonomic Neuroscience 200:21-28.

[11] Morgan C, de Groat WC, Nadelhaft I (1986), The spinal distribution of sympathetic preganglionic and visceral primary afferent neurons that send axons into the hypogastric nerves of the cat. Journal of Comparative Neurology 243:23-40.

[12] Bahns E, Halsband U, Janig W (1987), Responses of sacral visceral afferents from the lower urinary tract, colon and anus to mechanical stimulation. Pflugers Arch 410:296-303.

[13] Winter DL (1971), Receptor characteristics and conduction velocities in bladder afferents. Journal of Psychiatric Research 8:225-235.

[14] de Groat, WC.; Booth, AM (1993). Synaptic transmission in pelvic ganglia. In: Maggi, CA., editor. The Autonomic Nervous System. London: Harwood Academic Publishers; p. 291-347.

[15] Keast JR, Booth AM, de Groat WC (1989), Distribution of neurons in the major pelvic ganglion of the rat which supply the bladder, colon or penis. Cell Tissue Res 256:105-112.

[16] Jobling P, Lim R (2008), Anatomical and physiological properties of pelvic ganglion neurons in female mice. Autonomic neuroscience : basic & clinical 140:30-39.

[17] Burnstock G (2006), Purinergic signalling. Br J Pharmacol 147 Suppl 1:S172-S181.

[18] Palea S, Artibani W, Ostardo E, Trist DG, Pietra C (1993), Evidence for purinergic neurotransmission in human urinary bladder affected by interstitial cystitis. J Urol 150:2007-2012.

[19] Habler HJ, Janig W, Koltzenburg M (1993), Receptive properties of myelinated primary afferents innervating the inflamed urinary bladder of the cat. J Neurophysiol 69:395-405.

[20] Bruns TM, Gaunt RA, Weber DJ (2011), Multielectrode array recordings of bladder and perineal primary afferent activity from the sacral dorsal root ganglia. J Neural Eng 8:056010.

[21] Häbler HJ, Jänig W, Koltzenburg M (1993), Myelinated primary afferents of the sacral spinal cord responding to slow filling and distension of the cat urinary bladder. The Journal of physiology 463:449-460.

[22] Xu L, Gebhart GF (2008), Characterization of mouse lumbar splanchnic and pelvic nerve urinary bladder mechanosensory afferents. J Neurophysiol 99:244-253.

[23] Sengupta JN, Gebhart GF (1994), Mechanosensitive properties of pelvic nerve afferent fibers innervating the urinary bladder of the rat. J Neurophysiol 72:2420-2430.

[24] Barrington FJF (1914), The nervous mechanism of micturition. Quarterly Journal of Experimental Physiology 8:33-71.

[25] de Groat WC, Ryall RW (1969), Reflexes to sacral parasympathetic neurones concerned with micturition in the cat. The Journal of physiology 200:87-108.

[26] Mallory B, Steers WD, De Groat WC (1989), Electrophysiological study of micturition reflexes in rats. Am J Physiol 257:R410-421.

[27] Cheng C-L, Liu J-C, Chang S-Y, Ma C-P, de Groat WC (1999), Effect of capsaicin on the micturition reflex in normal and chronic spinal cord-injured cats. American Journal of Physiology-Regulatory, Integrative and Comparative Physiology 277:R786-R794.

[28] de Groat WC, Yoshimura N (2009), Afferent nerve regulation of bladder function in health and disease. Handb Exp Pharmacol:91-138.

[29] Carp JS, Tennissen AM, Liebschutz JE, Chen XY, Wolpaw JR (2010), External urethral sphincter motoneuron properties in adult female rats studied in vitro. J Neurophysiol 104:1286-1300.

[30] Fedirchuk B, Shefchyk SJ (1993), Membrane potential changes in sphincter motoneurons during micturition in the decerebrate cat. The Journal of Neuroscience 13:3090.

[31] Torrens M, Morrison JFB (1987), The Physiology of the Lower Urinary Tract . Springer-Verlag: Berlin.

[32] Thor KB, Morgan C, Nadelhaft I, Houston M, De Groat WC (1989), Organization of afferent and efferent pathways in the pudendal nerve of the female cat. J Comp Neurol 288:263-279.

[33] McKenna KE, Nadelhaft I (1986), The organization of the pudendal nerve in the male and female rat. J Comp Neurol 248:532-549.

[34] Todd JK (1964), Afferent impulses in the pudendal nerves of the cat. Quarterly Journal of Experimental Physiology and Cognate Medical Sciences 49:258-267.

[35] Bradley W, Griffin D, Teague C, Timm G (1973) Sensory innervation of the mammalian urethra. Invest Urol 10: 287–289.

[36] Thor KB, de Groat WC (2010), Neural control of the female urethral and anal rhabdosphincters and pelvic floor muscles. Am J Physiol Regul Integr Comp Physiol 299:R416-R438.

[37] Karicheti V, Langdale CL, Ukai M, Thor KB (2010), Characterization of a spinal, urine storage reflex, inhibitory center and its regulation by 5-HT1A receptors in female cats. Am J Physiol Regul Integr Comp Physiol 298:R1198-1208.

[38] Holstege G, Griffiths D, de Wall H, Dalm E (1986), Anatomical and physiological observations on supraspinal control of bladder and urethral sphincter muscles in the cat. J Comp Neurol 250:449-461.

[39] Kuru M, Iwanaga T (1966), Ponto-sacral connections in the medial reticulo-spinal tract subserving storage of urine. J Comp Neurol 127:241-266.

[40] McGuire E, Morrissey S, Zhang S, Horwinski E (1983), Control of reflex detrusor activity in normal and spinal injured non-human primates. J Urol 129:197-199.

[41] Peng CW, Chen JJ, Cheng CL, Grill WM (2008), Role of pudendal afferents in voiding efficiency in the rat. Am J Physiol Regul Integr Comp Physiol 294:R660-672.

[42] Burnett AL, Calvin DC, Chamness SL, Liu JX, Nelson RJ, Klein SL, Dawson VL, Dawson TM, et al. (1997), Urinary bladder-urethral sphincter dysfunction in mice with targeted disruption of neuronal nitric oxide synthase models idiopathic voiding disorders in humans. Nat Med 3:571-574.

[43] Anderson KE (1993), Pharmacology of lower urinary tract smooth muscles and penile erectile tissues. Pharmacol Rev 45:253-308.

[44] Andersson KE, Arner A (2004), Urinary bladder contraction and relaxation: physiology and pathophysiology. Physiol Rev 84:935-986.

[45] Hegde SS (2006), Muscarinic receptors in the bladder: from basic research to therapeutics. Br J Pharmacol 147 Suppl 2:S80-87.

[46] Uchiyama T, Chess-Williams R (2004), Muscarinic receptor subtypes of the bladder and gastrointestinal tract. J Smooth Muscle Res 40:237-247.

[47] Yoshida M, Miyamae K, Iwashita H, Otani M, Inadome A (2004), Management of detrusor dysfunction in the elderly: changes in acetylcholine and adenosine triphosphate release during aging. Urology 63:17-23.

[48] Michel MC, Vrydag W (2006), Alpha1-, alpha2- and beta-adrenoceptors in the urinary bladder, urethra and prostate. Br J Pharmacol 147 Suppl 2:S88-119.

[49] Michel MC, Barendrecht MM (2008), Physiological and pathological regulation of the autonomic control of urinary bladder contractility. Pharmacol Ther 117:297-312.

[50] Tabatai M, Booth AM, de Groat WC (1986), Morphological and electrophysiological properties of pelvic ganglion cells in the rat. Brain Res 382:61-70.

[51] Rogers H, Kennedy C, Henderson G (1990), Characterization of the neurons of the mouse hypogastric ganglion: morphology and electrophysiology. J Auton Nerv Syst 29:255-270.

[52] de Groat WC (1995), Mechanisms underlying the recovery of lower urinary tract function following spinal cord injury. Paraplegia 33:493.

[53] de Groat WC, Ryall RW (1969), Reflexes to sacral parasympathetic neurones concerned with micturition in the cat. The Journal of physiology 200:87-108.

[54] Mallory B, Steers WD, De Groat WC (1989), Electrophysiological study of micturition reflexes in rats. Am J Physiol 257:R410-421.

[55] Blackman JG, Crowcroft PJ, Devine CE, Holman ME, Yonemura K (1969), Transmission from pregnanglionic fibres in the hypogastric nerve to peripheral ganglia of male guinea-pigs. The Journal of physiology 201:723-743.

[56] Booth AM, DeGroat WC (1979), A study of facilitation in vesical parasympathetic ganglia of the cat using intracellular recording techniques. Brain Res 169:388-392.

[57] deGroat WC, Saum WR (1976), Synaptic transmission in parasympathetic ganglia in the urinary bladder of the cat. The Journal of physiology 256:137-158.

[58] Mangera A, Osman NI, Chapple CR (2013), Anatomy of the lower urinary tract. Surgery (Oxford) 31:319-325.

[59] Yucel S, Baskin LS (2004), An anatomical description of the male and female urethral sphincter complex. J Urol 171:1890-1897.

[60] Longhurst PA, Levendusky M (2000), Influence of gender and the oestrous cycle on in vitro contractile responses of the rat urinary bladder to cholinergic stimulation. Br J Pharmacol 131:177-184.

[61] Lee JG, Wein AJ, Levin RM (1994), Comparative pharmacology of the male and female rabbit bladder neck and urethra: involvement of nitric oxide. Pharmacology 48:250-259.

[62] Fry CH, Bayliss M, Young JS, Hussain M (2011), Influence of age and bladder dysfunction on the contractile properties of isolated human detrusor smooth muscle. BJU Int 108:E91-96.

[63] Morita T, Latifpour J, O'Hollaren B, Wheeler MA, Weiss RM (1987), Sex differences in function and distribution of alpha 1- and alpha 2-adrenoceptors in rabbit urethra. Am J Physiol 252:F1124-1128.

[64] Patra PB, Patra S (2013), Sex differences in the physiology and pharmacology of the lower urinary tract. Curr Urol 6:179-188.

[65] Coyne KS, Sexton CC, Vats V, Thompson C, Kopp ZS, Milsom I: National community prevalence of overactive bladder in the United States stratified by sex and age. Urology 2011;77:1081–1087.

[66] Cheung WW, Khan NH, Choi KK, Bluth MH, Vincent MT (2009), Prevalence, evaluation and management of overactive bladder in primary care. BMC Fam Pract 10:8.

[67] Al-Ghazo MA, Ghalayini IF, Al-Azab R, Hani OB, Matani YS, Haddad Y (2011), Urodynamic detrusor overactivity in patients with overactive bladder symptoms. Int Neurourol J 15:48-54.

[68] deGroat WC, Douglas JW, Glass J, Simonds W, Weimer B, Werner P (1975), Changes in somato-vesical reflexes during postnatal development in the kitten. Brain Res 94:150-154.

[69] Maggi CA, Santicioli P, Meli A (1986), Postnatal development of micturition reflex in rats. American Journal of Physiology-Regulatory, Integrative and Comparative Physiology 250:R926-R931.

[70] Thor KB, Blais DP, de Groat WC (1989), Behavioral analysis of the postnatal development of micturition in kittens. Developmental Brain Research 46:137-144.

[71] Kruse MN, De Groat WC (1990), Micturition reflexes in decerebrate and spinalized neonatal rats. Am J Physiol 258:R1508-1511.

[72] Sugaya K, Roppolo JR, Yoshimura N, Card JP, de Groat WC (1997), The central neural pathways involved in micturition in the neonatal rat as revealed by the injection of pseudorabies virus into the urinary bladder. Neurosci Lett 223:197-200.

[73] Tai C, Roppolo JR, de Groat WC (2006), Spinal reflex control of micturition after spinal cord injury. Restor Neurol Neurosci 24:69-78.

[74] McGee MJ, Grill WM (2016), Modeling the spinal pudendo-vesical reflex for bladder control by pudendal afferent stimulation. J Comput Neurosci 40:283-296.

[75] Boggs JW, Wenzel BJ, Gustafson KJ, Grill WM (2006), Frequency-dependent selection of reflexes by pudendal afferents in the cat. The Journal of physiology 577:115-126.

[76] Woock JP, Yoo PB, Grill WM (2008), Activation and inhibition of the micturition reflex by penile afferents in the cat. Am J Physiol Regul Integr Comp Physiol 294:R1880-R1889.

[77] McGee MJ, Danziger ZC, Bamford JA, Grill WM (2014), A spinal GABAergic mechanism is necessary for bladder inhibition by pudendal afferent stimulation. American Journal of Physiology-Renal Physiology 307:F921-F930.

[78] Yoo PB, Woock JP, Grill WM (2008), Bladder activation by selective stimulation of pudendal nerve afferents in the cat. Exp Neurol 212:218-225.

[79] Woock JP, Yoo PB, Grill WM (2011), Mechanisms of reflex bladder activation by pudendal afferents. Am J Physiol Regul Integr Comp Physiol 300:R398-R407.

[80] McGee MJ, Grill WM (2014), Selective co-stimulation of pudendal afferents enhances bladder activation and improves voiding efficiency. Neurourology and urodynamics 33:1272-1278.

[81] Drolet R, Kunov H (1975), On the peripheral bladder control system of the dog and urodynamics: in vivo characterisation and hybrid computer simulation. Med Biol Eng 13:40-55.

[82] Bastiaanssen EH, van Leeuwen JL, Vanderschoot J, Redert PA (1996), A myocybernetic model of the lower urinary tract. J Theor Biol 178:113-133.

[83] van Duin F, Rosier PF, Rijkhoff NJ, van Kerrebroek PE, Debruyne FM, Wijkstra H (1998), A computer model of the neural control of the lower urinary tract. Neurourol Urodyn 17:175-196.

[84] van Duin F, Rosier PF, Bemelmans BL, Debruyne FM, Wijkstra H (1999), A computer model for describing the effect of urethral afferents on simulated lower urinary tract function. Arch Physiol Biochem 107:223-235.

[85] Guntu V, Feng F, Alturki A, Nair A, Samarth P, Nair SS (2018) Amygdala Models. In: Computational Models of Brain and Behavior, vol., pp. 285-301.

[86] Tan H, Mawe GM, Vizzard MA (2007), Electrical properties of neurons in the intact rat major pelvic ganglion. Autonomic neuroscience : basic & clinical 134:26-37.

[87] Gray M, Lett KM, Garcia VB, Kyi CW, Pennington KA, Schulz LC, Schulz DJ (2019), Changes in excitability and ion channel expression in neurons of the major pelvic ganglion in female type II diabetic mice. Autonomic neuroscience : basic & clinical 220:102558.

[88] Tompkins JD, Vizzard MA, Parsons RL (2013), Synaptic transmission at parasympathetic neurons of the major pelvic ganglion from normal and diabetic male mice. J Neurophysiol 109:988-995.

[89] Yoshimura N, De Groat WC (1996), Characterization of voltage-sensitive Na+ and K+ currents recorded from acutely dissociated pelvic ganglion neurons of the adult rat. J Neurophysiol 76:2508-2521.

[90] Won YJ, Whang K, Kong ID, Park KS, Lee JW, Jeong SW (2006), Expression profiles of high voltage-activated calcium channels in sympathetic and parasympathetic pelvic ganglion neurons innervating the urogenital system. J Pharmacol Exp Ther 317:1064-1071.

[91] Lee J, Kim E, Park B-G, Kim K-H, Cha S-K, Kong ID, Lee J-W, Jeong S-W, Perez-reyes E, Kong IND: Identification of T-Type α1H Ca2+ Channels (Cav3.2) in Major Pelvic Ganglion Neurons. J Neurophysiol 2002, 87:2844–2850.

[92] Park KS, Jeong SW, Cha SK, Lee BS, Kong ID, Ikeda SR, Lee JW: Modulation of N-type Ca2+ currents by A1-adenosine receptor activation in male rat pelvic ganglion neurons. J Pharmacol Exp Ther 2001, 299:501–8.

[93] Park K-S, Cha S-K, Lee KI, Jun JY, Jeong SW, Kong ID, Lee J-W (2002), Identification of ATP-sensitive K+ conductances in male rat major pelvic ganglion neurons. Korean Journal of Physiology and Pharmacology 6:247-253.

[94] Akasu T, Nishimura T, Tokimasa T (1990), Calcium-dependent chloride current in neurones of the rabbit pelvic parasympathetic ganglia. The Journal of physiology 422:303-320.

[95] Park KS, Cha SK, Kim MJ, Kim DR, Jeong SW, Lee JW, Kong ID (2006), An alpha3beta4 subunit combination acts as a major functional nicotinic acetylcholine receptor in male rat pelvic ganglion neurons. Pflugers Arch 452:775-783.

[96] Felix B, Catalin D, Miolan JP, Niel JP (1998), Integrative properties of the major pelvic ganglion in the rat. J Auton Nerv Syst 69:6-11.

[97] Zvara P, Wright AJ, Roach K, Ursiny M, Shapiro B, Dagrosa LM, Nelson MT, Heppner TJ (2010), A non-anesthetized mouse model for recording sensory urinary bladder activity. Front Neurol 1:127.

[98] Birder L, Andersson KE (2013), Urothelial signaling. Physiol Rev 93:653-680.

[99] Mahapatra C, Brain KL, Manchanda R (2018), A biophysically constrained computational model of the action potential of mouse urinary bladder smooth muscle. PLoS One 13:e0200712.

[100] Dayan P, Abbott LF (2005) Theoretical Neuroscience: Computational and Mathematical Modeling of Neural Systems. The MIT Press.

[101] Kepper ME, Keast JR (2000), Transmitter profile and spinal inputs of pelvic ganglion cells projecting with preganglionic axons along the hypogastric and pelvic nerves of the male rat. Neurosci Lett 280:123-126.

[102] Snellings AE, Yoo PB, Grill WM (2012), Urethral flow-responsive afferents in the cat sacral dorsal root ganglia. Neuroscience letters 516:34-38.

[103] Szucs P, Odeh F, Szokol K, Antal M (2003), Neurons with distinctive firing patterns, morphology and distribution in laminae V-VII of the neonatal rat lumbar spinal cord. Eur J Neurosci 17:537-544.

[104] Lu Y, Inokuchi H, McLachlan EM, Li J-S, Higashi H (2001), Correlation between electrophysiology and morphology of three groups of neuron in the dorsal commissural nucleus of lumbosacral spinal cord of mature rats studied in vitro. Journal of Comparative Neurology 437:156-169.

[105] Miura A, Kawatani M, Araki I, de Groat WC (2000), Electrophysiological properties of lumbosacral preganglionic neurons in the neonatal rat spinal cord. Brain Research 872:54-63.

[106] Zimmerman A, Hochman S (2010), Heterogeneity of membrane properties in sympathetic preganglionic neurons of neonatal mice: evidence of four subpopulations in the intermediolateral nucleus. J Neurophysiol 103:490-498.

[107] Jule Y, Szurszewski JH (1983), Electrophysiology of neurones of the inferior mesenteric ganglion of the cat. J Physiol 344:277-292.

[108] Blok BF, Holstege G (2000), The pontine micturition center in rat receives direct lumbosacral input. An ultrastructural study. Neurosci Lett 282:29-32.

[109] Feng F, Headley DB, Amir A, Kanta V, Chen Z, Pare D, Nair SS (2019) Gamma oscillations in the basolateral amygdala: biophysical mechanisms and computational consequences, eNeuro 6(1) e0388-18.2018 1–25.

[110] Hummos A, Nair SS (2017) An integrative model of the intrinsic hippocampal theta rhythm, PLoS ONE 12(8): e0182648.

[111] Kim D, Samarth PS, Feng F, Pare D, Nair SS (2016) Synaptic competition in the lateral amygdala and the stimulus specificity of conditioned fear: A biophysical modeling study, Brain Structure & Function, 221:2163–2182.

[112] Carnevale NT, Hines ML (2006) The NEURON book (Cambridge UP, Cambridge, UK).

[113] Gratiy SL, Billeh YN, Dai K, Mitelut C, Feng D, Gouwens NW, Cain N, Koch C, et al. (2018), BioNet: A Python interface to NEURON for modeling large-scale networks. PLoS ONE 13:e0201630.

[114] Guntu V, Latimer B, Schulz DJ, Nair SS (2020), Modeling the neural circuit of lower urinary tract. (*In Preparation*)

FIGURES:

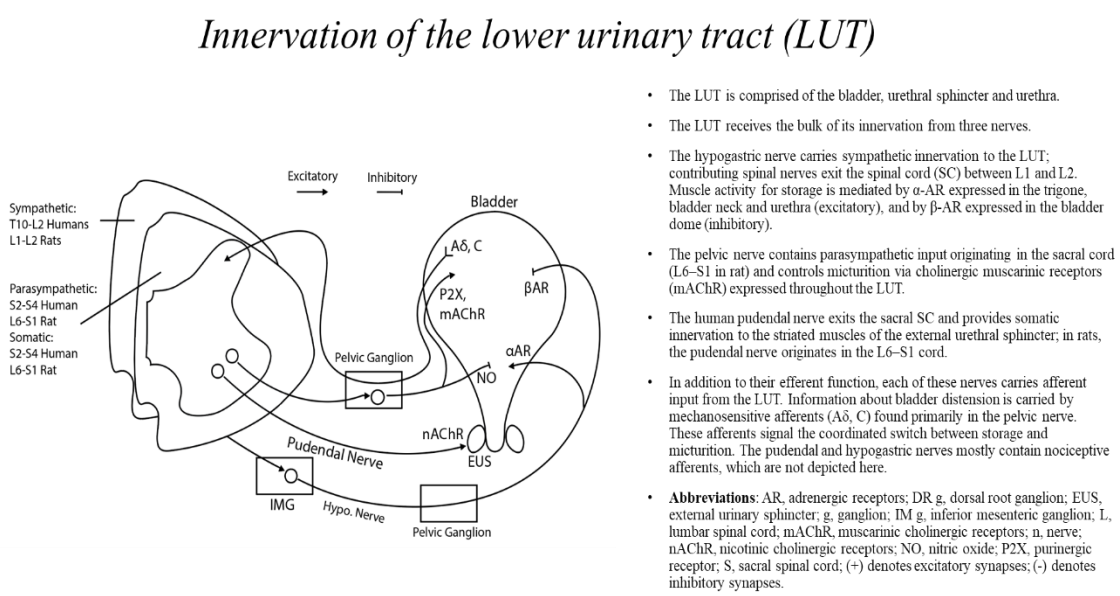

Figure 1: Consolidated biological figure of LUT innervation

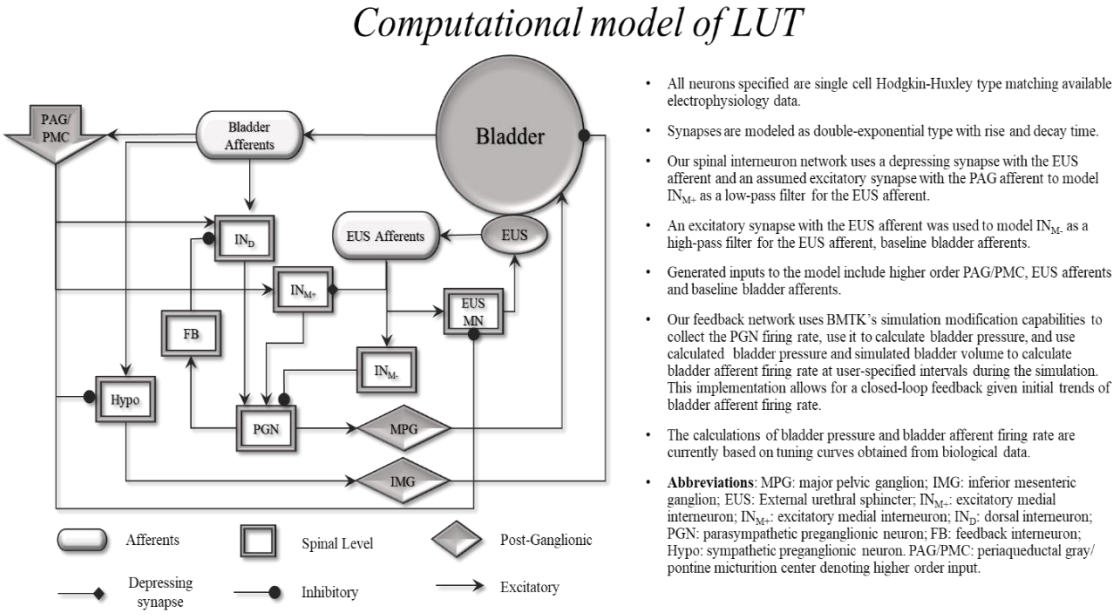

Figure2: Consolidated figure of LUT model

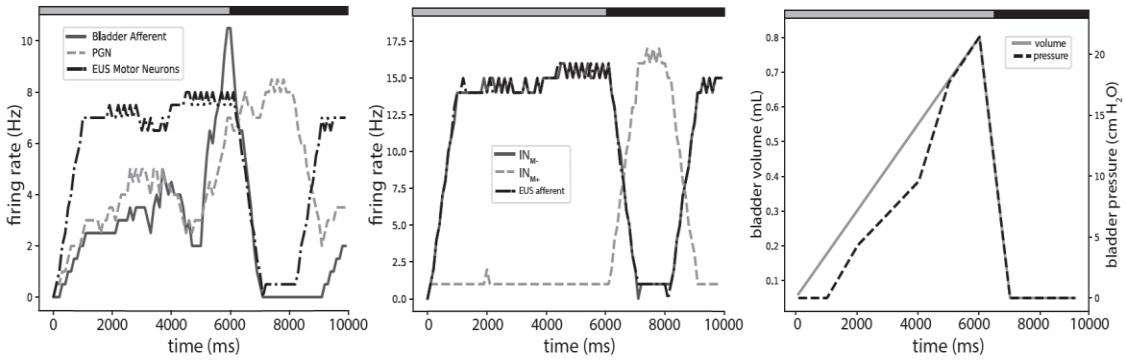

Figure 3: Filling vs Voiding in current biophysical model

(A) Firing rates of bladder afferents, preganglionic neurons (PGN) and EUs motor neurons; (B) Firing rates of medial interneurons (IN_{M+}, IN_{M-}) and EUS afferents; (C) Bladder volume and pressure profiles

TABLES:

Table 1: Electrophysiological properties of neurons in LUT circuit

Properties/ Neurons	V_{Rest} (mV)	Capacitance (pF)	R_{IN} (MΩ)	τ (msec)	Firing rate (Hz)
Bladder afferents [23][101]	-	-	-	-	0.06-40.4
EUS afferents [102]	-	-	-	-	1-65
IN_D [103]	-53.6 ± 2.54	-	822 ± 151	41.81 ± 5.4	21.83 ± 1.5
$IN_{M+/-}$ [104]	-60 ± 1	94.8 ± 7.9	270 ± 25	22 ± 1.5	-
FB	-	-	-	-	-
PGN [105]	-51.0 ± 1.1	26.5 ± 1.5	771.3 ± 70.7	-	-
HYPO [106]	-59.8 ± 7.4	32.8 ± 14.1	1140 ± 0.6	92.4 ± 43.7	-
MPG_T [16] [101]	-46.1 ± 1.64	28.9 ± 2.0	143.7 ± 14.0	4.0 ± 0.3	-
MPG_P [16] [101]	-47.4 ± 1.3	28.7 ± 2.3	157.2± 14.5	4.6 ± 0.5	-
IMG [9] [107]	-53.7 ± 2.45	-	83.0 ± 13.1	5.8 ± 1.4	-
EUS_{MN} [29]	-55.0 ± 8.0	-	11.1 ± 4.6	4.9 ± 1.5	-
PAG/PMC [108]	-	-	-	-	0-15

CHAPTER 3

MODELING THE NEURAL CIRCUIT OF LOWER URINARY TRACT

ABSTRACT

The rodent lower urinary tract (LUT, composed of the bladder and urethra) is used as a model system to study human LUT function and dysfunction. Studies of LUT dysfunction and their amelioration via stimulation are gaining importance due to increasing incidence of dysfunction of LUT including due to injury, e.g., spinal cord injury (SCI) and stroke, and increasing prevalence of conditions such as diabetes. Computational modeling provides an attractive complement to such studies by providing a tool to rapidly explore various hypotheses about both function and dysfunction, and to aid in the design and testing of closed-loop control strategies. We developed biophysical models of the cells in all major ganglia using information from the literature. Sensory bladder afferents are modeled presently using a regression fit with filling rate and bladder pressure. The closed-loop model reproduced the firing rates and bladder profiles in the normal fill and void cycle. The model also reproduced stimulation evoked contraction and inhibition with different frequencies of pudendal afferent stimulation and predicts intrinsic mechanisms that may underlie the observed behavior. Ongoing work focusses on providing insights into functioning of the guarding storage reflex and other reflexes responsible for non-voiding and voiding contractions.

INTRODUCTION

We provide a brief description of the LUT to illustrate what is being modeled, and then an overview of the mammalian LUT. The LUT contains two major segments, the bladder and the urethra. The bladder is composed of a smooth muscle chamber, denoted the body, and the neck, or posterior urethra, which serves to funnel urine into the urethra. At the base of the neck, a smooth muscle sphincter, the internal sphincter, prevents outflow to the urethra until a certain pressure is achieved. The urethra is a tube by which urine exits the bladder and flows to the exterior of the body. The structure of note in the urethra is the external urethral sphincter, which is a skeletal muscle sphincter, and the only voluntary component within the LUT. This sphincter allows conscious control over micturition and can be closed against fluid pressure by signal from the cortex (Hall JE and Guyton AC, 2011).

There are three main components to the neural anatomy of the LUT: sympathetic pathways, parasympathetic pathways, and the somatic pathways (Fowler CJ et al., 2008). These pathways have slightly differing functions in various studied mammals (rat/mouse, cat, human being the most common). Here, it is to be assumed to be for a mouse unless specified otherwise. The parasympathetic pathway constricts the bladder and relaxes the urethra; the sympathetic pathway does the opposite and inhibits the parasympathetic neurons near the bladder.

Sympathetic efferent neurons (located in the spinal cord, see below) innervate the body and neck of the bladder, and the urethra; these and the afferents (from bladder and

urethra) transmit via the hypogastric nerve. The urethral innervation is via the pelvic plexus. These attach to the spinal cord between T11 and L2, though primarily at L2, in lamina V-VII and X [1,2]. Two neuron types have been noted in the bladder and spinal ganglia, Aδ and C. The Aδ neurons are myelinated and carry tension information. C neurons tend to carry only noxious stimuli, though some small percentage may also carry mechanical information. Information is supplied via mechanoreceptors in the bladder wall that respond to tension as the bladder fills or voids. These neurons interface with the supraspinal micturition centers, namely the pontine micturition center, via spinal interneurons (Figure 4) (de Groat WC and Yoshimura N, 2009).

Parasympathetic efferent neurons (located as noted below) innervate the body and neck of the bladder and the urethra. The afferents relay volume and tension information from these structures via Aδ and C neurons similar to the sympathetic pathways, though there can be some variation in properties of these cells based on location, prompting further subclasses (Yoshimura N and Chancellor MB, 2003). The primary differences are between neurons arising in the body of the bladder and the urethra, the former utilizing stretch receptors and the latter being more sensitive to flow. These signals are transmitted via the pelvic nerve to L6 of the spinal column (lamina I, V-VII, and X), which forms a reflex arc back to the bladder to stimulate contraction (Figure 4).

The only somatic-LUT connection is to the external urethral sphincter (EUS) (Hall JE and Guyton AC, 2011). These motor neurons integrate via the pudendal nerve into the L6 regions of the spinal cord. Afferent pathways report on muscle activity and integrate with the parasympathetic reflex arc in the sacral spine, as well as sending information

to the supraspinal system, mainly integrating in Onuf's nucleus of laminia IX, though they notably interface with the parasympathetic system via dendritic extension in the areas noted in the parasympathetic section (de Groat WC and Yoshimura N, 2009;Fowler CJ,Griffiths D and de Groat WC, 2008)(Figure 4).

This section will present a broad overview of how the neurons of the LUT are believed to interact based on available data as well as how they regulate micturition.

The LUT can function without the sympathetic system, however, this causes lower sustainable bladder pressures before micturition is engaged. This leads to the conclusion that the sympathetic pathway serves to stabilize and inhibit the parasympathetic stimulation, as well as communicate information to the supraspinal centers, which in turn allows for better conscious control of micturition (de Groat WC and Yoshimura N, 2009). Sympathetic neurons from the bladder tend to be active even while empty, and those from the urethra only respond when under pressure (~>20mmHg). When active, they serve to relax the bladder wall and contract the urethral wall and EUS (the latter via spinal pathways).

Parasympathetic feedback loops drive the majority of LUT function. The Aδ neurons fire at higher frequency as bladder pressure increases (Mendez A et al., 2013). These signals, when combined with EUS pressure signals (and sympathetic feedback presented above) create a cycling feedback system where the pelvic nerve will periodically partially contract the bladder. Should the EUS not open, these contractions will absolve relatively quickly, in positive correlation to baseline bladder pressure (Hall

JE and Guyton AC, 2011).

The somatic portion of the LUT is the conscious control for micturition. As stated above, if the EUS does not open, the pudendal pressure sensors inhibit the pelvic centers in the sacral spine and stop micturition (Fowler CJ,Griffiths D and de Groat WC, 2008) At extreme levels of pressure, this is overridden by the parasympathetic spinal reflex arc. The motor neurons innervating the skeletal muscle of EUS are controlled by the supraspinal inputs.

We have chosen to divide the models in the literature into two categories: mechanical and neurological models. Mechanical models are more concerned with the bladder's urine output and simplify the neural component into some state-space relationship or strict differential equation relationship without processing. The neural models focus on creating some set of spiking neurons to reproduce effects measured experimentally.

The first computational models we found were developed in the 1970s, and were based on the dog bladder (Bastiaanssen EH et al., 1996;Drolet R and Kunov H, 1975). The model by Drolet and Kunov assumed the bladder to be a spherical collapsible tank with increasing pressure. They used recordings from stimulating female dogs' bladders to determine their feedback system with state space methods dependent on their measured motor neuron firing rates. This general approach remained throughout most of the modeling attempts. The model of the physical bladder was improved over time. Bastiaanssen et al. modeled the human bladder based on urine outflow data from patients, but further simplified their neural component to disregard firing rates, directly

converting pressures to muscular contraction via empirically determined state variables (Bastiaanssen EH,van Leeuwen JL,Vanderschoot J and Redert PA, 1996).

One of the earlier papers to attempt to model neural computation was done by Van Duin et al. where they created state-space transformations at each known neural ganglion by varying complexity (van Duin F et al., 2000;van Duin F et al., 1998). They added levels of neural components incrementally, then varied connectivity to include both excitatory and inhibitory connections. Though later research by de Groat's group showed some of their architecture to be incorrect, they were able to faithfully reproduce appropriate micturition patterns with varying levels of accuracy as they altered their model.

More recently several groups have taken a greater interest in faithfully modeling the neural side of micturition. Much of this has been devoted to determining the interactions between the supraspinal micturition centers (PMC/PAG, cortex, etc.) and the spinal ganglia or the interaction between the autonomic and somatic systems at the spinal level (de Groat WC et al., 2015;de Groat WC and Wickens C, 2013;McGee MJ and Grill WM, 2016). De Groat's group has focused on the former, while Grill's the latter. De Groat et al. created a model with simple monosynaptic weighed integration binary neurons in the spinal cord. Their supraspinal neurons were based on recordings taken from the PMC and PAG, as their overall goal was to understand the supraspinal switching circuitry's role in micturition (de Groat WC and Wickens C, 2013).

McGee et al. has developed an integrate-and-fire model of the lower urinary tract. Their primary research focuses on the pudendal neuron, and their model reflects this. They

have the most detailed model of spinal connectivity in the sacral spine; however, they ignore the sympathetic nervous system in their model. Their results centered on showing the depression of the micturition reflex – from the pudendal inputs (McGee MJ et al., 2014).

The present study. Our model builds on this previous work by using biologically realistic neurons to reproduce stimulation evoked contraction and inhibition of bladder depending on pudendal afferent stimulation. Experimentally it's been found that during bladder filling when stimulated with 33Hz pudendal afferent stimulation when volume is above 70% of volume required to trigger distension evoked contractions we can observe stimulation evoked contractions and after distention evoked contractions are triggered and pressure is high when we stimulate with 10Hz pudendal afferent stimulation we can inhibit the distension evoked contractions. We then investigate the mechanisms that might implement some of the reflexive loops, and the top-down control from supraspinal centers.

METHODS

The single cell and network models were developed using the parallel NEURON 7.4 simulator (Carnevale NT HM, 2009), and simulations were run with a fixed time step of 25 μs.

Mathematical equations for voltage-dependent ionic currents: The dynamics for soma followed the Hodgkin-Huxley formulation (Kim D et al., 2013) in eqn. 1,

$$C_m dV_s/dt = -g_L(V_s - E_L) - \sum I_{cur,s}^{int} - \sum I_{cur,s}^{syn} + I_{inj} \qquad (1)$$

where $I_{cur,s}^{int}$ and $I_{cur,s}^{syn}$ are the intrinsic and synaptic currents in the soma, I_{inj} is the electrode current applied to the soma, C_m is the membrane capacitance, g_L is the conductance of the leak channel. The intrinsic current $I_{cur,s}^{int}$, was modeled as $I_{cur,s}^{int} = g_{cur} m^p h^q (V_s - E_{cur})$, where g_{cur} is its maximal conductance, *m* its activation variable (with exponent *p*), *h* its inactivation variable (with exponent *q*), and E_{cur} its reversal potential (a similar equation is used for the synaptic current $I_{cur,s}^{syn}$ but without *m* and *h*). The kinetic equation for each of the gating variables *x* (*m* or *h*) takes the form

$$\frac{dx}{dt} = \frac{x_\infty\left(V,[Ca^{2+}]_i\right) - x}{\tau_x(V,[Ca^{2+}]_i)} \qquad (2)$$

where x_∞ is the steady state gating voltage- and/or Ca^{2+}- dependent gating variable and τ_x is the voltage- and/or Ca^{2+}- dependent time constant.

*Single cell models***:** We built single cells to represent neurons involved in parasympathetic, sympathetic and somatic pathways of LUT. Each of these cells were single compartment, as we could not find any data-based reason to use multiple compartments: these neurons are mostly transmitting signals straight though with some data compression at the ganglia. At postganglionic level we modeled MPG and IMG neurons, and both exhibit tonic and firing patterns. Tonic MPG neuron has Resting membrane potential (V_{Rest}): -45mV, Input resistance (R_{IN}): 145MΩ and time constant (τ): 4.6ms matching biological values (Jobling P and Lim R, 2008). IMG neuron was tuned to V_{Rest}: -54mV, R_{IN}: 82.7MΩ and τ: 5.5ms (Julé Y and Szurszewski JH, 1983).

At preganglionic level we have, parasympathetic preganglionic neuron (PGN): V_{Rest}: -51mV, R_{IN}: 772MΩ , Capacitance (C): 26.1pF and τ: 26.1ms which is known to exhibit both tonic and phasic firing patterns (Miura A et al., 2000) and sympathetic preganglionic neuron (HYPO): V_{Rest}: -58mV, R_{IN}: 1.15GΩ and τ: 94.6ms with tonic firing (Zimmerman A and Hochman S, 2010). At spinal level we have, dorsal interneuron (IN_D): V_{Rest}: -54mV, R_{IN}: 860MΩ and τ: 42.4ms and exhibit tonic firing with average spike frequency of 20Hz (Szûcs P et al., 2003), we use the same single cell to model excitatory medial interneuron(IN_{M+}), inhibitory medial interneuron (IN_{M-}): V_{Rest}: -60mV, R_{IN}: 286.6MΩ and τ: 20.8ms (Lu Y et al., 2001) and EUS motorneuron (EUS_{MN}): V_{Rest}: -55mV, R_{IN}: 11.1MΩ and τ: 4.9ms (Carp JS et al., 2010).

See figure 9 for firing properties of each neuron and tables 2-4 for equations of current kinetics and maximal densities.

Network size and cell type proportions: Estimates of number of neurons at each stage are not readily available. Number of neurons at each stage is as follows: PGN:25, EUS_{MN}:25, HYPO:25, IN_{M+}: 25, IN_{M-}: 25, IN_D: 25, IMG:250, MPG:250 and FB:25. the connection ratios between them are 1:10 between bladder afferents and IN_D & HYPO, 10:1 for PGN-MPG & HYPO-IMG and 1:1 for the rest. However, these numbers and connection ratios are varied for SNR tests. Connections between cells were generated randomly, based on the Gaussian probabilities.

Mathematical equations for synaptic currents: All excitatory transmission was mediated by AMPA/NMDA receptors, and inhibitory transmission by $GABA_A$

receptors. The corresponding synaptic currents were modeled by dual exponential functions (Destexhe A MZ, Sejnowski TJ, 1998) as shown in eqns. 3-5,

$$I_{AMPA} = w \times G_{AMPA} \times (V - E_{AMPA})$$

$$G_{AMPA} = g_{AMPA,max} \times F_{AMPA} \times r_{AMPA}$$

$$r_{AMPA}{}' = \alpha Tmax_{AMPA} \times ON_{AMPA} \times (1 - r_{AMPA}) - \beta_{AMPA} \times r_{AMPA} \quad (3)$$

$$I_{NMDA} = w \times G_{NMDA} \times (V - E_{NMDA})$$

$$G_{NMDA} = g_{NMDA,max} \times F_{NMDA} \times s(V) \times r_{NMDA}$$

$$r_{NMDA}{}' = \alpha Tmax_{NMDA} \times ON_{NMDA} \times (1 - r_{NMDA}) - \beta_{NMDA} \times r_{NMDA} \quad (4)$$

$$I_{GABAa} = w \times G_{GABAa} \times (V - E_{GABAa})$$

$$G_{GABAa} = g_{GABAa,max} \times F_{GABAa} \times r_{GABAa}$$

$$r_{GABAa}{}' = \alpha Tmax_{GABAa} \times ON_{GABAa} \times (1 - r_{GABAa}) - \beta_{GABAa} \times r_{GABAa} \quad (5)$$

where V is the membrane potential (mV) of the compartment (dendrite or soma) where the synapse is located, I is the current injected into the compartment (nA), G is the synaptic conductance (μS), w is the synaptic weight (unitless), and E is the reversal potential of the synapse (mV). $g_{x,max}$ is the maximal conductance (μS), F implements short term plasticity as defined in the next section, and r_x determines the synaptic current rise and decay time constants based on the terms $\alpha Tmax$ and β (Destexhe A MZ, Sejnowski TJ, 1998). The voltage-dependent variable $s(V)$ which implements the Mg^{2+} block was defined as $s(V) = [1 + 0.33 \exp(-0.06\ V)]^{-1}$ (Volo Md et al., 2019) The terms

ON_{NMDA} and ON_{AMPA} are set to 1 if the corresponding receptor is open, else to 0. Synaptic parameter values are listed in table 4 as mean ± std. For all connections, synaptic weight *w* was distributed log-normally with a cutoff of three times the mean to prevent non-physiological values.

Short-term presynaptic plasticity: Short-term depression was modeled at EUS afferent->IN_{M+} synapse. Short term plasticity was implemented as follows (Hummos A et al., 2014): For depression, the factor D was calculated using the equation: $\tau_D * \frac{dD}{dt} = 1 - D$ and *D* constrained to be ≤ 1. After each stimulus, *D* was multiplied by a constant d (≤ 1) representing the amount of depression per pre-synaptic action potential and updated as $D \rightarrow D * d$. Between stimuli, *D* recovered exponentially back toward 1. We modeled depression using two factors d_1 and d_2 with d_1 being fast and d_2 being slow subtypes, and $d = d_1 * d_2$. The parameters for modeling short-term plasticity are (τ_{D1} = 400msec, D1 = 0.5, τ_{D2} = 400msec, D2 = 0.5 and synaptic strength set to 0.5). Our model did not have long-term synaptic plasticity.

Implementation of feedback: Simulated bladder pressure (P_B) was recurrently calculated using functions of bladder volume at the previous time step and PGN output firing rate in a sliding window. (does not include IMG firing)

The PGN firing rate calculation was generated from a polynomial fit of prior experimental results in cats (Sasaki 1998).

$$PB(t) = f(\int_{t-wl}^{t-1} FRPGN(t)dt + f(VolB(t-1)) \quad (6)$$

Where,

$$f(FR\text{PGN}) = 2x10^{-3}FR\text{PGN}^3 - 3.3x10^{-2}FR\text{PGN}^2 + 1.8FR\text{PGN} - 0.5 \quad (7)$$

Model is using the following equation to simulate bladder filling:

$$v(t) = v(0) + fill * spk * scale\_factor \quad (8)$$

v(t): current volume of bladder, v(0): initial volume of bladder (0.05 ml) , fill: bladder fill rate (assumed constant: 0.05 ml/min), spk: current time in simulation, scale_factor: because we are working in a short period (10,000 ms) we need to scale the biological values we are using so that the filling/voiding cycle can fit in the shorter time frame (150), scaled to units of ml/ms for model 1/(1000*60)

Model is using the following equation to simulate bladder voiding

$$v(t) = v(t - 1) - void * spk \quad (9)$$

v(t): current volume of bladder, v(t – 1): previous volume of bladder, void: bladder void rate (assumed constant: 4.6 ml/min (Streng T et al., 2002) and voiding should be about 100x faster than filling), spk: current time in simulation There is a maximum bladder volume of 0.76 ml being used as a guide for ending voiding.

Pelvic afferent firing rate (Sengupta JN and Gebhart GF, 1994)

$$FR\text{Pel}(t) = f\big(P\text{B}(t-1)\big)$$

$$= 3x10^{-8}P\text{B}^5 + 1x10^{-5}P\text{B}^4 - 1.5x\,10^{-3}P\text{B}^3 + 7.9x\,10^{-2}P\text{B}^2 - 0.6P\text{B} \quad (10)$$

Within the existing bladder feedback loop, we have added a connection between the EUS afferent firing rate and bladder pressure assumed to exist based on literature (Livingston BP, 2016)

$$\text{If, } \Delta P\text{B} = P\text{B}(t) - P\text{B}(t-1) > 10\ cm\ H_20$$

EUS afferent neurons are set to fire at a rate given by the following equation

$$FR\text{EUS} = constant1 * P\text{B}(t) + constant2 * \Delta P\text{B} \quad (11)$$

Inputs to the model:

Current high firing rate for EUS, PAG afferent used in model is 15 Hz. Documented in literature as high firing rate for PAG (Blok BF and Holstege G, 2000). Current low firing rate for EUS, PAG afferent used in model is 1 Hz. Documented in literature as basal firing rate of pudendal (EUS) afferent (Habler HJ et al., 1993).

RESULTS

The biophysical model included all reported details about the neural LUT circuit. The model was used to investigate both normal and abnormal functioning of the circuit, including how they affect the storage and voiding reflexes.

Biologically realistic model of LUT

The model successfully reproduces the firing rate and pressure profiles during filling and voiding cycles (Figure 5-6) with insights into reflexes involved in each stage. We

implement a feedback mechanism in the model based on (McGee MJ and Grill WM, 2016) where, the parasympathetic efferent firing rate is used to recurrently calculate pressure at constant rate bladder filling and the pressure calculated is used to estimate bladder afferent firing rate . The estimated bladder afferent firing rate is fed back into the model. We used synaptic depression to model documented connection between EUS afferent and $IN_{M}+$ (Roppolo JR et al., 1985;Thor KB et al., 1989). Synaptic depression can be used to model a low-pass filter so that a post-synaptic neuron will only fire when the pre-synaptic neuron is firing low. According to the functional role of IN_{M+} , this excitatory interneuron should fire high when EUS afferent firing is low and vice-versa. We modeled this using a depressive synapse between the EUS afferent and IN_{M+} and a normal excitatory synaptic between the PAG input and IN_{M+}

Insights related to storage reflex

When a small amount of urine enters the urethra without conscious voiding control from the cortex, the bladder pressure increases, causing a contraction in the EUS (Park JM et al., 1997). This EUS contraction is modeled by an increase in the EUS motor neurons firing. We are assuming that the guarding reflex depends on bladder pressure and results in brief increases in the EUS afferent firing rate. To implement this in our model, we used a feedback loop modification (See Methods). The steps involved are 1) measure firing rate of the PGN. 2) Uses this firing rate to calculate bladder pressure. 3) Detects when bladder pressure is spiking (sharp increase). 4) At each spike, a corresponding spike in the EUS motor neurons firing rate is generated. The results are reported in (Fig 2) we can clearly see the result of these fluctuations in EUS motor neuron firing.

Distension evoked contractions (DECs)

To further study the role of each reflex involved in the LUT circuit we identified and studied the sub-circuits involved. Example, parasympathetic pathway is mostly involved in micturition reflex and is mostly silent during filling process. Bladder is filled at constant rate from low volume to all the way beyond the maximum volume needed to evoke distention evoked contractions. The sub-circuit involved and the bladder response are shown in figure 7. The spinal neurons involved in this reflex are dorsal interneuron (IN_D) which receives excitation from bladder afferents and supraspinal input from PAG/PMC, PGN which are the primary pre-ganglionic neurons located in sacral parasympathetic nucleus (SPN) in lumbosacral cord. At postganglionic level we have major pelvic ganglion (MPG) which are known to have some filtering properties but mostly relay excitation to detrusor muscle. When bladder afferents fire higher than 10Hz PAG/PMC switches ON and provides an excitation of 15Hz to IN_D and is required to produce DECs. The network connections, synaptic properties and single neuron electrophysiological properties produce the observed bladder pressure profile.

Stimulation evoked contractions (SECs)

We expanded on the sub-circuit which produced the DECs to include pudendal stimulation effects, this include two spinal interneurons located medially and provide excitation and inhibition to PGN. These medial interneurons play a key role in producing pudendal stimulation based contraction and inhibition (SEI). Only SEC case is shown here and SEI will be explored in future work. Pudendal afferents which are disconnected

from bladder and EUS feedback are artificially stimulated with 33Hz input. These afferents in this case provide excitation to IN_D also which is a converging point for bladder afferents, supraspinal input and pudendal stimulation. The sub-circuit and the bladder profiles showing SECs are shown in figure 8. We show the volume dependence of the contractions produced by pudendal stimulation, when 33Hz pudendal stimulation is give at 45% max volume the contractions produced are not at the level produced during DECs. However when pudendal stimulation is provided at or above 70% max volume the circuit produces robust contractions thus highlighting the volume dependence of this pudendal initiated reflex.

DISCUSSION

We developed a biophysical network model of the mammalian neural circuits mediating the storage and micturition reflexes. The model includes afferent firing rate generation, spinal network model and also incorporates post ganglionic level processing. The model is constrained to fit firing rates of neurons involved and show how guarding reflex can be implemented. The model also provides an ideal framework to study several aspects of information theory such as signal-to-noise ratio, signal filtering and robustness of the network.

CONCLUSION AND FUTURE WORK

Models provide an ideal framework to provide insights into functional roles of different cells, connectivity, synapses in reflexes of LUT. Important aspects such as SNR, filtering properties of different stages can be studied with ease. Model can be easily adapted to include SCI related physiological changes and to test out hypothesis which can help in understanding possible therapeutic targets to restore normal function.

Future work:

a) What's needed to make this model more biologically realistic. Continue adding biological values to model.
b) Expand PAG model: There exists a circuit for an extended model of the higher-level neurons involved in micturition (Zare, et al. 2019). Apply this to the current model and observe its effects on the output.

SCI Injury/ dysfunctions and how circuit goes to reflex mode?

1. ***Reflex mode operation***: We introduced an interneuron which receives input from (1) bladder afferents (2) EUS afferents and inhibits EUS motorneuron to test out involuntary reflex. This could also be the urinary incontinence case. In this case PAG/PMC input is set to 0. This is to show EUS relaxation during reflex contraction of bladder.
2. ***de Groats hypothesis*** (Organization of parasympathetic excitatory reflex pathway) : To see the effects of high threshold C-fibers after spinal transection, change the afferent firing rate set to (0.9±0.4 Hz at rest; 34±2.5 Hz at Vol_{thres};

13.3±3.0 Hz at 80mmHg and 17.4±3.3 Hz at 100mmHg) if there is a tuning curve with P_B to c-fiber firing rate we should use that.

Biology: After SCI at or above lumbosacral level eliminates voluntary supraspinal control of voiding, leading initially to an loss of coordination between bladder and EUS with complete urinary retention, followed by spinal micturition take over and neurogenic detrusor overactivity (NDO) that is mediated by spinal reflex pathways (de Groat WC and Yoshimura N, 2006). However, voiding is commonly inefficient causing detrusor–sphincter dyssynergia.

In cats when supraspinal influence is removed by spinal lesions, a segmental sacral spinal reflex emerges that drives reflex bladder contractions and is mediated by capsaicin-sensitive C-fiber afferents. This causes reflex detrusor contractions in response to low-volume filling and is responsible for NDO in experimental models (de Groat WC et al., 1990). The emergence of C-fibre bladder reflexes seems to be mediated by several mechanisms, including changes in central synaptic connections and alterations in the properties of the peripheral afferent receptors that lead to sensitization of the ‘silent’ C-fibres and the unmasking of responses to mechanical stimuli (de Groat WC,Kawatani M,Hisamitsu T,Cheng CL,Ma CP,Thor K,Steers W and Roppolo JR, 1990) (de Groat WC, 1995)

REFERENCES

Bastiaanssen EH, van Leeuwen JL, Vanderschoot J, Redert PA (1996), A myocybernetic model of the lower urinary tract. J Theor Biol 178:113-133.

Blok BF, Holstege G (2000), The pontine micturition center in rat receives direct lumbosacral input. An ultrastructural study. Neurosci Lett 282:29-32.

Carnevale NT HM (2009), The NEURON Book. Cambridge University Press.

Carp JS, Tennissen AM, Liebschutz JE, Chen XY, Wolpaw JR (2010), External urethral sphincter motoneuron properties in adult female rats studied in vitro. J Neurophysiol 104:1286-1300.

de Groat WC (1995), Mechanisms underlying the recovery of lower urinary tract function following spinal cord injury. Paraplegia 33:493.

de Groat WC, Griffiths D, Yoshimura N (2015), Neural control of the lower urinary tract. Compr Physiol 5:327-396.

de Groat WC, Kawatani M, Hisamitsu T, Cheng CL, Ma CP, Thor K, Steers W, Roppolo JR (1990), Mechanisms underlying the recovery of urinary bladder function following spinal cord injury. J Auton Nerv Syst 30 Suppl:S71-77.

de Groat WC, Wickens C (2013), Organization of the neural switching circuitry underlying reflex micturition. Acta Physiol (Oxf) 207:66-84.

de Groat WC, Yoshimura N (2006), Mechanisms underlying the recovery of lower urinary tract function following spinal cord injury. Prog Brain Res 152:59-84.

de Groat WC, Yoshimura N (2009), Afferent nerve regulation of bladder function in health and disease. Handb Exp Pharmacol:91-138.

Destexhe A MZ, Sejnowski TJ (1998), Kinetic models of synaptic transmission. Methods Neuronal Model 2:1-25.

Drolet R, Kunov H (1975), On the peripheral bladder control system of the dog and urodynamics: in vivo characterisation and hybrid computer simulation. Med Biol Eng 13:40-55.

Fowler CJ, Griffiths D, de Groat WC (2008), The neural control of micturition. Nat Rev Neurosci 9:453-466.

Habler HJ, Janig W, Koltzenburg M (1993), Receptive properties of myelinated primary afferents innervating the inflamed urinary bladder of the cat. J Neurophysiol 69:395-405.

Hummos A, Franklin Charles C, Nair Satish S (2014), Intrinsic mechanisms stabilize encoding and retrieval circuits differentially in a hippocampal network model. Hippocampus 24:1430-1448.

Jobling P, Lim R (2008), Anatomical and physiological properties of pelvic ganglion neurons in female mice. Auton Neurosci 140:30-39.

Julé Y, Szurszewski JH (1983), Electrophysiology of neurones of the inferior mesenteric ganglion of the cat. J Physiol 344:277-292.

Kim D, Pare D, Nair SS (2013), Assignment of model amygdala neurons to the fear memory trace depends on competitive synaptic interactions. J Neurosci 33:14354-14358.

Livingston BP (2016), Anatomy and Neural Control of the Lower Urinary Tract and Pelvic Floor. Topics in Geriatric Rehabilitation 32:280-294.

Lu Y, Inokuchi H, McLachlan EM, Li J-S, Higashi H (2001), Correlation between electrophysiology and morphology of three groups of neuron in the dorsal commissural nucleus of lumbosacral spinal cord of mature rats studied in vitro. J Comp Neurol 437:156-169.

McGee MJ, Danziger ZC, Bamford JA, Grill WM (2014), A spinal GABAergic mechanism is necessary for bladder inhibition by pudendal afferent stimulation. American Journal of Physiology-Renal Physiology 307:F921-F930.

McGee MJ, Grill WM (2016), Modeling the spinal pudendo-vesical reflex for bladder control by pudendal afferent stimulation. J Comput Neurosci 40:283-296.

Mendez A, Sawan M, Minagawa T, Wyndaele JJ (2013), Estimation of bladder volume from afferent neural activity. IEEE Trans Neural Syst Rehabil Eng 21:704-715.

Miura A, Kawatani M, Araki I, de Groat WC (2000), Electrophysiological properties of lumbosacral preganglionic neurons in the neonatal rat spinal cord. Brain Res 872:54-63.

Park JM, Bloom DA, McGuire EJ (1997), The guarding reflex revisited. Br J Urol 80:940-945.

Roppolo JR, Nadelhaft I, de Groat WC (1985), The organization of pudendal motoneurons and primary afferent projections in the spinal cord of the rhesus monkey revealed by horseradish peroxidase. J Comp Neurol 234:475-488.

Sengupta JN, Gebhart GF (1994), Mechanosensitive properties of pelvic nerve afferent fibers innervating the urinary bladder of the rat. J Neurophysiol 72:2420-2430.

Streng T, Santti R, Talo A (2002), Similarities and differences in female and male rat voiding. Neurourol Urodyn 21:136-141.

Szûcs P, Odeh F, Szokol K, Antal M (2003), Neurons with distinctive firing patterns, morphology and distribution in laminae V-VII of the neonatal rat lumbar spinal cord. Eur J Neurosci 17:537-544.

Thor KB, Morgan C, Nadelhaft I, Houston M, De Groat WC (1989), Organization of afferent and efferent pathways in the pudendal nerve of the female cat. J Comp Neurol 288:263-279.

van Duin F, Rosier PF, Bemelmans BL, Wijkstra H, Debruyne FM, van Oosterom A (2000), Comparison of different computer models of the neural control system of the lower urinary tract. Neurourol Urodyn 19:289-310.

van Duin F, Rosier PF, Rijkhoff NJ, van Kerrebroek PE, Debruyne FM, Wijkstra H (1998), A computer model of the neural control of the lower urinary tract. Neurourol Urodyn 17:175-196.

Volo Md, Romagnoni A, Capone C, Destexhe A (2019), Biologically Realistic Mean-Field Models of Conductance-Based Networks of Spiking Neurons with Adaptation. Neural Comput 31:653-680.

Yoshimura N, Chancellor MB (2003), Neurophysiology of Lower Urinary Tract Function and Dysfunction. Reviews in Urology 5:S3-S10.

Zimmerman A, Hochman S (2010), Heterogeneity of membrane properties in sympathetic preganglionic neurons of neonatal mice: evidence of four subpopulations in the intermediolateral nucleus. J Neurophysiol 103:490-498.

FIGURES:

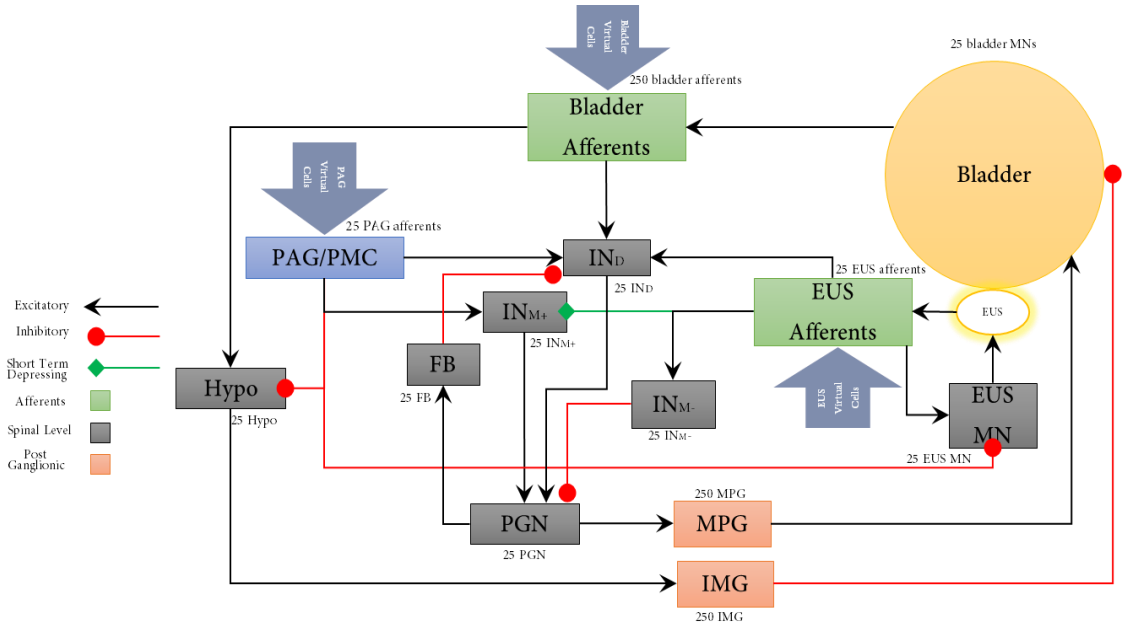

Figure 4: Proposed model of mouse LUT modeled

Abbreviations*: MPG: major pelvic ganglion; IMG: inferior mesenteric ganglion; EUS: External urethral sphincter;* IN_{M+}*: excitatory medial interneuron;* IN_{M+}*: excitatory medial interneuron;* IN_D*: dorsal interneuron; PGN: parasympathetic preganglionic neuron; FB: feedback interneuron; Hypo: sympathetic preganglionic neuron. PAG/PMC: periaqueductal gray/ pontine micturition center denoting higher order input.*

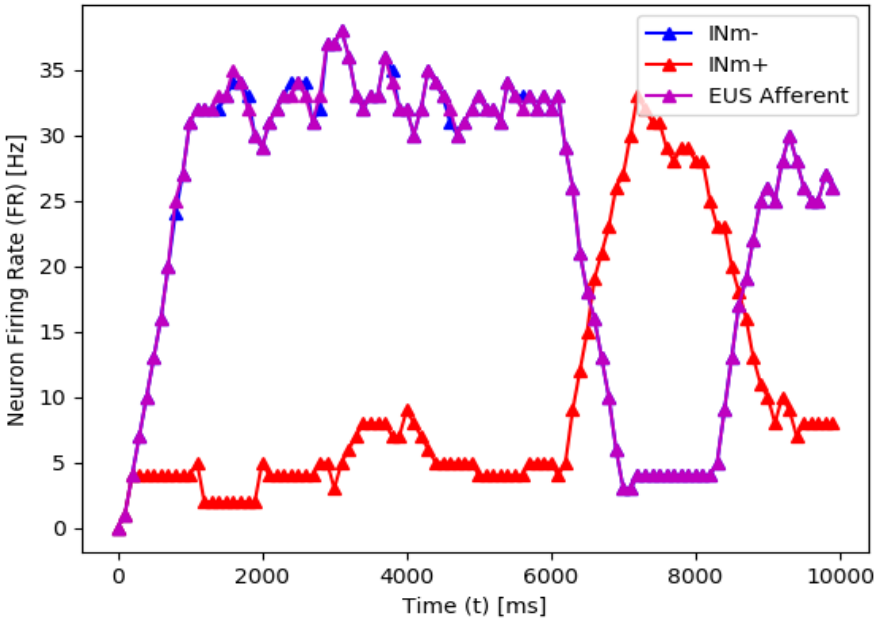

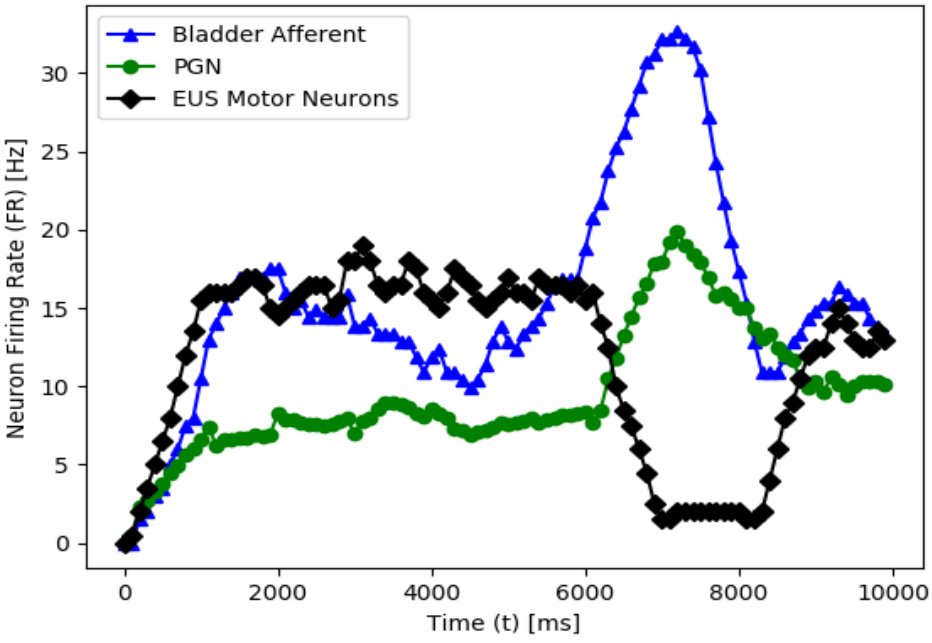

Figure 5: Firing rates of model neurons during filling and voiding

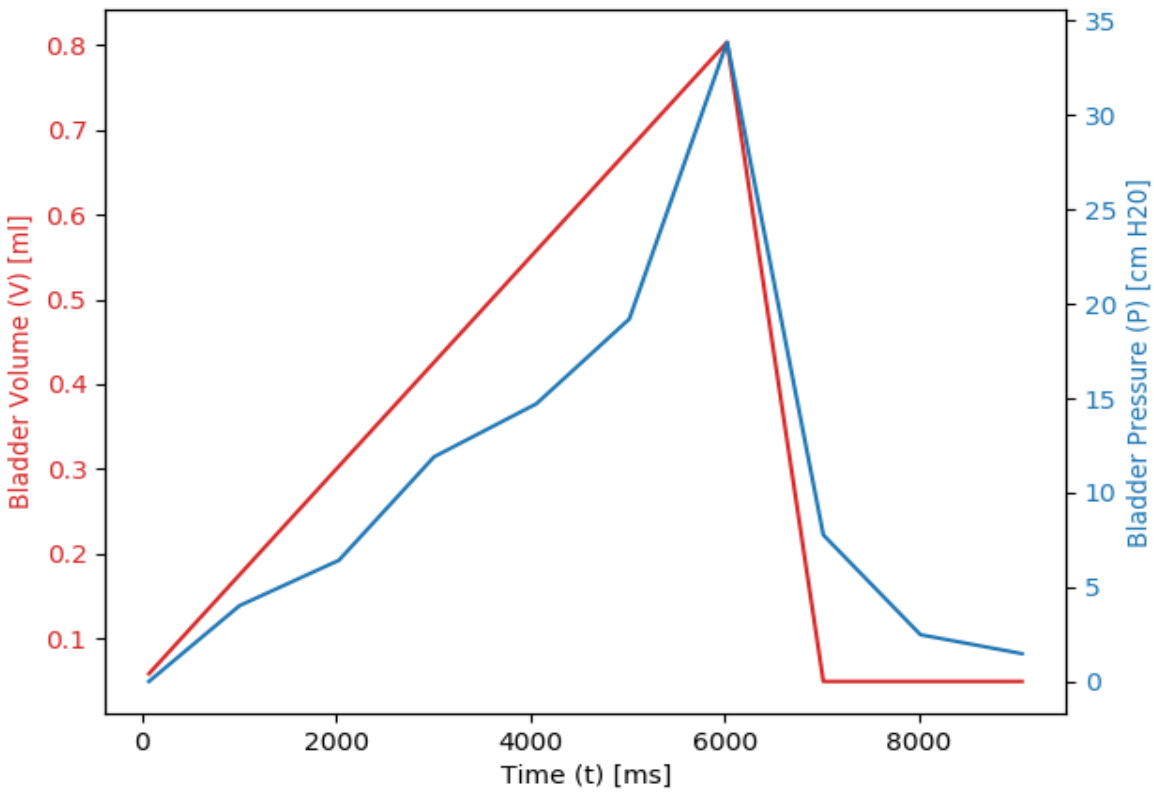

Figure 6: Constant rate filling of bladder with pressure profile

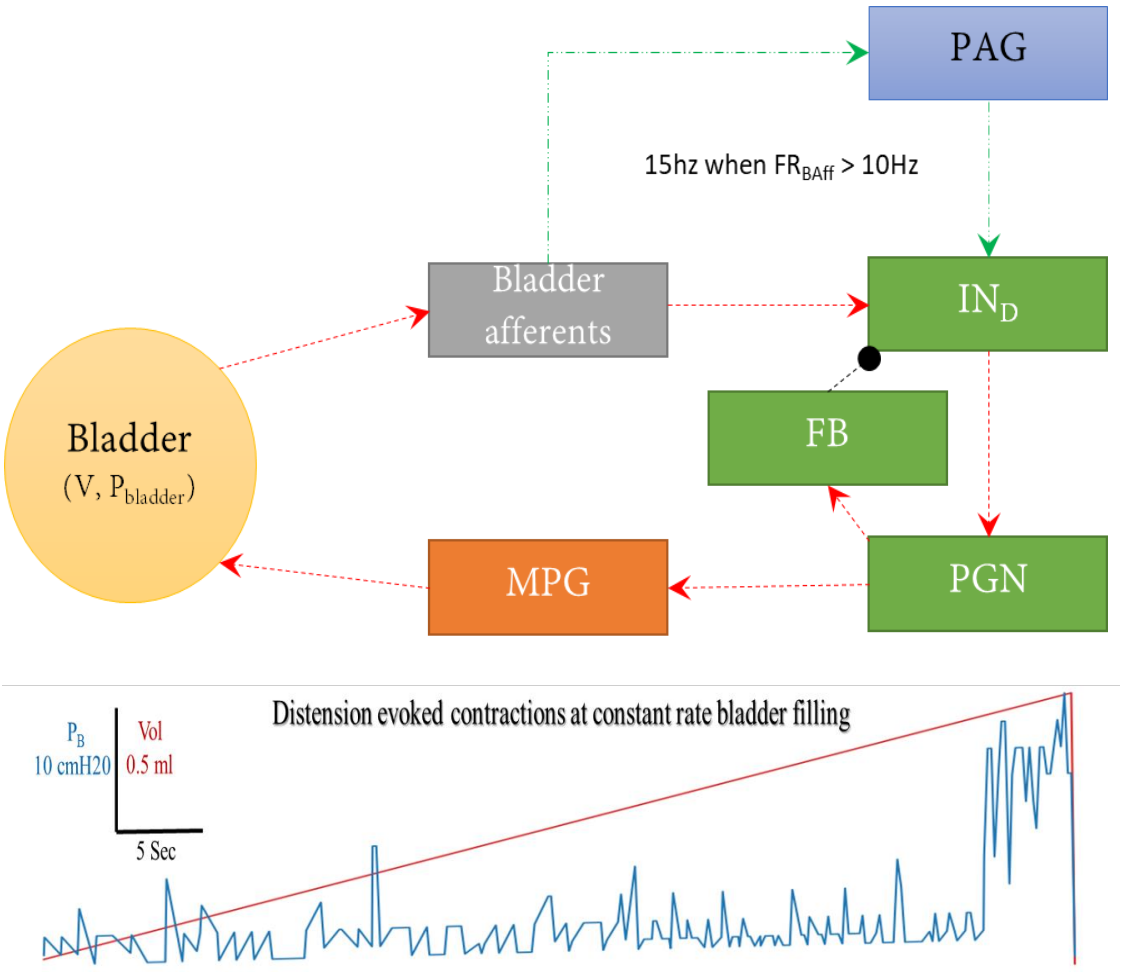

Figure 7: Parasympathetic sub-circuit with DECs

(above) Sub circuit highlighting parasympathetic pathway which is responsible for micturition reflex, (below) figure shows constant rate volume fill from 0%-150% max volume (1.05ml). Supraspinal input from PAG is turned ON when bladder afferent rate goes above 10Hz and it fires at 15Hz providing descending excitation to PGN vis IN_D to produce distension evoked contractions (DECs) which results in rapid rise in bladder pressure (P_B) and in turn help facilitate micturition.

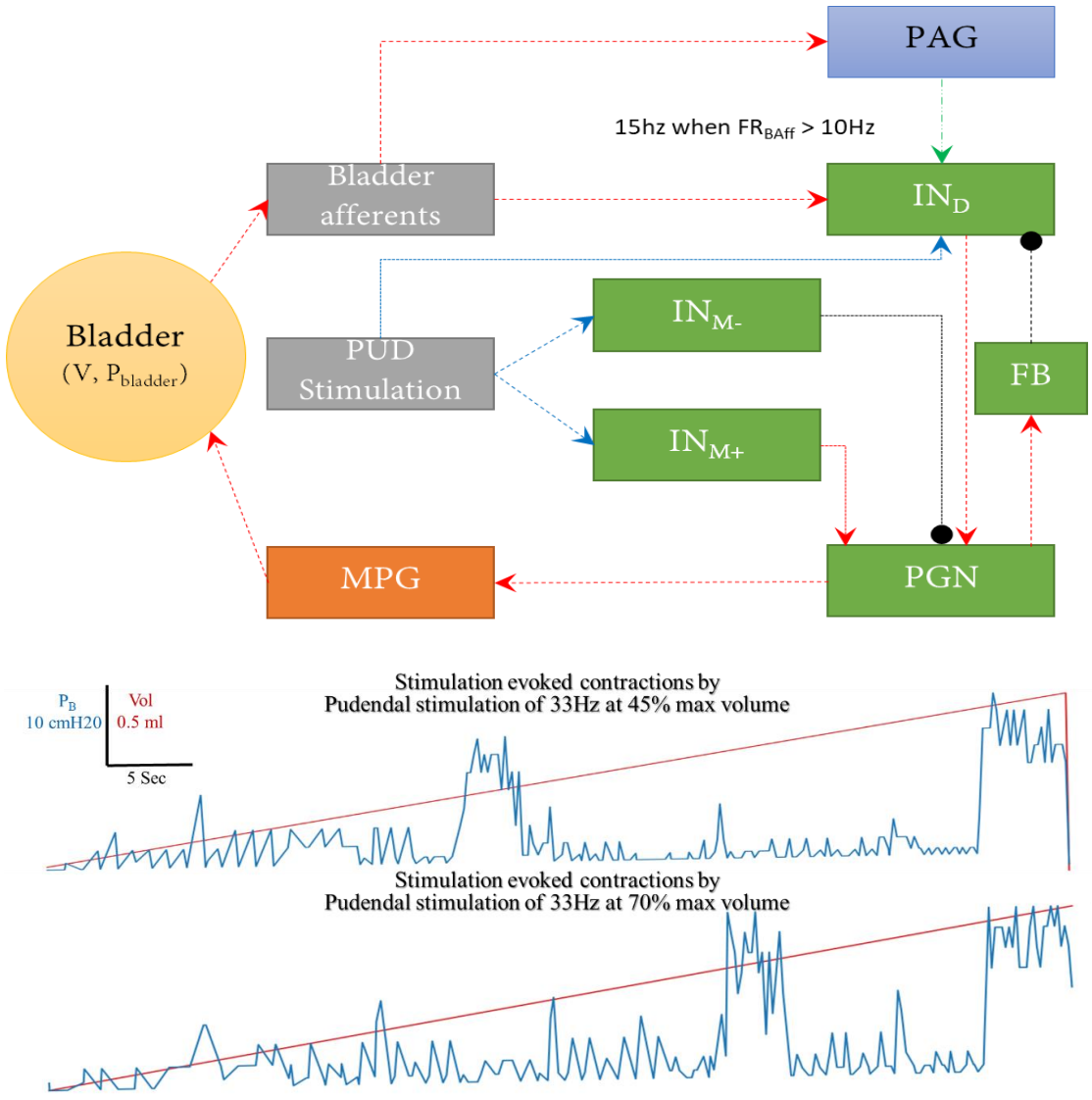

Figure 8: LUT sub-circuit with pudendal stimulation

(below) Pudendal stimulation at 33Hz can evoke simulation evoked contractions (SECs) but are dependent on volume since 33Hz provided when volume is at 45% max volume doesn't elicit contractions at same level as DECs but at 70% max volume SECs are at same pressure level as DECs which shows heavy volume dependency of SECs and the suggests a role of convergence of inputs from bladder afferents and pudendal afferents.

Figure 9: Models for Individual Cells

Tonic MPG neuron	
Current injection plots (Biology)	Matching current injection plots (Model)
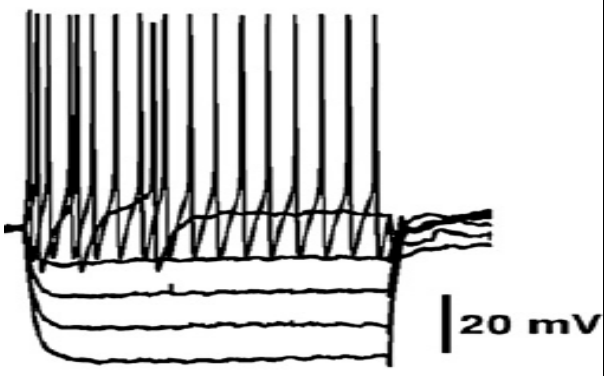	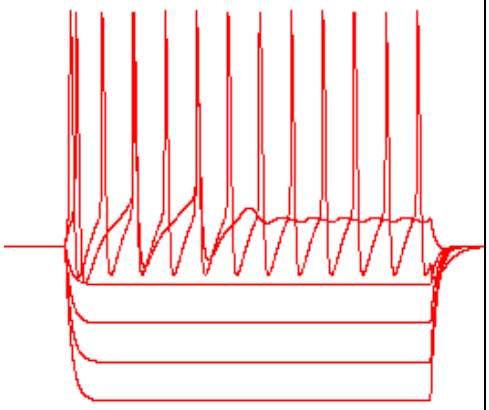

Responses to current injections of [-0.4,-0.3,-0.2,-0.1,0.1,0.2] nA with 250 ms duration.

Phasic MPG neuron	
Current injection plots (Biology)	Matching current injection plots (Model)
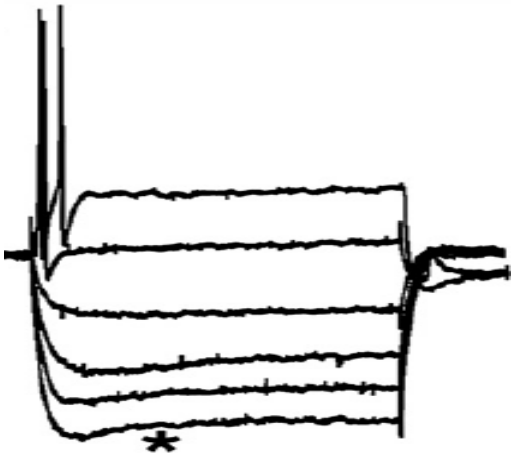	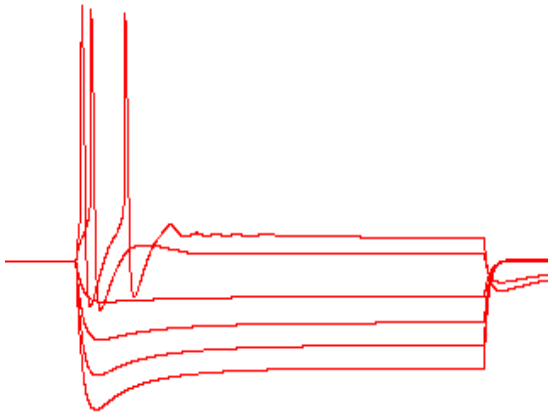

Responses to current injections of [-0.4,-0.3,-0.2,-0.1,0.1,0.2] nA with 250 ms duration.

Sympathetic postganglionic neuron (IMG) phasic	
Current injection plots (Biology)	Matching current injection plots (Model)
	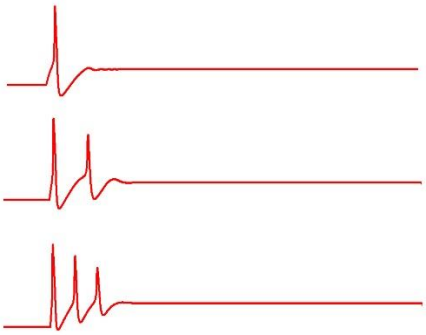

Responses to current injections of [0.5,1,2] nA with 750 ms duration.

Tonic PGN neuron	
Current injection plots (Biology)	Matching current injection plots (Model)
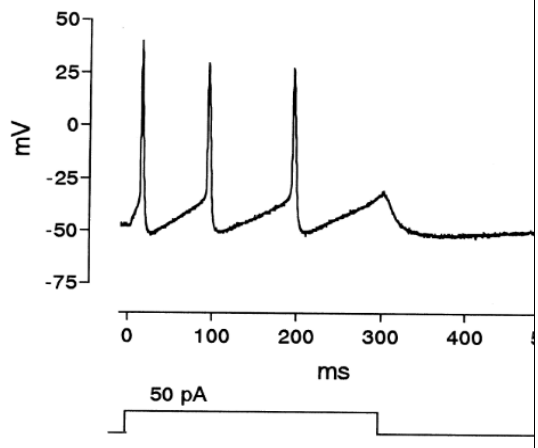	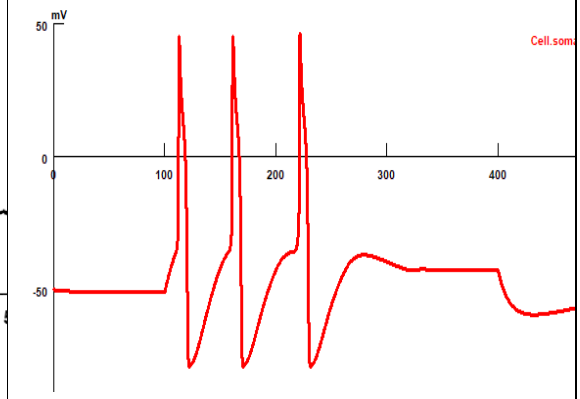

*Model follows trend of increased number of spikes with increased current injection consistent with biology (Data not shown)

Phasic PGN neuron	
Current injection plots (Biology)	Matching current injection plots (Model)
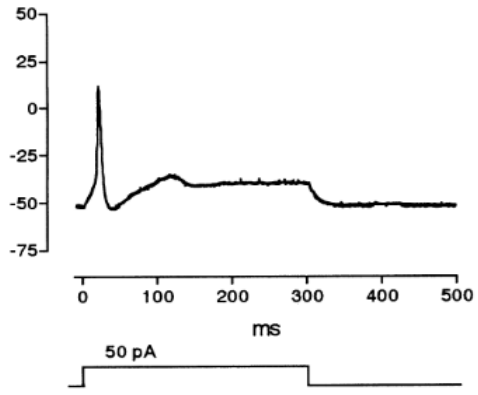	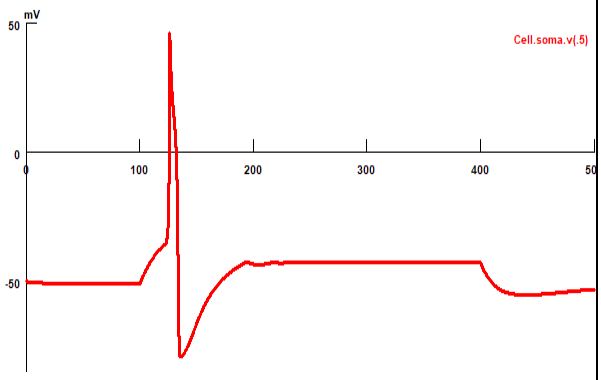

*Model gives 1 spike for current injections from 30pA – 120pA consistent with biology

Sympathetic preganglionic neuron (Hypo)	
Current injection plots (Biology)	Matching current injection plots (Model)
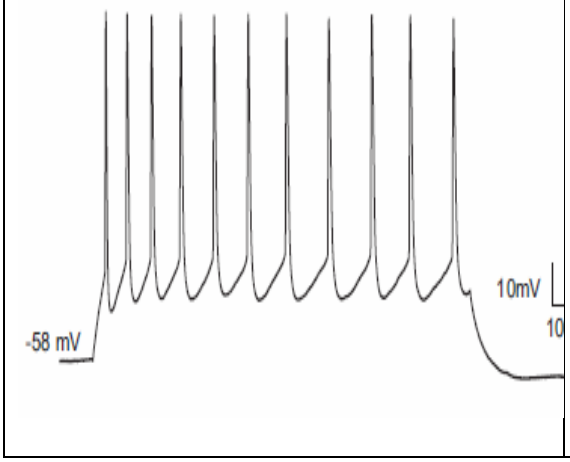	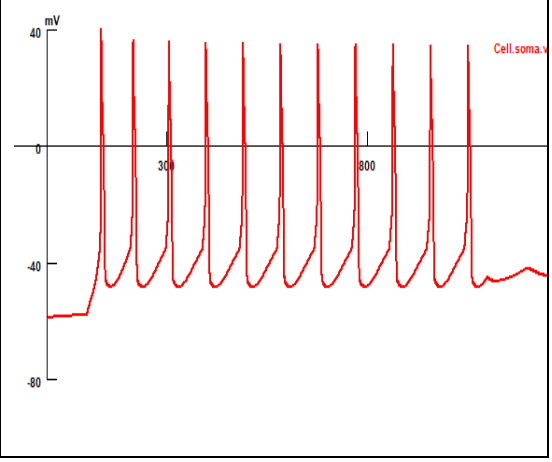

Responses to current injection of 20pA for 1s duration

Dorsal interneuron (IN_D)	
Current injection plots (Biology)	Matching current injection plots (Model)
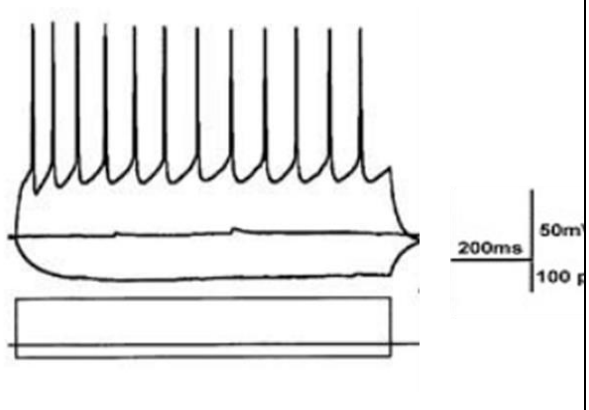	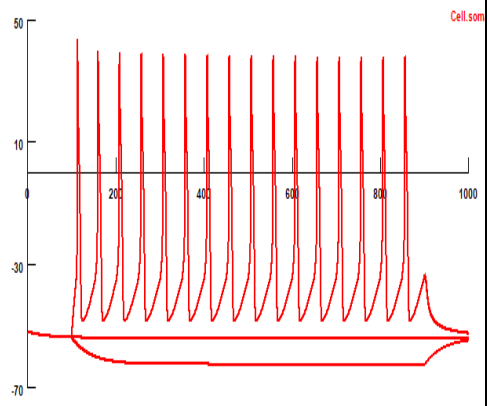

Responses to current injection of [-10, 0, 100] pA for 800 ms duration

Medial interneuron (IN_{M+} & IN_{M-})	
Current injection plots (Biology)	Matching current injection plots (Model)
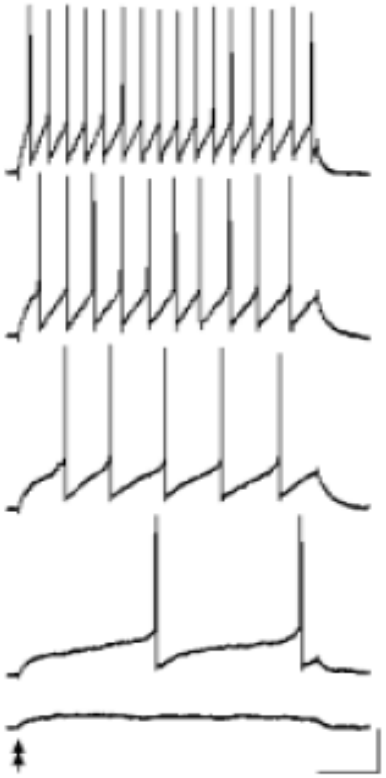	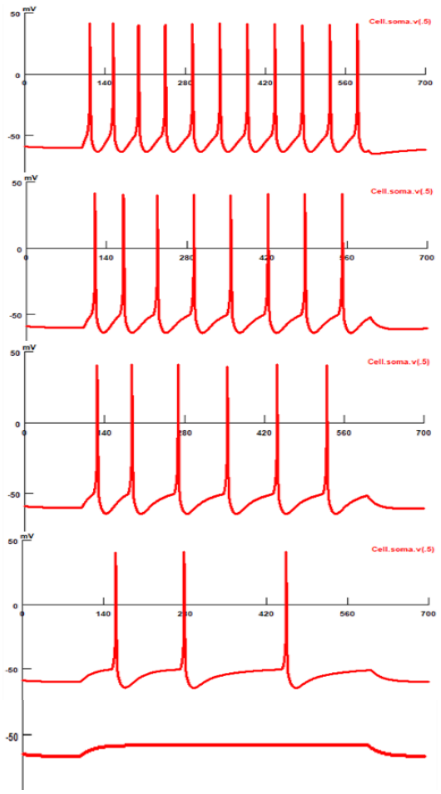

Responses to current injection of [109, 72, 54, 36, 18] pA for 500 ms duration; scale bar left 20mV, 100ms

TABLES:

Table 2: Passive properties of neurons in LUT circuit

Cell	Passive properties	RMP (mV)	R_{in} (MΩ)	τ (ms)	C (pF)
MPG	*Biology*	-46.1 ± 1.64	143.7 ± 14.0	4.0 ± 0.3	-
	Model	-45	145	4.6	-
IMG	*Biology*	-53.7 ± 2.45	83.0 ± 13.1	5.8 ± 1.4	-
	Model	-54	82.7	5.5	-
PGN	*Biology*	-51.0 ± 1.1	771.3 ± 70.7	20.4	26.5 ± 1.5
	Model	-51	772	20.2	26.1
HYPO	*Biology*	-59.8 ± 7.4	1.14 ± 0.6	92.4 ± 43.7	-
	Model	-58	1.148	94.6	-
IN_D	*Biology*	-53.6 ± 2.54	822 ± 151	41.81 ± 5.4	-
	Model	-54	860	42.4	-
$IN_{M\pm}$	*Biology*	-60 ± 1	270 ± 25	22 ± 1.5	-
	Model	-60	286.6	20.8	-

Table 3: Gating parameters of ion channels

Current Type	Gating Variable	α	β	x_∞	τ_x (ms)
I_{Na}[1]	*p=3*	$\frac{-0.4(V+30)}{\exp[-(V+30)/7.2]-1}$	$\frac{0.124(V+30)}{\exp[(V+30)/7.2]-1}$	$\frac{\alpha}{\alpha+\beta}$	$\frac{0.6156}{\alpha+\beta}$
	q=1	$\frac{-0.03(V+45)}{\exp[-(V+45)/1.5]-1}$	$\frac{0.01(V+45)}{\exp[(V+45)/1.5]-1}$	$\frac{1}{\exp[(V+50)/4]+1}$	$\frac{0.6156}{\alpha+\beta}$
I_{Kdr}[1]	*p=1*	$\exp[-0.1144(V+15)]$	$\exp[-0.0801(V+15)]$	$\frac{1}{\exp[(-V-15)/11]+}$	$\frac{50*\beta}{1+\alpha}$
I_H[2]	*q=1*	$\exp[0.0832(V+75)]$	$\exp[0.0333(V+75)]$	$\frac{1}{\exp[(V+81)/8]+1}$	$\frac{\beta}{0.0081(1+\alpha)}$
I_{KM}[3]	*p=2*	$\frac{0.016}{\exp[-(V+52.7)/23]}$	$\frac{0.016}{\exp[(V+52.7)/18.8]}$	$\frac{1}{\exp[(-V-52.7)/10.3}$	$\frac{1}{\alpha+\beta}$
I_{Ca}[3]	*p=2*	—	—	$\frac{1}{\exp[(-V-30)/11]+}$	$\frac{2.5}{\exp\left[\frac{-(V+37.1)}{32.3}\right]+e}$
	q=1	—	—	$\frac{1}{\exp[(V+12.6)/18.9]}$	420
I_{Nap}[4]	*p=1*	—	—	$\frac{1}{\exp[(-V-48)/5]+1}$	$2.5+14$ $*\exp[-\lvert V+40\rvert$
I_{sAHP}[3]	*p=1*	$\frac{0.0048}{\exp[-5\log_{10}([Ca]_{i2})-17.5]}$	$\frac{0.012}{\exp[2\log_{10}([Ca]_{i2})+20]}$	$\frac{\alpha}{\alpha+\beta}$	48
I_A[1]	*p=1*	$exp\left[0.0381(V-11)\left[-1.5 - \frac{1}{\exp[(V+40)/5+1]}\right]\right]$	$exp\left[0.021(V - 11)\left[-1.5\right.\right.$	$\frac{1}{1+\alpha}$	$\frac{6.4826\,\beta}{1+\alpha}$
	q=1	$\exp[0.1144V+56]$	—	$\frac{1}{1+\alpha}$	$0.26(V+50)$

1 – Migliore et al. 1999, 2 – Magee et al. 1998, 3 – Kim et al. 2013, 4 – Traub 2002

Table 4: Parameters of single cell models

Parameters	**MPG_P**	**MPG_T**	**IMG_P**	**PGN_P**	**PGN_T**	**Hypo**	**IN_M**	**IN_D**
Cm (µF/cm^2)	0.65	0.65	1.5	0.9	0.9	1.12	2.5	1.7
Ra (Ωcm)	200	200	200	200	200	200	200	200
Conductance (mho/cm^2)								
gNabar	0.25	0.35	0.1	0.5	0.5	0.2	0.5	0.3
gKdrbar	0.002	0.0013	0.014	0.01	0.01	0.01	0.1	0.01
gLeak	1.6e-4	1.6e-4	2.7e-4	4.5e-5	4.5e-5	3.13e-5	1.2e-4	4e-5
gNapbar	--	--	--	--	--	2e-4	0.004	--
gHdbar	0.0001	--	--	--	--	--	--	--
gCabar	--	--	--	0.005	0.005	0.003	0.004	2.35e-3
gMbar	--	--	--	--	--	0.0012	0.001	--
gsAHPbar	0.15	1.1e-5	0.1	0.0003	5e-5	1e-4	0.001	1.1e-4
gKapbar	--	--	--	--	--	0.0025	0.001	--

CHAPTER 4

INTERPLAY OF RHYTHMIC AND NON-RHYTHMIC THETA GENERATORS IN A BIOLOGICALLY REALISTIC HIPPOCAMPAL MODEL

ABSTRACT

Rhythmic activity characterizes neuronal processing in multiple brain areas. Study of rhythms indicate the involvement of a multitude of rhythm generators, likely through a variety of mechanisms. Considering the multitude of involved mechanisms in rhythm generation, inactivation of circuit components can produce complex and unpredictable results. We use computational modeling to examine interaction between circuit components that participate in rhythm generation. We distinguish between resonant components and synchronizing components and demonstrate that this categorization permits predicting the rules of which components can interfere with one another and which can substitute for one another. Resonant mechanisms inherently produce rhythmic signals as a product of their dynamics and include spike-frequency adaptation, slow inhibition, rhythmic external input, and slow neuronal currents. Synchronizing mechanisms promote coordinated activity and include inhibitory feedback, non-rhythmic external input, and recurrent excitatory connections. Some circuit components can provide both resonance and synchronization. We found the most robust rhythm generation to require at least one resonant component and one synchronizing component. We found that pyramidal cells adaptation can interfere with theta produced

by slow inhibition, and fast inhibition can either substitute for or interfere with rhythm generation by slow inhibition, depending on the cholinergic state. These results begin to shed light on the conflicting evidence produced by studies inactivating circuit components, and also predicts circuit states where inactivating a component known to participate in rhythm generation might paradoxically enhance rhythmic activity. We conclude that effects of component inactivation can only be predicted in the context of what other components are present and on the neuromodulatory state of the circuit.

INTRODUCTION

NOTE: This chapter originated as work done by a previous student. The advancement over that work is primarily the conversion of the entire model from an Izhikevich version to a biological realistic version. Preliminary single cell model results are provided in Figures 10A, 10B, and 10C, with parameter values in Tables A1, A2, and A3. The other figures are not yet complete and since the work is being written up as a journal paper presently, we use the same text as before and will be updating the figures related to the results once they are ready.

The hippocampus is a well-studied and easily accessible part of the brain with a wealth of physiological data and computational models. It displays a prominent slow rhythmic activity in the theta band (4-12 Hz) (Vanderwolf, 1969). In rodents, evidence points to a hippocampal role in navigation, both spatial (O'Keefe and Dostrovsky, 1971) and temporal (Pastalkova et al., 2008; MacDonald et al., 2011), but also in encoding and retrieval of episodic-like memories (Steckler et al., 1998; Mumby et al., 2002; Eacott and Norman, 2004; Fortin et al., 2004).

The hippocampal theta rhythm is understood to be generated intrinsically, through a number of mechanisms (Kocsis et al., 1999; Buzsáki, 2002; Hummos and Nair, 2017), and also entrained from external input. Theta oscillations can be driven by medial septal and entorhinal cortex input in vivo, as found in experiments that inactivated the external input altogether, i.e., both its non-rhythmic and its rhythmic components (Petsche et al., 1962; Brazhnik and Vinogradova, 1986; Stewart and Fox, 1990; Vinogradova, 1995; Boyce et al., 2016). While multiple mechanisms are suspected, biological and theoretical studies of hippocampal oscillations have typically focused on individual intrinsic oscillatory mechanisms, and the individual contributions of the multiple intrinsic mechanisms to theta activity are not well understood.

The rise of optogenetic tools, and detailed realistic computer models, popularized inactivation studies that aim to 'dissect' rhythm generating circuits in the hippocampus, by inactivating one component at a time and observing changes rhythmic activity. While these studies generated multiple insights, divergent findings have been reported (Table 5). For instance, despite in vitro reports of a role for the slow inhibition from oriens-lacunosum moleculare cells (OLM cells) in theta generation (Pouille and Scanziani, 2004; Gloveli et al., 2005), *in vivo* optogenetic inactivation of slow and fast inhibitory cells (OLM, and BC) revealed no role in ongoing theta activity (Royer et al., 2012). However, an in vitro study showed no role for OLM cells but rather inactivation of BCs severely attenuated theta activity (Amilhon et al., 2015). Nagode and colleagues (2014), on the other hand, found no effect from inactivating BCs on CA1 theta activity, but a reduction in CA3 gamma activity. A highly detailed model of CA1 region confirmed attenuation of theta with BCs inactivation but found no contribution from

OLM cells (Bezaire et al., 2016). Computational models have suggested a contribution to hippocampal theta from intrinsic membrane conductances such as the spike-frequency adaptation currents (Crook et al., 1998; Fuhrmann et al., 2002; Hu et al., 2002; Gigante et al., 2007; Augustin et al., 2013), or the h-current (Gloveli et al., 2005; Rotstein et al., 2005; Orbán et al., 2006; Zemankovics et al., 2010; Neymotin et al., 2013a; Rotstein, 2015). Spike-frequency adaptation currents remain difficult to inactivate experimentally, while a genetic knockout of the h-current (HCN1 channels) did not disrupt theta (Nolan et al., 2004; Giocomo et al., 2011).

These inconsistent results highlight the need for a deeper understanding of how the multiple mechanisms of theta interact. We used our previously developed model, that showed a multitude of interacting theta generators, to discover more specific rules that govern how the generators might substitute for others in some cases, and under what conditions. For this, we suggest that the approach should distinguish between network components that generate oscillatory resonance from those that synchronize neuronal activity (Table 6). By considering this distinction, we were able to better describe the effects of inactivating one component, in the presence of other components, and to describe several minimal circuits for robust rhythm generation. We also found that theta generators can also compete and interfere with each other, and the model predicts conditions under which inactivation of one theta generator can paradoxically enhance the power of ongoing theta activity.

RESULTS

We used our previously published computational model of the hippocampal CA3 network that included pyramidal, OLM, and basket cells, modeled using the Izhikevich

formulation (Izhikevich, 2003), with cellular characteristics matched to physiological data. The model had synapses with realistic dynamics and short-term plasticity. Physiologically recorded place cells showed firing rates that were lognormally distributed (Mizuseki and Buzsáki, 2013), so our model pyramidal cells received Poisson inputs at rates drawn from a lognormal distribution, to match physiological firing patterns. The model reproduced the physiological aspects of theta rhythmic activity in the hippocampus (Mizuseki et al., 2012; Mizuseki and Buzsáki, 2013).

In the present study, we inactivated components of the circuit individually or in combination, to discern their effect on the theta rhythm. Expectedly, these inactivation runs led to variations in firing rates. To allow for an interpretable comparison of spectral power peaks across experimental conditions, we added a constant current injection to each cell to bias their activity level. The amplitude of these current injections was adjusted across experiments to maintain a realistic average firing rate for pyramidal cells as a population, keeping it within the reported 7 Hz reported for place cell activity *in vivo* (Mizuseki and Buzsáki, 2013). The application of a bias current maintained the lognormal distribution of firing rates and we only matched the average firing rate for the population (see figures 10A-10C, current injection values are given in figure legends).

In examining as many potential network components involved in rhythm generation, we found it useful to describe components as either resonance generators or synchronizing mechanisms. This distinction has parallels with current understanding of rhythmic activity generation in a single neuron where neuronal currents are categorized into resonant and amplifying currents. Another helpful distinction between ‘resonance

generators' and 'current generators' was previously considered in literature (Buzsáki, 2002).

OLMs and slow currents in pyramidal cells are the resonant mechanisms in CA3

To identify the resonant components of our model, we began with isolated pyramidal cells, with their slow currents (adaptation and h-current) inactivated. Pyramidal cells also received unique Poisson input and had no correlations in their external input. We then ran simulations with only one model component activated including the recurrent connections, BCs, non-rhythmic correlated external input from EC, OLM cells, and pyramidal cells slow currents. The results showed that only OLM cells and the pyramidal cells slow currents produced a peak in theta range (Fig. 2), indicating that the two components are the resonant components in this network. Recurrent connections, and input from EC enhanced power in the delta range (2-6 Hz).

Resonant mechanisms can substitute for or compete with one another

Resonant mechanisms are defined as network components possessing dynamics consistent with rhythmic activity at certain frequencies. It follows from this definition that one resonant mechanism, at a minimum, is critical for the generation of oscillatory activity in the corresponding oscillatory band. To test this hypothesis in our model, we considered that the OLM-pyramidal cells loop and the slow currents in pyramidal cells (adaptation and h-current) are the only two active resonant mechanisms.

We ran experiments with four combinations of model components. First, the full model with all components of the CA3 network active. Second, we inactivated OLM cells

(denoted “-OLM”), and third we activated OLM cells back on again and inactivated slow currents in pyramidal cells (denoted “-sPYR”), through decreasing the time constant of the adaptation current to 10 ms (from 100 ms), and removing the h-current. The last experiment was to inactivate both OLM cells and slow currents together (denoted “-Both”). Power spectra of these experiments showed that the presence of either resonant mechanisms, OLM-pyramidal cells or slow current, was sufficient to produce theta rhythmic activity, whereas inactivating both abolished all theta activity (Fig. 2). These results are made more evident by calculating the relative power in the theta band (Fig. 2, power in the 4-12 Hz range divided by power in the 0-50 Hz range). The firing rate was kept within 0.5 Hz of the physiologically reported value of 7 Hz (Fig. 2, see Methods).

In this experiment other synchronizing mechanisms of theta remained intact, such as the recurrent connections and the reciprocal inhibition to BCs. But in the absence of any resonant mechanisms rhythm generation fails. This suggests a rule of a minimum of one resonant mechanism to generate rhythms. An interesting interaction observed indicated that pyramidal cells slow currents has the potential to compete with OLM-pyramidal cell ability to generate rhythmic activity. The observation that theta power increases with the activation of pyramidal cells slow currents indicates potential interference between resonating mechanisms (Fig. 2)

Cholinergic states separate resonant mechanisms functionally and reduce interference.

We found that there is a potential for interference between the two resonant mechanisms in our model. Our previous findings indicated that different cholinergic

states engage different theta mechanisms (Hummos and Nair, 2017), accordingly, we theorized that by functionally separating the two mechanisms, cholinergic modulation might reduce the interference between the two resonant mechanisms.

For this experiment, we performed the four experimental conditions (full model, OLM inactivated, slow currents inactivated, both inactivated) in three cholinergic states, low, med, and high (by setting the ACh variable to 0, 1, and 2 respectively, see Methods). Examination of relative theta power in these conditions revealed that in the extremes of cholinergic modulation (low and high), the pattern of slow currents interfering with OLM generated theta disappeared (Fig.3).

Interactions between slow and fast inhibitory cells in theta generation

We next considered interactions between interneuronal subtypes in theta generation across cholinergic states. We examined the OLM-pyramidal cells and the BC-pyramidal cells subnetworks and ran experiments with other synchronizing mechanisms inactivated (recurrent connections were inactivated, and non-rhythmic external input was substituted with direct Poisson inputs to pyramidal cells).

In the baseline cholinergic state, both mechanisms appeared to have an additive effect on producing theta spectral peak. Inactivating either subtype of interneurons produced a moderate drop in theta power. We have previously shown that the OLM-pyramidal cells subnetwork becomes increasingly engaged in theta generation in high cholinergic states (Hummos and Nair, 2017). Here we observed that at increasing cholinergic levels, OLM-pyramidal subnetwork is becoming more engaged in generating higher levels of theta power, meanwhile, BCs effects remained the same. In high cholinergic states,

interestingly, BCs began to interfere with the theta activity generated through the OLM-pyramidal subnetwork, and their inactivation increased rhythmic power in the theta range (Fig. 4). A similar analysis with a circuit including the recurrent connections and basket cells revealed little interaction between the two synchronizing mechanisms (Fig. 5). Specifically, recurrent connections appeared to have the most significant role in lower cholinergic states, while BCs had a consistent role with little change across cholinergic states.

DISCUSSION

We used our previously developed model of the hippocampal CA3 to provide in-depth concepts to assimilate what is known about hippocampal theta generation, in a well-grounded conceptual framework. Our study shows a complex interaction between theta generators. The effects of inactivating one theta component can be complex and dependent on other generators present and on neuromodulatory states.

Multiple interacting mechanisms

Comprehensive models have been developed recently allowing the examination of a number of these generators in one model (Neymotin et al., 2013a; Bezaire et al., 2016; Ferguson et al., 2017; Hummos and Nair, 2017). We here used our biologically realistic model, with many theta generating components, to show that theta generators act to provide a context in which inactivation of one component can be interpreted. Inactivation of on component can have no effect, reduce or even enhance rhythmic activity, depending on which other components are active. Our previous study showed that results of component inactivation can also depend strongly cholinergic neuromodulation (Hummos and Nair, 2017). Here we also extend these results to show

a complex interaction between the component inactivated, other active components, in addition to the cholinergic state, to determine the effects of inactivation on the power spectrum.

These insights can be used to interpret results from experiments. For example, our results are consistent with findings by Royer et al., where optogenetic inactivation of either BCs or OLM did not impact theta generation significantly. As far as can be gleaned from their Methods, the animals were not exposed to any novel stimuli or environments during testing, and because cholinergic modulation is tied to novelty (Miranda et al., 2000; Giovannini et al., 2001), one can assume a low cholinergic state in this study. Their results are consistent with our inactivation results, where, in low cholinergic states, BCs and OLMs were able to compensate for one another to generate theta (Fig. 4). However, our model predicts that in a high cholinergic state, the same experiment could show a dramatic drop in theta with OLM inactivation, and an increase in theta power with BCs inactivation (Fig. 4); this remains to be shown in experiments.

Resonant and synchronizing mechanisms act in concert to generate rhythms

We here provide a broad stroke conceptualization by distinguishing between resonant mechanisms and synchronizing mechanisms. We note another distinction between ‘resonance generators’, and ‘current generators’ suggested by Buzsaki (2002). BCs have recently been shown in a computational model to be significant current generators, even if not directly involved in rhythm generation (Neymotin et al., 2013b).

Parallels can be seen between this conceptual division and the requirements for generating subthreshold membrane oscillations in a single cell. Individual neurons were

described to require at least one resonant current and at least one amplifying current to display significant membrane oscillations (Hutcheon et al., 2000).

Recently another comprehensive model of CA1 showed that theta power was sensitive to silencing several of the interneuronal cell types including silencing PV+ BCs, CCK+ BCs, neurogliaform, bistratified, and axo-axonic cells (Bezaire et al., 2016). Our work suggests that almost any interneuronal population, if reciprocally connected to pyramidal cells, can participate in rhythm generation, as a synchronizing component. The sensitivity of the theta rhythm in that study to the inactivation of as many types of interneurons might be related to changes in the levels of network excitability, as the study indicates theta was sensitive to level of excitation. A contribution of our study was to examine effects of inactivating interneurons while maintaining excitation levels within physiological limits. We provided pyramidal cells with a constant current injection to offset the effects of inactivating inhibitory interneurons on level of excitation. Isolating effect of interneurons on excitation level, revealed their role in rhythm generation by acting as synchronizing mechanisms.

Most interneuronal types are capable of participating in theta rhythm generation, including OLM cells. We here emphasized the role of the OLM-pyramidal cells sub-network in providing resonance in theta frequency, however OLM cells also do participate, as do many interneurons, as a synchronizing mechanism.

Fast spiking basket cells as synchronizing component for theta generation

Inhibition by fast spiking basket cells, which tightly controls the timing of pyramidal cells firing, was proposed to play a role in theta generation (Buzsaki 2002), but later

studies focused on the role of the pyramidal-basket cells sub-network as a generator of gamma power (for review, see Buzsáki and Wang, 2012). However, recent experimental and computational findings have highlighted a role for basket cells in the generation of theta activity. Inactivation of PV+ basket cells diminished theta activity in an intact hippocampus preparation (Amilhon et al., 2015), and in a detailed computational model of CA1 (Bezaire et al., 2016), and a minimal circuit with pyramidal cells and BCs was found sufficient to produce theta activity (Stark et al., 2013; Ferguson et al., 2017; Hummos and Nair, 2017).

Two more recent modeling studies, Hummos et al. (2017) and Ferguson et al. (2017), demonstrated a role for BCs in synchronizing a population of excitatory pyramidal cells to generate theta activity. In these models, pyramidal cells had spike frequency adaptation matched to experimental data, and generated theta spiking oscillations, i.e. a predominance of theta interval spikes in pyramidal cells (ISI peak ~ 90 ms), robustly at a wide range of input levels (Hummos and Nair, 2017). Through reciprocal connections, BCs synchronize these theta spikes. Intuitively, we theorize that BCs can synchronize pyramidal cells spikes to a degree where BCs themselves begins to receive increasingly synchronized excitation from pyramidal cells, and in turn provides theta rhythmic inhibition, thus amplifying the rhythmic activity. This mechanism is relatively independent of the specific properties of BCs or their connections to pyramidal cells but is rather a general property of pyramidal-interneuronal interactions. Considering that pyramidal cells have both subthreshold and spiking oscillations in the theta range, any common input might add sufficient synchrony in their activity to create more coherent rhythmic activity (Cobb et al., 1995). This common input can come from any type of

inhibitory cells reciprocally connected to pyramidal cells, independent from the specific dynamics of the inhibitory cells or their inhibitory current, although faster inhibitory currents might control pyramidal cells spiking with higher precision.

We demonstrate this effect in a simulation with two populations of BCs and pyramidal cells and their interconnections (Fig. 1D). This subnetwork is capable of generating theta rhythmic activity that is robust to a range of input levels to pyramidal cells. This current study extends these results and show that the role of BCs in ongoing theta oscillations is dependent on the involvement of OLM cells, and on the neuromodulatory state of the circuit.

Competition and interference

This study provides examples of interference and competition amongst resonant mechanisms and amongst synchronizing mechanisms, in a biologically realistic model. The results accordingly predict conditions were inactivation of a resonant or a synchronizing mechanism might enhance rhythmic activity, indicating that their presence interfered with other active generators. We note, however, that interference is not a destructive phenomenon in this context. Indeed, interference between oscillators has been theorized to encode the location of an animal by producing grid cells firing patterns in EC (Burgess, 2008). In addition, competition of multiple peripheral oscillators to synchronization with a central oscillator have been theorized to serve as a mechanism for attention controlled by executive function (Kazanovich et al., 2013).

Limitation and future direction

As discussed above, theta appears to be generated in the hippocampus due to the effects

of external input, both its rhythmic and non-rhythmic components, and a consortium of intrinsic mechanisms. Our model falls short of representing the diversity of these theta generators and analyzing more complex interactions that involve a larger number of rhythm generators. With the current community effort to make more detailed models increasingly available, these complexities can be examined comprehensively. In addition to complexity added by more theta generators, neuromodulators (such as endocannabinoids, and serotonin) have effects of theta generation and likely have a role in determining which theta generators are actively engaged. The h-current model used matched experiments of subthreshold resonance in pyramidal cells (see Methods), however it remained mathematically difficult to separate from the adaptation current in pyramidal cells. A more detailed model of the h-current can allow examination of its role specifically and separate from spike-frequency adaptation.

Another area of future interest would be to examine how individual theta generators interact with rhythmic external input. Results can vary from competition and interference to synergy. Combinations of intrinsic theta generators might also respond differently than individual ones. These questions in addition to cholinergic dependence can help future conceptualization of how the hippocampus responds to its rhythmic inputs.

CONCLUSIONS

- As a conceptual framework for hippocampal theta generation, we propose a useful distinction between resonant and synchronizing components.

• Many interneuronal types can be involved in theta generation through a general role for interneurons as synchronizing mechanisms. These effects can be more evident if inactivation studies would compensate for variation in excitation levels.

• We predict conditions when inactivation of a rhythm generator might paradoxically raise the power in the particular rhythmic band.

METHODS

We developed a network model of the rodent hippocampus in a prior study using Izhikevich single cell models, synaptic currents, spatial connectivity patterns, short- and long-term plasticity and known neuromodulator effects (Hummos et al. 2014). The model included CA3 and DG regions that received inputs from EC. The present study used the same model, except for replacing the Izhikevich single cell models with biophysical conductance-based models matched to biological data. We provide information related to the single cell models followed by an overview of the network model and key features. The reader is referred to our previous study for details, including a complete listing of other parameters (Hummos et al. 2014).

Single cell models

Single neurons were modeled using the Hodgkin-Huxley formulation (Byrne et al. 2014) and included multiple compartments with known currents and neuromodulator receptors. CA3 model cells included PNs and the two most abundant interneuron types, BCs and OLM cells (Vida 2010). DG model cells included granule cells, BCs, and Hilar Perforant Path-associated (HIPP) cells. All model neurons were matched to the salient features reported in biology. CA3 PNs fire in bursts of 2-3 action potentials as well as individual spikes (Tropp Sneider et al. 2006). These PNs respond to current injections

with an initial burst followed by either silence or tonic firing at different frequencies (Brown and Randall 2009; Hemond et al. 2008) and are also capable of bursting in response to a very short (2-5 ms) current pulse with a burst of action potentials that out-live the stimulus (Brown and Randall 2009; Wong and Prince 1981). Model CA3 PNs had a resting potential of -75 mV, input resistance of 80 MΩ and time constant of 21 ms. Parvalbumin-positive basket cells (BCs) are characterized by fast spiking patterns and a small membrane time constant (~10 ms) and little spike frequency adaptation (Bartos and Elgueta 2012). The cell model had these characteristics, with a resting potential of -64 mv and firing rate vs. current injection relationship that matched data in (Buhl et al. 1996). OLM cells have a high input resistance (496 MΩ) and slow membrane time constant (71 ms) (Lawrence et al. 2006). Action potentials are followed by a characteristic long-lasting, slow after-hyperpolarization with rebound spikes occurring commonly on repolarization. Model OLM cells captured these characteristics, and had a resting membrane potential of -68 mv (Ali and Thomson 1998). OLM model cells were also tuned to produce the observed slow AHP, rebound spikes and the characteristic sag with negative current injections. Granule cells in DG display a very low basal firing rate in vivo with an average < 0.5 Hz, and bursts shorter than those in CA3 cells (Jung and McNaughton 1993). These cells predominantly fire in single spikes with spike frequency adaptation (Staley et al. 1992). DG model cells had resting membrane potential of -73 mV (Staley et al. 1992) and matched biological data including passive properties and responses to current injections (Staley et al. 1992). Interneurons in DG used the same BC model and used the OLM model for HIPP cells (Katona et al. 1999).

EC Layer II Stellate cell. The medial EC Layer II is composed primarily of "stellate" cells (Tahvildari et al. 2005). For the purpose of this study, because we needed the cells responsible for hippocampal input to the CA3 and Dentate Gyrus only the stellate cell of EC layer II was modeled (Heinemann et al., 2006). This cell consisted of two Hodgkin-Huxley type compartments with individual properties: These included a soma and an apical dendrite. Current injection responses from electrophysiological experiments (Alonso et al., 1993) were matched in the cell model.

Ion currents in the Stellate cell model. The ion currents inserted into each compartment were adapted from existing biophysical hippocampal and entorhinal cortex models (Acker et al., 2003, Fransén et al., 2004 , Li et al., 2008). The soma compartment contained sodium (I_{Na}), persistent sodium (I_{NaP}), delayed-rectifier potassium (I_{KDR}), L-type calcium ($I_{Ca,L}$), hyperpolarization-activated (I_H), calcium-activated potassium (I_{AHP}), high voltage-activated calcium (I_{Ca}) and calcium and voltage-activated potassium (I_C) currents. The apical dendrite contained the same currents as that of the soma except for I_C *and* I_{Ca} (Fransén et al., 2004). The specific properties of the Stellate cell model are shown in Table 1A, and the equations used for each ion current are shown in Table 1B.

Dentate Gyrus Granule cell. Neurons in the DG consist primarily of pyramidal, granule and stellate cell types of which we have modeled the granule cell. For the purpose of this study, we needed the cells involved in memory formation and storage in the hippocampal circuit and so only the granule cell was modeled. This cell consisted of two Hodgkin-Huxley type compartments with individual properties: These included a

soma and an apical dendrite. Current injection responses from electrophysiological experiments (Zhang et al.,1993, Spruston et al., 1992 and Staley et al. 1992) were matched in the cell model.

Ion currents in the Granule cell model. The ion currents inserted into each compartment were adapted from existing biophysical dentate gyrus model (Aradi and Holmes, 1999). The soma compartment contained sodium (I_{Na}), fast (I_{fKDR}) and slow (I_{sKDR}) delayed-rectifier potassium, L-type ($I_{Ca,L}$), T-type($I_{Ca,T}$) and N-type ($I_{Ca,N}$) calcium, fast transient potassium current (I_A), calcium-activated potassium (I_{AHP}) and calcium and voltage-activated potassium (I_C) currents. The apical dendrite contained the same currents as that of the soma except for I_A (Aradi and Holmes, 1999).

CA3 Spiny Pyramidal Cell. Neurons in the CA3 consist primarily of spiny and aspiny pyramidal and basket cell types of which we have modeled the spiny pyramidal cell. For the purpose of this study, we needed the cells responsible for memory formation and storage in the hippocampal circuit and so only the CA3 cell was modeled. This cell consisted of two Hodgkin-Huxley type compartments with individual properties: These included a soma and an apical dendrite. Current injection responses from electrophysiological experiments (Scharfman (1993) were matched in the cell model.

Ion currents in the CA3 cell model. The ion currents inserted into each compartment were adapted from existing biophysical CA3 cell models (Traub et al. (1991), Traub et al. (1994) and Migliore (1995)). The soma compartment contained sodium (I_{Na}), delayed-rectifier potassium (I_{KDR}), L-type ($I_{Ca,L}$), T-type($I_{Ca,T}$) and N-type ($I_{Ca,N}$) calcium, calcium activated potassium (I_{KCa}), fast transient potassium current (I_A),

calcium-activated potassium (I_{AHP}) and voltage-gated persistent muscarinic (I_M) currents. The apical dendrite contained the same currents as that of the soma.

Interneuron. The interneurons were modeled after interneurons of the lateral amygdala (LA) as described in Li et al. (2009).

Equations for Modeling A Cell

For each Hodgkin-Huxley type cell compartment, the membrane voltage was computed by Eq. 1, where C_i and V_i represent the total capacitance and membrane voltage of compartment *i*, and I_{ion} and I_{axial} represent the sums of intrinsic membrane currents, axial cytoplasmic currents, respectively, for that compartment.

$$C_i \frac{dV_i}{dt} = I_{ion,i} + I_{axial,i} \qquad (1)$$

Ion currents. Each ion current was modeled according to Eq. 2, where the kinetics of the gating variables *m* and *h* were governed by Eq. 3, with *x* representing either *m* or *h*. *V* is the membrane voltage of the compartment in which the current was inserted, G_{max} is its maximal conductance, and E_{rev} is its reversal potential. Each current is assigned its own value of these parameters, and these values are shown in Table 1B.

$$I = -G_{max} m^p h^q (V - E_{rev}) \qquad (2)$$

$$\frac{dx}{dt} = \frac{x_\infty([Ca^{2+}]) - x}{\tau_x(V)} \qquad (3)$$

Axial currents. Axial currents flowing between neuron sections are handled in the NEURON simulation environment for connected sections according to section geometry and cytoplasmic resistivity. For the connected sections *i* and *j*, the axial current flowing to section *i* is computed according to the equation $I_{axial} = (V_j - V_i)/R_i$,

where R_i is the cumulative axial resistance between the end-most points at which Eq. 1 is evaluated.

Network structure and connectivity

The rat hippocampus contains approximately 1.6 million cells (Hosseini-Sharifabad and Nyengaard, 2007). For computational efficiency and to maintain minimum model complexity, the numbers were scaled down while maintaining reported ratios (Hummos et al., 2014), as in our previous models (Li et al., 2011; Kim et al., 2013a, 2013b; Pendyam et al., 2013). The model DG region had 384 granule cells, 32 BCs, and 32 HIPP interneurons, while the model CA3 region contained 63 pyramidal cells, 8 BCs, and 8 OLM cells (Seress and Pokorny, 1981; Kosaka et al., 1987; Baude et al., 2007; Hosseini-Sharifabad and Nyengaard, 2007). The model EC region had 30 regular spiking cells.

The entorhinal cortex provides inputs to the hippocampus through the perforant pathway that projects to the entire hippocampal formation. The standard view describes a unidirectional connectivity with a direct path from EC to CA3 and an indirect path through DG (Fig. 1D in Hummos and Nair, 2017) (Naber et al., 1997; Witter, 2010). The perforant path projections follow a lamellar organization across the longitudinal axis of the hippocampus, as follows: Lateral and posterior parts of the EC are connected to the dorsal parts of CA3 and DG, while the more medial and anterior parts of EC project to the ventral parts of CA3 and DG (Witter, 2010). This lamellar organization transitions gradually from one extreme to the other on the longitudinal axis of the hippocampus, and a single neuron in EC can project to about 25% of the longitudinal

length of CA3 (Witter, 2010). Projections from DG to CA3 also follow a similar longitudinal organization; however, these projections target a more limited longitudinal extent (Witter, 2010).

Model cells were distributed uniformly in 3D space separated into the three regions, EC, DG, and CA3, with dimensions that approximate the respective dimensions of the rat hippocampus (Hummos et al., 2014). Projections from EC to both pyramidal cells and BCs in DG and CA3 followed a lamellar pattern where neurons were most likely to connect to neurons in of their longitudinal neighborhood with a decreasing probability towards the periphery. This spatial connectivity was modeled using a Gaussian connection probability function that depended on the longitudinal distance between the two connected cells. The Gaussian function had a peak probability of 0.4 and a standard deviation of 3 mm for the perforant path projections to both pyramidal cells and BCs in CA3. Perforant path projections to DG had similar values (see (Hummos et al., 2014)).

Similarly, the mossy fiber projections from DG to CA3 followed the same lamellar pattern but with a more limited longitudinal extent by setting the standard deviation of the Gaussian probability function to 2 mm. In addition, to preserve the sparseness of the mossy fiber connections from DG to CA3 (Witter, 2010), each DG granule cell was limited to contacting two CA3 pyramidal neurons. Projections from DG granule cells to CA3 BCs are more diffuse and out-number projections to CA3 pyramidal neurons by a ratio of 10:1 (Acsady et al., 1998). Accordingly, DG projections to BC followed a Gaussian distribution with a peak probability of 0.2 and standard deviation of 3 mm. Recurrent CA3 connections reveal relatively more diffuse spatial

organization (Ishizuka et al., 1990; Wittner et al., 2007), and were therefore distributed homogenously with a fixed probability of 0.3.

The dendritic projecting OLM cells are thought to be involved in feedback inhibitory loops (Maccaferri, 2005) and while they have a more limited axonal arborization (Buhl and Whittington, 2007) they make many more synapses compared to BCs (Sik et al., 1995). In contrast, BCs have a more diffuse axonal arborization with the highest connection probability to pyramidal cells in their immediate neighborhood and a decreasing connection probability towards the periphery of their axonal arbors (Sik et al., 1995). Similarly, BCs project to neighboring OLM cells (Bartos et al., 2010). As before, we used a Gaussian function to approximate these spatial probabilities. We also assumed that BC projections to both pyramidal cells and to OLM cells shared the same spatial domain. In the reverse direction, OLMs receive reciprocal connections from the same pyramidal cells they projected to, in line with their function as local feedback cells (Maccaferri, 2005). On the other hand, granule cells in DG and pyramidal cells in CA3 projected homogenously to BCs with a fixed probability of 0.15, consistent with the lack of specific topography reported at these projections (Wittner et al., 2006).

The network was constructed by generating connections randomly between cells while maintaining the connection probabilities and spatial patterns of connectivity described above. The spatial connectivity patterns and parameter values are summarized in table 7 (also see (Hummos et al., 2014)).

Synaptic currents

Synaptic currents were modeled using the kinetic model described in Destexhe

et al. (1998). AMPA, NMDA, $GABA_A$, and $GABA_B$ currents were modeled and their dynamics such as rise and decay time constants and delays were matched to available literature (Hummos et al., 2014). In particular, CA3 pyramidal cell AMPA currents were fastest for the mossy fiber inputs from DG and slowest for perforant path inputs from EC, while recurrent CA3 inputs from other pyramidal cells had intermediate values (Hoskison et al., 2004; Tóth, 2010), as summarized in table 7. Additionally, inhibitory currents from OLM had slower dynamics compared to those from BC (Table 7) (Geiger et al., 1997; Bartos et al., 2010). Synaptic weights were assigned in accordance with literature where available (for details, see Hummos and Nair, 2017).

Long-term synaptic plasticity

Biological studies have shown classical Hebbian associative long-term potentiation (LTP) at the glutamatergic perforant path synapses to DG (Bliss and Gardner-Medwin 1973) and to CA3 (Do et al. 2002). Many types of synaptic plasticity exist at GABAergic synapses (for a review, see (Maffei 2011)). (Woodin et al. 2003) reported LTP between hippocampal cells if the pre- and post-synaptic spikes were within 20ms of each other, LTD if within 50ms, and no change if longer. They also found plasticity to be dependent on activation of postsynaptic L-type voltage dependent calcium channels (VDCCs).

Consistent with these findings, the model implemented LTP using a learning rule based on the concentration of a post-synaptic calcium pool at each modifiable synapse (Shouval et al. 2002a). At excitatory synapses, calcium entered post-synaptic pools via NMDA receptors, and at inhibitory synapses, calcium entered through VDCCs. The postsynaptic pool also received Ca^{2+} from internal stores upon $GABA_B$

receptor stimulation. This approach has been used in other models by our group (Kim et al. 2013b; Li et al. 2009). For both types of synapses, a calcium concentration above a lower threshold caused synaptic weight depression, while a concentration exceeding an upper threshold cause synaptic weight potentiation. Because the characteristics of DG to CA3 mossy fiber potentiation are controversial (Neves et al. 2008), we only modeled short-term plasticity in the MF connections, as described below. Long-term plasticity in all synapses was constrained to 100%.

Short-term synaptic plasticity

In addition to long-term plasticity described above, we included short-term plasticity in the model based on the formulation by (Varela et al. 1997). We modeled short-term facilitation reported at the DG to CA3 mossy fiber connections (Toth et al. 2000) and frequency-dependent synaptic depression reported at the recurrent CA3 connections (Hoskison et al. 2004). In CA1, projections from pyramidal cells to OLM cells have been shown to experience short-term facilitation (Ali and Thomson 1998), while projections to BC cells experience short-term depression (Ali et al. 1998). In the opposite direction, inhibitory currents from OLM cells to CA3 pyramidal cells show no short term facilitation or depression (Maccaferri 2005), while inhibitory currents from BC cells to CA3 pyramidal cells show depression (Hefft and Jonas 2005).

Acetylcholine effects

The hippocampus receives widespread volume transmission of cholinergic inputs from the septum-diagonal band complex (Woolf, 1991).Cholinergic stimulation has differential effects on synaptic transmission of different pathways in the hippocampus (Barry et al., 2012). Synaptic transmission through the perforant pathway

projections to CA3 is suppressed by 50%, compared to a suppression by 85% at the recurrent connections in CA3 (Hasselmo et al., 1995; Kremin and Hasselmo, 2007). On the other hand, the mossy fibers transmission is enhanced by 49% (Vogt and Regehr, 2001). To model ACh effects on synapses, AMPA synaptic currents were scaled by the value of ACh. A parameter bACh determined the direction and magnitude of ACh effects on a particular synapse. Values of bACh for different synapses were set according to experimental results as summarized in table 7 (also see Hummos et al. (Hummos et al., 2014)).

In addition to the synapse specific effects, cholinergic stimulation enhanced cellular excitability and depolarized the resting membrane potential of principal cells, eliminated AHP, decreased spike frequency adaptation and induced rhythmic burst activity (Madison and Nicoll, 1984; Misgeld et al., 1989). Furthermore, effects on interneurons were subtype-dependent (McQuiston and Madison, 1999a, 1999b). Muscarinic stimulation of OLM interneurons depolarized the resting membrane potential, and lowered both spike frequency adaptation and AHP (Lawrence et al., 2006). In contrast, PV-BCs respond to muscarinic receptor activation with a limited depolarization in resting membrane potential (Cea-del Rio et al., 2010; Cobb and Lawrence, 2010). Effects of ACh on neurons were modeled by linearly scaling the neuronal model parameters by the ACh state as detailed in Hummos et al. (see fig. S4 in (Hummos et al., 2014)). Considering the slow dynamics of ACh effects (onset time constant approximated between 1 and 2 s; Hasselmo and Fehlau, 2001), ACh state was set to a given value at the beginning of each experiment and had no dynamics.

Spontaneous firing rates

DG. 0.5 Hz (Bower, 2008); 2 to 4 Hz for mossy cells (Santhakumar, 2005)

CA3. 0.1 to 0.2 Hz (Hausser, 2004); The highest mean firing rates were observed during RUN (CA1 = 0.88 ± 1.23 Hz; CA3 = 0.50 ± 0.78 Hz), followed by SWS (CA1 = 0.72 ± 0.78 Hz; CA3 = 0.42 ± 0.44 Hz) and REM (CA1 = 0.67 ± 1.00 Hz; CA3 = 0.24 ± 0.38 Hz), in both regions.

Note: RUN: is during task performance. SWS is slow wave sleep and REM is REM sleep. (Miuseki, 2012)

In our model, the DG cells had an average spontaneous firing frequency of 2.98 Hz and the CA3 cells had an average firing frequency of 0.49 Hz. Both values are within reported values in the literature.

Inputs and data analysis

For the full model and sub-circuit cases considered, either EC cells or CA3 pyramidal cells (identified in the figures) received external input as trains of Poisson-distributed spikes, triggering an influx of AMPA and NMDA currents into the cell. We studied two model cases: one with external input arriving at EC, and the other with input arriving directly at CA3 pyramidal cells. The two types of inputs differed in the weight of the associated input synapses, and the base rate of the Poisson spike trains arriving at these synapses. Input to EC arrived at synapses with a 100% spike transmission rate to ensure that EC firing pattern was dictated by the Poisson input, whereas input to CA3 pyramidal cells had a lower weight value with parameters matching the EC to CA3 synapses (Table 7).

To determine the base rates of the Poisson processes generating these input trains, we considered place cells in CA3. Place cells respond to certain areas in the environment and their firing rates approximate a lognormal distribution (Mizuseki and Buzsáki, 2013) with an average of ~7 Hz (Mizuseki et al., 2012). In our model case where external inputs arrived at EC, each EC cell received a unique train of Poisson input spikes at a base rate of 15 Hz, which produced firing rates in CA3 pyramidal cells with a lognormal distribution and an average of 7 Hz. In the model case where external inputs arrived directly to CA3 pyramidal cells, the input rates to different cells had to be drawn from a lognormal distribution (average: 50 Hz, standard deviation: 40 Hz), to produce firing rates with a lognormal distribution that matched experimental data. Following titration of the Poisson input, a constant current injection was added to the voltage equation and the current amplitude was adjusted to maintain the physiologically reported average firing rate and lognormal distribution of firing rates. The current values used for each experimental condition are listed in the corresponding figure legend.

For spectral analysis, we summed the spikes of all cells of each type in a region (e.g., CA3 pyramidal cells) in 0.1 ms bins and computed the fast-Fourier transform of the resulting vector, using the Matlab function psautospk.m (Koch and Segev, 1998), with a moving window of size 1024 ms, and overlap of 512 ms. Spike data was used in spectral calculations as a proxy for LFP as used in network models (e.g., Brunel and Wang, 2003; Hoseini and Wessel, 2016; Samarth et al., 2016), with the assumption that these spikes are received by a downstream local neuron and translated into membrane currents that generate an LFP signal.

The model was developed using the NEURON software package (Carnevale and Hines, 2009) and run on a PC with an Intel i7-core processor with an integration time-step of 0.1 ms (key results were also verified with a time-step of 0.01 ms). The code is available as part of our previous publication via the public database ModelDB at Yale University. The recorded spike times were then analyzed using MATLAB (Mathworks, Inc.). All simulations ran for 5 seconds.

TABLES

Table 5: Summary of inactivation studies

Study	Type	Component inactivated	Evidence for	Evidence against	Cholinergic effects	Region
(Amilhon et al., 2015)	*In vitro* intact preparation	Optogenetic BCs and OLM inactivation	Role of BCs	OLM cells	Not considered	CA1
(Wulff et al., 2009)	In vivo	$GABA_A$ receptors on BCs	Role for inhibition of BCs in theta	Role for inhibition of BCs in gamma	Not considered	CA1
(Gillies et al., 2002)	In vitro	AMPA transmission	Inhibitory currents	Recurrent connections (But not in CA3)	Inhibition based theta was atropine-resistant	CA1, CA3
(Nolan et al., 2004)	In vivo	HCN1		h-current	Not considered	CA1
(Leung and Shen, 2004)	In vivo	AMPA transmission	None	Recurrent connections	Not considered.	CA1, theta dropped by 47%
(Nagode et al., 2014)	in vitro		Role of CCK cells	Role of BCs	Rhythms cholinergically induced	CA1
(Royer et al., 2012)	In vivo	OLM cells and BCs	None	OLM cells or BCs cells	Not considered, but animals not exposed to novelty.	CA3
(Buzsáki et al., 1983)	In vivo	EC input	Rhythmic EC input		Inactivating EC input made the remaining theta atropine-sensitive	Theta dropped but more markedly became atropine sensitive.

Table 6: Classification of theta rhythm mechanisms

Mechanism	Resonant	Synchronizing
E-E		X
E-Slow I	X	X
E-Fast I		X
Adaptation	X	
h-current	X	
Non-rhythmic external input		X
Rhythmic external input	X	X

Table 7: Chapter 4 supplementary tables

Table A1: Parameter values for CA3 PNs.

Current Type	Soma G_{max} (S/cm2)	Dend$_P$ G_{max}	Gating Variable	α	β
I_{Na}	0.031	0.015	p = 3	$\frac{0.32(13.1-v)}{\exp[(13.1-v)/4]-1}$	$\frac{0.28(v-40.1)}{\exp[(v-40.1)/5]-1}$
			q = 1	$0.128\exp[(17-v)/18]$	$\frac{4}{\exp[(40-v)/5]+1}$
I_{Kdr}	0.06	0.03	p = 3	$\frac{-0.07(v-47)}{\exp[(v-47)/-6]-1}$	$\frac{0.264}{\exp[(v-22)/40]}$
			q = 1	$0.001\exp\left(-2(v+61).\frac{F}{RT}\right)]$	0.001
I_{KCa}	0.00055135	0.00055	p =1	$\frac{0.28[Ca^{2+}]}{[Ca^{2+}]+\exp1(0.00048,0.84,v)}$	$\frac{0.48}{1+[Ca^{2+}]/\exp1(0.13e^{-6},1,v)}$
I_M	0.007	0.001	p = 4	$-0.006\exp\left(0.6(v+55).\frac{F}{RT}\right)]$	$0.06\exp\left(-9.4(v+55).\frac{F}{RT}\right)]$
I_{CaL}	0.025	0.025	p = 2	$\frac{15.69(81.5-v)}{\exp[(81.5-v)/10]-1}$	$0.29\exp[-v/10.86]$
I_{CaN}	0.01	0.0001	p =2	$\frac{0.1967(19.98-v)}{\exp[(19.98-v)/10]-1}$	$0.046\exp[-v/20.73]$
			q = 1	$0.00016\exp[-v/48.4]$	$\frac{1}{\exp[(39-v)/10]+1}$
I_{CaT}	0.0079	0.007	p =2	$\frac{0.2(19.26-v)}{\exp[(19.26-v)/10]-1}$	$0.009\exp[-v/22.03]$
			q = 1	$0.00016\exp[-v/16.26]$	$\frac{1}{\exp[(29.79-v)/10]+1}$
I_{KAHP}	0.001	0.0004	p = 1	$1.3*10^{13}[Ca^{2+}]_i^4$	0.005
I_A	0.0012	0.001	p = 1	$0.02\exp\left(1.8(v+33.6).\frac{F}{RT}\right)]$	$0.02\exp\left(-1.2(v+33.6).\frac{F}{RT}\right)]$
			q = 1	$0.08\exp\left(4(v+83).\frac{F}{RT}\right)]$	0.08
Diam	16	3	C_m = 1.0	R_{axial} = 210 Ω-cm	G_{leak} = 0.00018
Length	16.8	150	E_{Na} = 45	E_K = -85 mV	E_{leak} = -70 mV
				$x_\infty = \frac{\alpha}{\alpha+\beta}$	τ_x (ms) = $\frac{1}{\alpha+\beta}$

Table A2: Parameter values for DG PNs.

Current Type	Soma G_{max}	Dend$_P$ G_{max}	Gating Variable	α	β
I_{Na}	0.08	0.08	p = 3 q = 1	$\frac{-0.3(v-25)}{\exp[(v-25)/-5]-1}$ $\frac{0.23}{\exp[(v-3)/20]}$	$\frac{0.3(v-53)}{\exp[(v-53)/5]-1}$ $\frac{3.33}{\exp[(v-55.5)/-10]+1}$
I_{fKdr}	0.04	0.04	p = 4	$\frac{-0.07(v-47)}{\exp[(v-47)/-6]-1}$	$\frac{0.264}{\exp[(v-22)/40]}$
I_{sKdr}	0.13889	0.012	p = 4	$\frac{-0.028(v-35)}{\exp[(v-35)/-6]-1}$	$\frac{0.1056}{\exp[(v-10)/40]}$
I_C	0.0001	0.0001	p =2	$\frac{-0.00642Vm-0.1152}{\exp[-(Vm+18)/12]-1}$ $Vm = v + 40\log(1000[Ca]_{i2})$	$1.7\exp[-(Vm+152)/30]$ $Vm = v + 40\log(1000[Ca]_{i2})$
I_{CaL}	0.0004	0.0004	p = 2	$\frac{15.69(81.5-v)}{\exp[(81.5-v)/10]-1}$	$0.29\exp[-v/10.86]$
I_{CaN}	0.0005	0.0005	p =2 q = 1	$\frac{0.19(19.98-v)}{\exp[(19.98-v)/10]-1}$ $0.00016\exp[-v/48.4]$	$0.046\exp[-v/20.73]$ $\frac{1}{\exp[(39-v)/10]+1}$
I_{CaT}	0.0005	0.0005	p =2 q = 1	$\frac{0.19(19.98-v)}{\exp[(19.98-v)/10]-1}$ $0.00016\exp[-v/48.4]$	$0.046\exp[-v/20.73]$ $\frac{1}{\exp[(39-v)/10]+1}$
I_{AHP}	0.00005	0.00005	p = 1	$\frac{0.0048}{\exp[-0.5(Vm-35)]}$ $Vm = 10\log(1000[Ca]_{i1})$	$\frac{0.012}{\exp[0.2(Vm+100)]}$ $Vm = 10\log(1000[Ca]_{i1})$
I_{KA}	0.005	–	p = 1 q = 1	$\frac{-0.05(v+25)}{\exp[(v+25)/-15]-1}$ $\frac{0.00015}{\exp[(v+13)/15]}$	$\frac{0.1(v+15)}{\exp[(v+15)/8]-1}$ $\frac{0.06}{\exp[(v+68)/-12]+1}$
Diam. (μm)	16	3	C_m = 1.0	R_{axial} = 210 Ω-cm	G_{leak} = 0.0002
Length (μm)	16.8	150	E_{Na} = 45	E_K = -85 mV	E_{leak} = -70 mV
$\tau_{[Ca^{2+}]}$ (sAHP)(msec)	1000	1000	$[Ca^{2+}]_{rest}$ = 50 nM	$x_\infty = \frac{\alpha}{\alpha+\beta}$	τ_x (ms) = $\frac{1}{\alpha+\beta}$
$\tau_{2[Ca^{2+}]}$ (C)(msec)	1	1			

Table A3: Parameter values for BC and OLM cells (*all values for are for both unless otherwise indicated)*.

Current	Soma G_{max}	Dend$_P$ G_{max} (S/cm2)	Gat. Var.	α	β
I_{Na}	BC-0.12; OLM-0.08	BC-0.12; OLM-0.08	p = 3 q = 1	$\frac{-0.3(v-43)}{\exp[(v-43)/-5]-1}$ $\frac{0.23}{\exp[(v-65)/20]}$	$\frac{0.3(v-15)}{\exp[(v-15)/5]-1}$ $\frac{3.33}{\exp[(v-12.5)/-10]+1}$
I_{fKdr}	BC-0.0013; OLM-0.01	BC-0.0013; OLM-0.01	p = 4	$\frac{-0.07(v-47)}{\exp[(v-47)/-6]-1}$	$\frac{0.264}{\exp[(v-22)/40]}$
I_{sKdr}	BC-0.0013; OLM-0.01	BC-0.0013; OLM-0.01	p = 4	$\frac{-0.028(v-35)}{\exp[(v-35)/-6]-1}$	$\frac{0.1056}{\exp[(v-10)/40]}$
I_{KCa} (BC)	0.0002	0.0002	p =1	$\frac{0.28[Ca^{2+}]}{[Ca^{2+}]+\exp1(0.00048,0.84,v)}$	$\frac{0.48}{1+[Ca^{2+}]/\exp1(0.13e^{-6},1,v)}$
I_H (OLM)	0.00002	0.00002	p = 1	$\exp1 -0.00048\exp[\frac{0.12Fv}{}]$ $x_\infty = \frac{1}{\exp[(84.1-v)/10.2]+1}$	$\exp1 -0.13e^{-6}\exp[\frac{Fv}{}]$ τ_x (ms) = $\frac{1}{\exp[0.116v-17.9]+\exp[0.09v-1.84]}$
I_{CaL}	0.09	0.09	p = 2	$\frac{15.69(81.5-v)}{\exp[(81.5-v)/10]-1}$	$0.29\exp[-v/10.86]$
I_{CaN} (BC)	0.0008	0.0008	p =2 q = 1	$\frac{0.19(19.98-v)}{\exp[(19.98-v)/10]-1}$ $0.00016\exp[-v/48.4]$	$0.046\exp[-v/20.73]$ $\frac{1}{\exp[(39-v)/10]+1}$
I_{CaT} (OLM)	0.0005	0.0005	p =2 q = 1	$\frac{0.2(19.26-v)}{\exp[(19.26-v)/10]-1}$ $0.00016\exp[-v/16.26]$	$0.009\exp[-v/22.03]$ $\frac{1}{\exp[(29.79-v)/10]+1}$
I_{KAHP}	0.00002	0.00002	p = 1	$1.25*10^{13}[Ca^{2+}]_i^4$	0.00025
I_A	BC-0.00015; OLM-0.08	BC-0.00015; OLM-0.0001	p = 1 q = 1	$0.02\exp[\left(1.8(v+33.6).\frac{F}{RT}\right)]$ $0.08\exp[\left(4(v+83).\frac{F}{RT}\right)]$	$0.02\exp[\left(-1.2(v+33.6).\frac{F}{RT}\right)]$ 0.08
Diam. (μm) Length(μm)	BC-15; OLM-10 20	BC-2.5; OLM-3 BC-300;	C_m = BC-2.5; E_{Na} = 55	R_{axial} = BC-100; OLM-150 Ω-cm E_K = -90 mV $x_\infty = \frac{\alpha}{\alpha+\beta}$	G_{leak} = BC-0.0002; OLM-0.0003 E_{leak} = -64 (BC); -60 (OLM) mV τ_x (ms) = $\frac{1}{\alpha+\beta}$

FIGURES

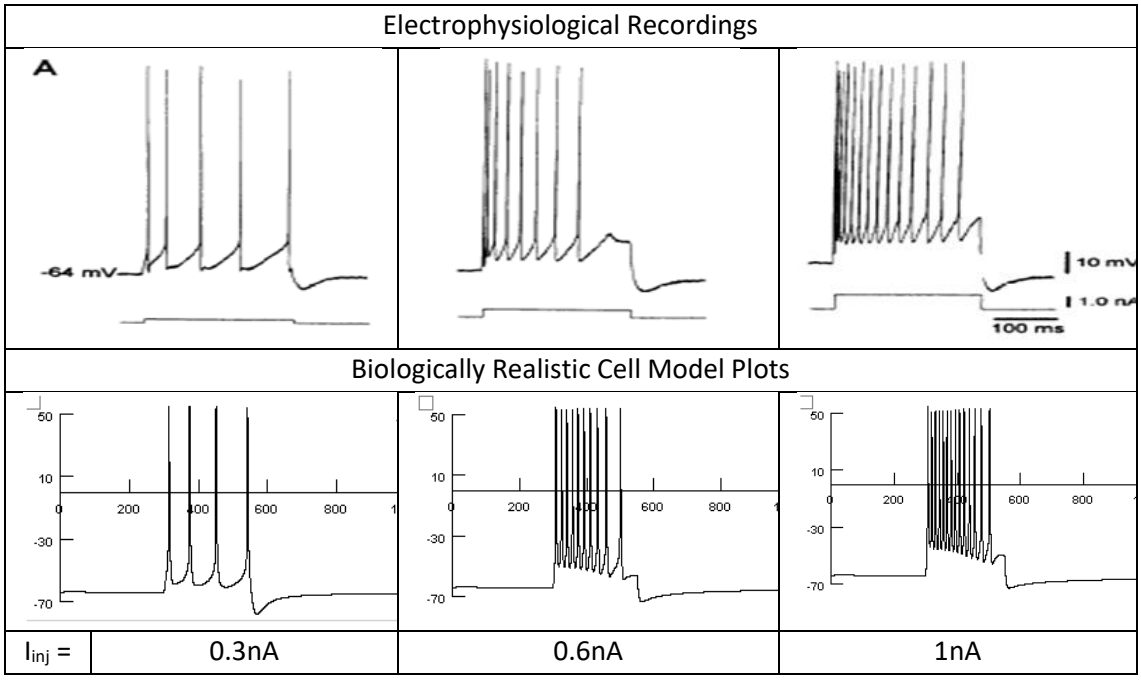

Figure 10A: Electrophysiological recordings and cell model voltage plots of Entorhinal Cortex Layer II Stellate Cell to current injections of 0.3, 0.6 and 1.0nA for 500ms. The biological recordings are shown above with the model simulations below for several current injections.

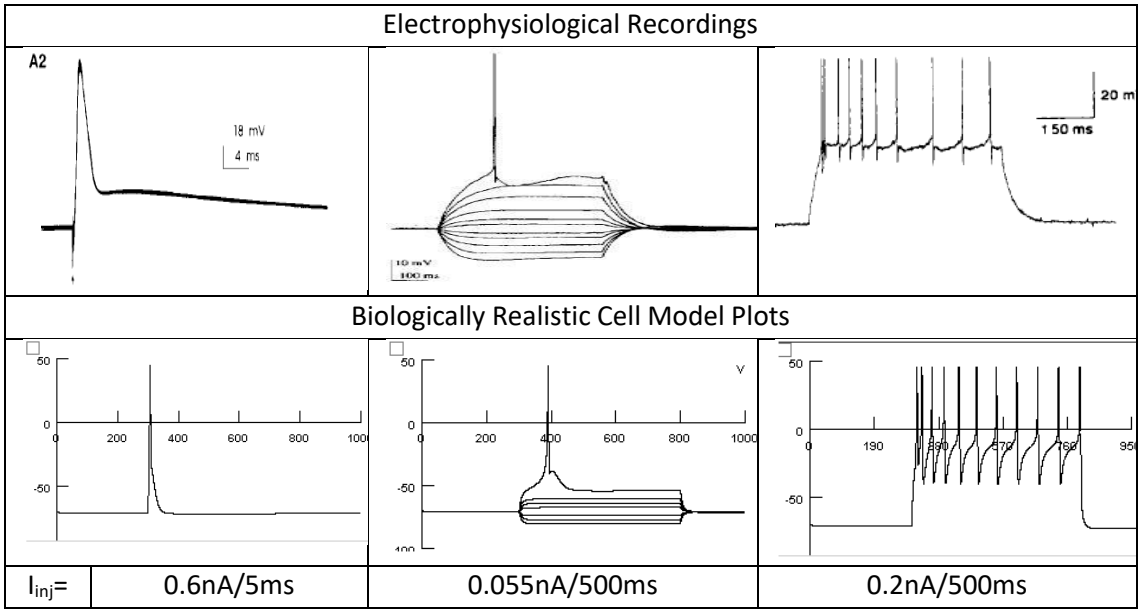

Figure 10B: Electrophysiological recordings and cell model plots of Dentate Granule Cell to current injections of 0.6nA for 5ms, 0.055 and 0.2 nA for 500ms. The biological recordings are shown above with the model simulations below for several current injections.

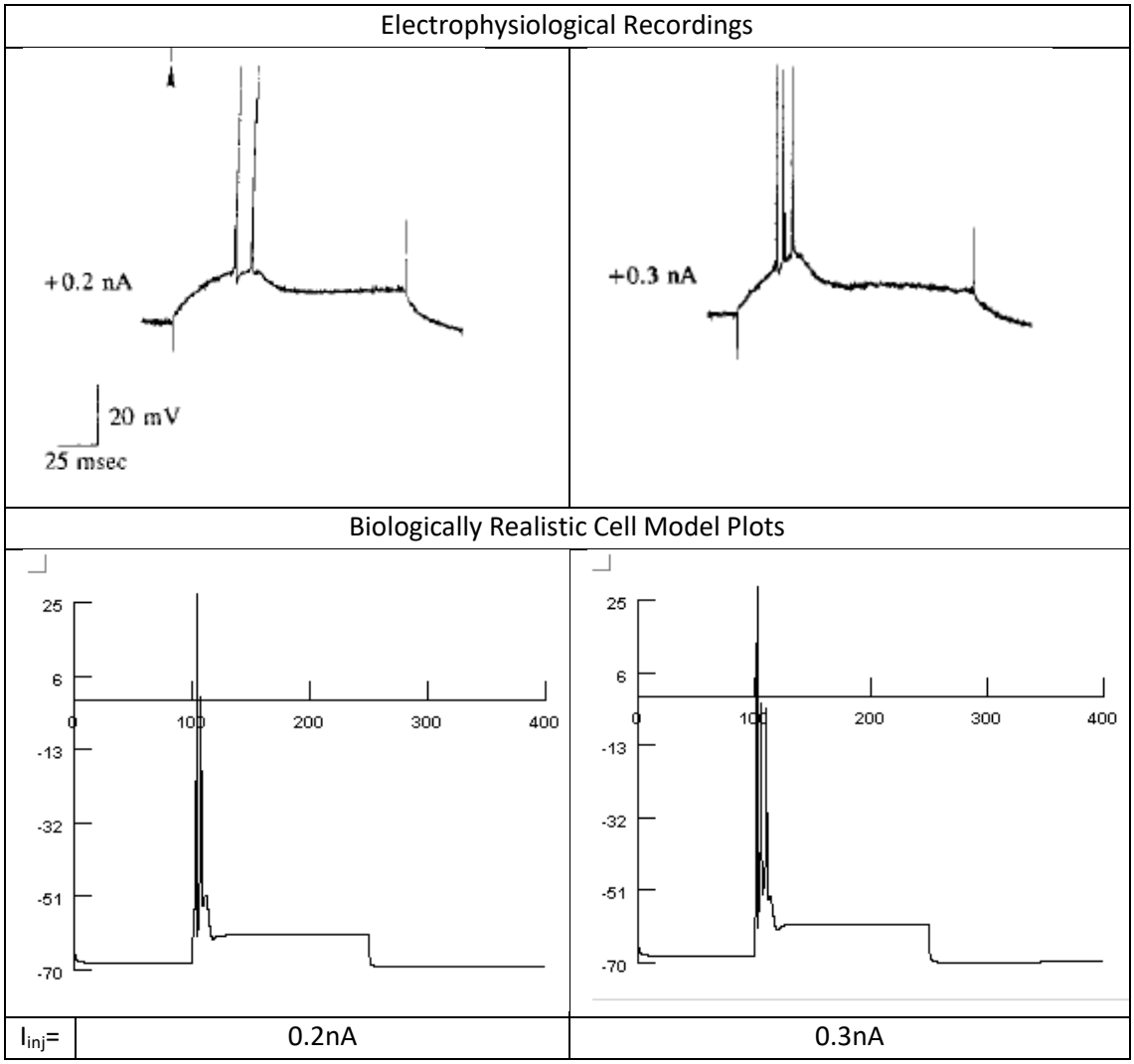

Figure 10C: Electrophysiological recordings and cell model plots of CA3 Spiny Pyramidal Cell to current injections of 0.2 and 0.3nA for 250ms. The biological recordings are shown above with the model simulations below for several current injections.

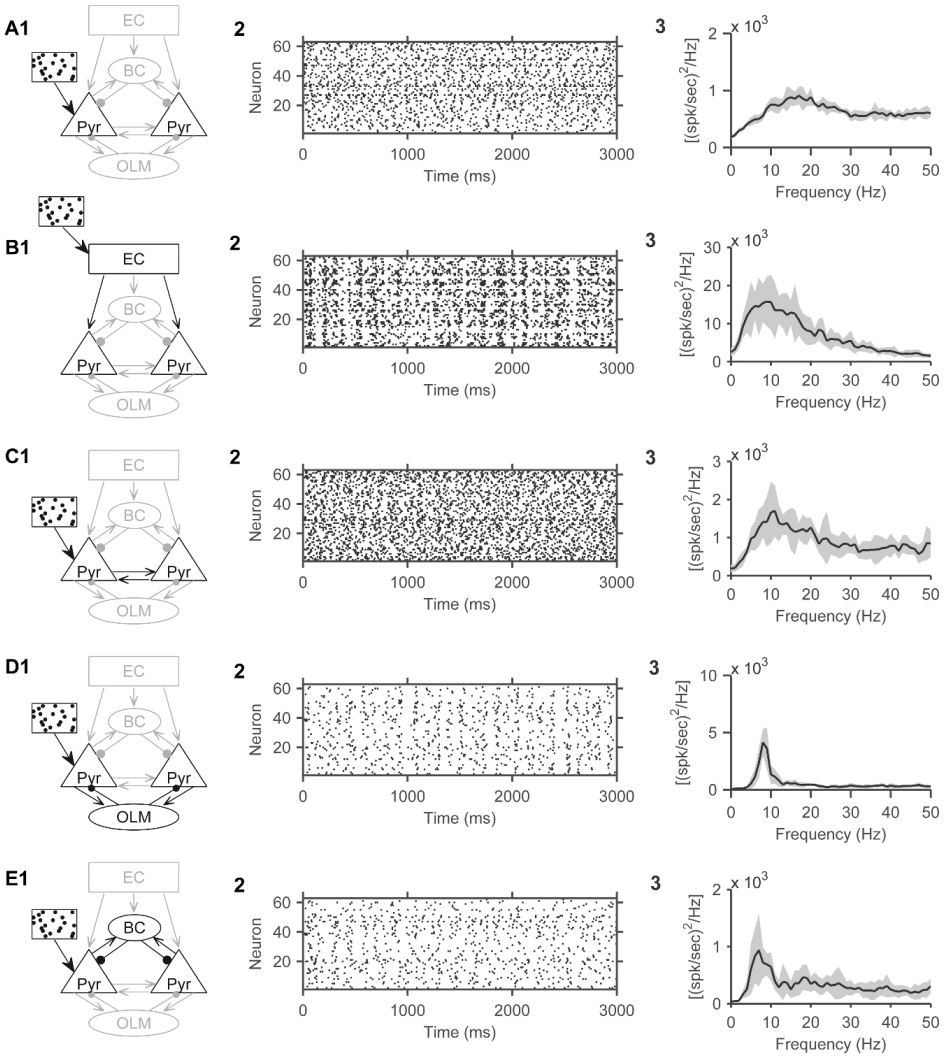

Figure 10D. Multiple generators of theta oscillations in the hippocampal ca3 network.

Adapted from Hummos and Nair (2017).

Suggested figures for future work:

Figure 2: Pyramidal cells slow currents and olm-pyramidal cells loop are the two resonant mechanisms.

A) The power spectra of 6 simulations. The 'None' experiment had no theta generating components with isolated pyramidal cells with no slow currents, and direct unique Poisson input with no correlations. The following experiments activated one theta component at a time and examined the power spectrum. The recurrent connections were activated in '+RC' and produced a small bump in the 2-4 Hz range. BCs activated in '+BC' produced no spectral peaks. Routing input through the EC added correlations in the external input and shift the power to low frequencies but did not produce theta peaks. Adding OLM cells '+OLM' produced a robust theta peak. Activating the slow currents in pyramidal cells also produced a small but significant peak in theta frequencies '+RES'. B) relative theta calculations. '+RC', '+EC' increased relative theta due to a less specific increase in slow frequency power. C) firing rates were kept within physiological range using the following current injections. None: 7 mA, +RC 8 mA, +BC 5 mA, +EC 10 mA, +OLM 1 mA, +RES 1 mA.

Figure 3: Resonant mechanisms can substitute for and compete with each other.

A) Schematic of this experiment with EC inactivated and input directly arriving at CA3 pyramidal cells. Both OLM cells, BCs, and the recurrent excitatory connections were active.

B) The power spectra of four experiments as follows: "full" simulated with both OLM cells and adaptation in pyramidal cells intact, "-OLM" was run with OLM cells inactivated, "-sPYR" had OLM cells intact but adaptation and h-current were removed from pyramidal cells, and finally "-both" had both pyramidal cells slow currents and OLM cells inactivated. The power spectra indicate that theta activity persisted with at least one resonant mechanism intact, but also interestingly showed that pyramidal cells adaptation as a resonant component may have interfered with the OLM-pyramidal cells resonator.

C) Relative power in the theta band (4-12 Hz) divided by total power (0-50 Hz) and normalized to the value of the "full" model run.

D) Shows the results of our procedure using constant current injections to cells to maintain a population average firing rate consistent with physiological data, to compensate for the variation in firing rates resulting from inactivating various network components. Current injections to pyramidal cells in the different experiments were as follows. Full: 3.5 mA, -OLM: 4.2 mA, -sPYR: 3 mA, -Both: 8.2 mA.

Figure 4: Functional separation at the extremes of cholinergic modulation minimizes interference between resonating mechanisms.

Current injections to compensate for variation in firing rates: ACh 0: Full: -2 mA, -OLM: -2 mA, -sPYR: 0 mA, -Both: 2 mA. ACh 1: Full: 3.5 mA, -OLM: 4.2 mA, -sPYR: 3 mA, -Both: 8.2 mA. ACh 2: Full: 4 mA, -OLM: 5 mA, -sPYR: 3.5 mA, -Both: 8.5 mA.

Figure 5: Synchronizing Mechanisms Can Substitute for Or Interfere With One Another

Recurrent connections and EC were inactivated, leaving the two synchronizing mechanisms in the model, OLM cells and BC cells. We tested three conditions, first with both OLM and BC cells active (+OLM +BC), and then with BCs inactivated (+OLM -BC) and finally, with OLM cells inactivated (-OLM +BC). Running the three conditions under three different cholinergic states revealed different interaction modes between the two synchronizing mechanisms. In low ACh, they were equally effective at generating theta, and only one mechanism appeared necessary. With increasing cholinergic levels, BCs contribution to theta diminished, and in high cholinergic states they interfered with OLM generated theta. Current injections to compensate for variation in firing rates: ACh 0: +both: -7 mA, -BC: -6.5 mA, -OLM: -7.5 mA. ACh 1: +both: -3 mA, -BC: 1 mA, -OLM: -6.1 mA. ACh 2: +both: -1 mA, -BC: 2.8 mA, -OLM: 1.4 mA.

Figure 6: Recurrent connections and bcs cooperatively synchronize theta oscillations.

OLM cells and EC were inactivated, leaving the two synchronizing mechanisms in the model, recurrent connections and BC cells. We tested three conditions, first with both recurrent connections and BC cells active (+RC +BC), and then with BCs inactivated (+RC -BC) and finally, with recurrent connections inactivated (-RC +BC). Running the three conditions under three different cholinergic states revealed a stable engagement of BCs in theta generation while recurrent connection had a stronger engagement in lower cholinergic states. Current injections to compensate for variation in firing rates: ACh 0: +both: 5 mA, -BC: 6 mA, -RC: 1 mA. ACh 1: +both: 2 mA, -BC: 5 mA, -RC: -2 mA. ACh 2: +both: -2 mA, -BC: 5 mA, -RC: -2 mA

REFERENCES

Acsady L, Kamondi A, Sik A, Freund T, Buzsaki G (1998), GABAergic cells are the major postsynaptic targets of mossy fibers in the rat hippocampus. J Neurosci 18:3386-3403.

Ali AB, Deuchars J, Pawelzik H, Thomson AM (1998), CA1 pyramidal to basket and bistratified cell EPSPs: dual intracellular recordings in rat hippocampal slices. J Physiol 507 (Pt 1):201-217.

Ali AB, Thomson AM (1998), Facilitating pyramid to horizontal oriens-alveus interneurone inputs: dual intracellular recordings in slices of rat hippocampus. J Physiol 507 (Pt 1):185-199.

Alonso A, Garcia-Austt E (1987), Neuronal sources of theta rhythm in the entorhinal cortex of the rat. II. Phase relations between unit discharges and theta field potentials. Exp Brain Res 67:502-509.

Amilhon B, Huh CY, Manseau F, Ducharme G, Nichol H, Adamantidis A, Williams S (2015), Parvalbumin Interneurons of Hippocampus Tune Population Activity at Theta Frequency. Neuron 86:1277-1289.

Augustin M, Ladenbauer J, Obermayer K (2013), How adaptation shapes spike rate oscillations in recurrent neuronal networks. Front Comput Neurosci 7:9.

Barry C, Heys JG, Hasselmo ME (2012), Possible role of acetylcholine in regulating spatial novelty effects on theta rhythm and grid cells. Front Neural Circuits 6:5.

Bartos M, Sauer J-F, Vida I, Kulik Á (2010) Fast and Slow GABAergic Transmission in Hippocampal Circuits. In: Hippocampal Microcircuits: A Computational Modeler's Resource Book, vol. (Cutsuridis V, Graham B, Cobb S, Vida I, eds), pp. 129-161. New York, NY: Springer New York.

Baude A, Bleasdale C, Dalezios Y, Somogyi P, Klausberger T (2007), Immunoreactivity for the GABAA receptor alpha1 subunit, somatostatin and

Connexin36 distinguishes axoaxonic, basket, and bistratified interneurons of the rat hippocampus. Cereb Cortex 17:2094-2107.

Bezaire MJ, Raikov I, Burk K, Vyas D, Soltesz I (2016), Interneuronal mechanisms of hippocampal theta oscillations in a full-scale model of the rodent CA1 circuit. eLife 5:e18566.

Boyce R, Glasgow SD, Williams S, Adamantidis A (2016), Causal evidence for the role of REM sleep theta rhythm in contextual memory consolidation. Science 352:812-816.

Brazhnik ES, Vinogradova OS (1986), Control of the neuronal rhythmic bursts in the septal pacemaker of theta-rhythm: effects of anaesthetic and anticholinergic drugs. Brain Res 380:94-106.

Brown JT, Randall AD (2009), Activity-dependent depression of the spike after-depolarization generates long-lasting intrinsic plasticity in hippocampal CA3 pyramidal neurons. J Physiol 587:1265-1281.

Brunel N, Wang XJ (2003), What determines the frequency of fast network oscillations with irregular neural discharges? I. Synaptic dynamics and excitation-inhibition balance. J Neurophysiol 90:415-430.

Buhl EH, Szilagyi T, Halasy K, Somogyi P (1996), Physiological properties of anatomically identified basket and bistratified cells in the CA1 area of the rat hippocampus in vitro. Hippocampus 6:294-305.

Burgess N (2008), Grid cells and theta as oscillatory interference: theory and predictions. Hippocampus 18:1157-1174.

Buzsáki G (2002), Theta Oscillations in the Hippocampus. Neuron 33:325-340.

Buzsaki G, Leung LW, Vanderwolf CH (1983), Cellular bases of hippocampal EEG in the behaving rat. Brain Res 287:139-171.

Buzsáki G, Wang X-J (2012), Mechanisms of Gamma Oscillations. Annu Rev Neurosci 35:203-225.

Carnevale NT HM (2009), The NEURON Book. Cambridge University Press.

Cea-del Rio CA, Lawrence JJ, Tricoire L, Erdelyi F, Szabo G, McBain CJ (2010), M3 muscarinic acetylcholine receptor expression confers differential cholinergic modulation to neurochemically distinct hippocampal basket cell subtypes. J Neurosci 30:6011-6024.

Cobb S, Lawrence JJ (2010) Neuromodulation of Hippocampal Cells and Circuits. In: Hippocampal Microcircuits: A Computational Modeler's Resource Book, vol. (Cutsuridis V, Graham B, Cobb S, Vida I, eds), pp. 187-246. New York, NY: Springer New York.

Cobb SR, Buhl EH, Halasy K, Paulsen O, Somogyi P (1995), Synchronization of neuronal activity in hippocampus by individual GABAergic interneurons. Nature 378:75-78.

Colgin LL (2013), Mechanisms and Functions of Theta Rhythms. Annu Rev Neurosci 36:295-312.

Crook SM, Ermentrout GB, Bower JM (1998), Spike frequency adaptation affects the synchronization properties of networks of cortical oscillations. Neural Comput 10:837-854.

Destexhe A MZ, Sejnowski TJ (1998), Kinetic models of synaptic transmission. Methods Neuronal Model 2:1-25.

Eacott MJ, Norman G (2004), Integrated Memory for Object, Place, and Context in Rats: A Possible Model of Episodic-Like Memory? The Journal of Neuroscience 24:1948.

Eberhard B, Miles W (2009), Local Circuits. The Hippocampus Book.

Ferguson KA, Chatzikalymniou AP, Skinner FK (2017), Combining Theory, Model, and Experiment to Explain How Intrinsic Theta Rhythms Are Generated in an In Vitro Whole Hippocampus Preparation without Oscillatory Inputs. eNeuro 4:ENEURO.0131-0117.2017.

Fortin NJ, Wright SP, Eichenbaum H (2004), Recollection-like memory retrieval in rats is dependent on the hippocampus. Nature 431:188-191.

Fuhrmann G, Markram H, Tsodyks M (2002), Spike frequency adaptation and neocortical rhythms. J Neurophysiol 88:761-770.

Geiger JR, Lubke J, Roth A, Frotscher M, Jonas P (1997), Submillisecond AMPA receptor-mediated signaling at a principal neuron-interneuron synapse. Neuron 18:1009-1023.

Gigante G, Del Giudice P, Mattia M (2007), Frequency-dependent response properties of adapting spiking neurons. Math Biosci 207:336-351.

Gillies MJ, Traub RD, LeBeau FE, Davies CH, Gloveli T, Buhl EH, Whittington MA (2002), A model of atropine-resistant theta oscillations in rat hippocampal area CA1. J Physiol 543:779-793.

Giocomo LM, Hussaini SA, Zheng F, Kandel ER, Moser MB, Moser EI (2011), Grid cells use HCN1 channels for spatial scaling. Cell 147:1159-1170.

Giovannini MG, Rakovska A, Benton RS, Pazzagli M, Bianchi L, Pepeu G (2001), Effects of novelty and habituation on acetylcholine, GABA, and glutamate release from the frontal cortex and hippocampus of freely moving rats. Neuroscience 106:43-53.

Gloveli T, Dugladze T, Rotstein HG, Traub RD, Monyer H, Heinemann U, Whittington MA, Kopell NJ (2005), Orthogonal arrangement of rhythm-generating microcircuits in the hippocampus. Proc Natl Acad Sci U S A 102:13295-13300.

Hasselmo ME, Fehlau BP (2001), Differences in time course of ACh and GABA modulation of excitatory synaptic potentials in slices of rat hippocampus. J Neurophysiol 86:1792-1802.

Hasselmo ME, Schnell E, Barkai E (1995), Dynamics of learning and recall at excitatory recurrent synapses and cholinergic modulation in rat hippocampal region CA3. J Neurosci 15:5249-5262.

Hefft S, Jonas P (2005), Asynchronous GABA release generates long-lasting inhibition at a hippocampal interneuron-principal neuron synapse. Nat Neurosci 8:1319-1328.

Hoseini MS, Wessel R (2016), Coherent and intermittent ensemble oscillations emerge from networks of irregular spiking neurons. J Neurophysiol 115:457-469.

Hoskison MM, Connor JA, Shuttleworth CW (2004), GABA(B)-receptor modulation of short-term synaptic depression at an excitatory input to murine hippocampal CA3 pyramidal neurons. Neurosci Lett 365:48-53.

Hosseini-Sharifabad M, Nyengaard JR (2007), Design-based estimation of neuronal number and individual neuronal volume in the rat hippocampus. J Neurosci Methods 162:206-214.

Hu H, Vervaeke K, Storm JF (2002), Two forms of electrical resonance at theta frequencies, generated by M-current, h-current and persistent Na+ current in rat hippocampal pyramidal cells. J Physiol 545:783-805.

Hummos A, Franklin Charles C, Nair Satish S (2014), Intrinsic mechanisms stabilize encoding and retrieval circuits differentially in a hippocampal network model. Hippocampus 24:1430-1448.

Hummos A, Nair SS (2017), An integrative model of the intrinsic hippocampal theta rhythm. PLoS One 12:e0182648.

Hutcheon B, Yarom Y (2000), Resonance, oscillation and the intrinsic frequency preferences of neurons. Trends Neurosci 23:216-222.

Ishizuka N, Weber J, Amaral DG (1990), Organization of intrahippocampal projections originating from CA3 pyramidal cells in the rat. J Comp Neurol 295:580-623.

Jung MW, McNaughton BL (1993), Spatial selectivity of unit activity in the hippocampal granular layer. Hippocampus 3:165-182.

Katona I, Acsady L, Freund TF (1999), Postsynaptic targets of somatostatin-immunoreactive interneurons in the rat hippocampus. Neuroscience 88:37-55.

Kazanovich Y, Burylko O, Borisyuk R (2013), Competition for synchronization in a phase oscillator system. Physica D: Nonlinear Phenomena 261:114-124.

Kim D, Pare D, Nair SS (2013), Assignment of model amygdala neurons to the fear memory trace depends on competitive synaptic interactions. J Neurosci 33:14354-14358.

Kim D, Pare D, Nair SS (2013), Mechanisms contributing to the induction and storage of Pavlovian fear memories in the lateral amygdala. Learn Mem 20:421-430.

Koch C SI (1998), Methods in neuronal modeling: from ions to networks. MIT Press.

Kocsis B, Bragin A, Buzsaki G (1999), Interdependence of multiple theta generators in the hippocampus: a partial coherence analysis. J Neurosci 19:6200-6212.

Kosaka T, Katsumaru H, Hama K, Wu JY, Heizmann CW (1987), GABAergic neurons containing the Ca2+-binding protein parvalbumin in the rat hippocampus and dentate gyrus. Brain Res 419:119-130.

Kremin T, Hasselmo ME (2007), Cholinergic suppression of glutamatergic synaptic transmission in hippocampal region CA3 exhibits laminar selectivity: Implication for hippocampal network dynamics. Neuroscience 149:760-767.

Lawrence JJ, Statland JM, Grinspan ZM, McBain CJ (2006), Cell type-specific dependence of muscarinic signalling in mouse hippocampal stratum oriens interneurones. J Physiol 570:595-610.

Leung LS, Shen B (2004), Glutamatergic synaptic transmission participates in generating the hippocampal EEG. Hippocampus 14:510-525.

Li G, Amano T, Pare D, Nair SS (2011), Impact of infralimbic inputs on intercalated amygdala neurons: a biophysical modeling study. Learn Mem 18:226-240.

Maccaferri G (2005), Stratum oriens horizontal interneurone diversity and hippocampal network dynamics. J Physiol 562:73-80.

MacDonald Christopher J, Lepage Kyle Q, Eden Uri T, Eichenbaum H (2011), Hippocampal “Time Cells” Bridge the Gap in Memory for Discontiguous Events. Neuron 71:737-749.

Madison DV, Nicoll RA (1984), Control of the repetitive discharge of rat CA 1 pyramidal neurones in vitro. J Physiol 354:319-331.

McQuiston AR, Madison DV (1999), Muscarinic receptor activity has multiple effects on the resting membrane potentials of CA1 hippocampal interneurons. J Neurosci 19:5693-5702.

McQuiston AR, Madison DV (1999), Nicotinic receptor activation excites distinct subtypes of interneurons in the rat hippocampus. J Neurosci 19:2887-2896.

Miranda MaI, Ramírez-Lugo L, Bermúdez-Rattoni F (2000), Cortical cholinergic activity is related to the novelty of the stimulus. Brain Res 882:230-235.

Misgeld U, Muller W, Polder HR (1989), Potentiation and suppression by eserine of muscarinic synaptic transmission in the guinea-pig hippocampal slice. J Physiol 409:191-206.

Mizuseki K, Buzsaki G (2013), Preconfigured, skewed distribution of firing rates in the hippocampus and entorhinal cortex. Cell Rep 4:1010-1021.

Mizuseki K, Royer S, Diba K, Buzsaki G (2012), Activity dynamics and behavioral correlates of CA3 and CA1 hippocampal pyramidal neurons. Hippocampus 22:1659-1680.

Mumby DG, Gaskin S, Glenn MJ, Schramek TE, Lehmann H (2002), Hippocampal damage and exploratory preferences in rats: memory for objects, places, and contexts. Learn Mem 9:49-57.

Naber PA, Caballero-Bleda M, Jorritsma-Byham B, Witter MP (1997), Parallel input to the hippocampal memory system through peri- and postrhinal cortices. Neuroreport 8:2617-2621.

Nagode DA, Tang A-H, Yang K, Alger BE (2014), Optogenetic identification of an intrinsic cholinergically driven inhibitory oscillator sensitive to cannabinoids and opioids in hippocampal CA1. The Journal of Physiology 592:103-123.

Neymotin SA, Hilscher MM, Moulin TC, Skolnick Y, Lazarewicz MT, Lytton WW (2013), Ih tunes theta/gamma oscillations and cross-frequency coupling in an in silico CA3 model. PLoS One 8:e76285.

Nolan MF, Malleret G, Dudman JT, Buhl DL, Santoro B, Gibbs E, Vronskaya S, Buzsaki G, et al. (2004), A behavioral role for dendritic integration: HCN1 channels constrain spatial memory and plasticity at inputs to distal dendrites of CA1 pyramidal neurons. Cell 119:719-732.

O'Keefe J, Dostrovsky J (1971), The hippocampus as a spatial map. Preliminary evidence from unit activity in the freely-moving rat. Brain Res 34:171-175.

Orban G, Kiss T, Erdi P (2006), Intrinsic and synaptic mechanisms determining the timing of neuron population activity during hippocampal theta oscillation. J Neurophysiol 96:2889-2904.

Pastalkova E, Itskov V, Amarasingham A, Buzsaki G (2008), Internally generated cell assembly sequences in the rat hippocampus. Science 321:1322-1327.

Pendyam S, Bravo-Rivera C, Burgos-Robles A, Sotres-Bayon F, Quirk GJ, Nair SS (2013), Fear signaling in the prelimbic-amygdala circuit: a computational modeling and recording study. J Neurophysiol 110:844-861.

Pouille F, Scanziani M (2004), Routing of spike series by dynamic circuits in the hippocampus. Nature 429:717-723.

Rotstein HG (2015), Subthreshold amplitude and phase resonance in models of quadratic type: Nonlinear effects generated by the interplay of resonant and amplifying currents. J Comput Neurosci 38:325-354.

Rotstein HG, Pervouchine DD, Acker CD, Gillies MJ, White JA, Buhl EH, Whittington MA, Kopell N (2005), Slow and fast inhibition and an H-current interact to create a theta rhythm in a model of CA1 interneuron network. J Neurophysiol 94:1509-1518.

Royer S, Zemelman BV, Losonczy A, Kim J, Chance F, Magee JC, Buzsaki G (2012), Control of timing, rate and bursts of hippocampal place cells by dendritic and somatic inhibition. Nat Neurosci 15:769-775.

Samarth P, Ball JM, Unal G, Paré D, Nair SS (2017), Mechanisms of memory storage in a model perirhinal network. Brain Structure and Function 222:183-200.

Seress L, Pokorny J (1981), Structure of the granular layer of the rat dentate gyrus. A light microscopic and Golgi study. J Anat 133:181-195.

Sik A, Penttonen M, Ylinen A, Buzsaki G (1995), Hippocampal CA1 interneurons: an in vivo intracellular labeling study. J Neurosci 15:6651-6665.

Staley KJ, Otis TS, Mody I (1992), Membrane properties of dentate gyrus granule cells: comparison of sharp microelectrode and whole-cell recordings. J Neurophysiol 67:1346-1358.

Stark E, Eichler R, Roux L, Fujisawa S, Rotstein HG, Buzsaki G (2013), Inhibition-induced theta resonance in cortical circuits. Neuron 80:1263-1276.

Steckler T, Drinkenburg WHIM, Sahgal A, Aggleton JP (1998), RECOGNITION MEMORY IN RATS—I.CONCEPTS AND CLASSIFICATION. Prog Neurobiol 54:289-311.

Steckler T, Drinkenburg WHIM, Sahgal A, Aggleton JP (1998), Recognition memory in rats—II. Neuroanatomical substrates. Prog Neurobiol 54:313-332.

Steckler T, Sahgal A, Aggleton JP, Drinkenburg WH (1998), Recognition memory in rats--III. Neurochemical substrates. Prog Neurobiol 54:333-348.

Stewart M, Fox SE (1990), Do septal neurons pace the hippocampal theta rhythm? Trends Neurosci 13:163-168.

Stumpf C, Petsche H, Gogolak G (1962), The significance of the rabbit's septum as a relay station between the midbrain and the hippocampus. II. The differential influence of drugs upon both the septal cell firing pattern and the hippocampus theta activity. Electroencephalogr Clin Neurophysiol 14:212-219.

Tóth K (2010) Glutamatergic Neurotransmission in the Hippocampus. In: Hippocampal Microcircuits: A Computational Modeler's Resource Book, vol. (Cutsuridis V, Graham B, Cobb S, Vida I, eds), pp. 99-128. New York, NY: Springer New York.

Toth K, Suares G, Lawrence JJ, Philips-Tansey E, McBain CJ (2000), Differential mechanisms of transmission at three types of mossy fiber synapse. J Neurosci 20:8279-8289.

Vanderwolf CH (1969), Hippocampal electrical activity and voluntary movement in the rat. Electroencephalogr Clin Neurophysiol 26:407-418.

Varela JA, Sen K, Gibson J, Fost J, Abbott LF, Nelson SB (1997), A quantitative description of short-term plasticity at excitatory synapses in layer 2/3 of rat primary visual cortex. J Neurosci 17:7926-7940.

Vida I (2010) Morphology of Hippocampal Neurons. In: Hippocampal Microcircuits: A Computational Modeler's Resource Book, vol. (Cutsuridis V, Graham B, Cobb S, Vida I, eds), pp. 27-67. New York, NY: Springer New York.

Vinogradova OS (1995), Expression, control, and probable functional significance of the neuronal theta-rhythm. Prog Neurobiol 45:523-583.

Vogt KE, Regehr WG (2001), Cholinergic modulation of excitatory synaptic transmission in the CA3 area of the hippocampus. J Neurosci 21:75-83.

Witter MP (2010) Connectivity of the Hippocampus. In: Hippocampal Microcircuits: A Computational Modeler's Resource Book, vol. (Cutsuridis V, Graham B, Cobb S, Vida I, eds), pp. 5-26. New York, NY: Springer New York.

Wittner L, Henze DA, Zaborszky L, Buzsaki G (2006), Hippocampal CA3 pyramidal cells selectively innervate aspiny interneurons. Eur J Neurosci 24:1286-1298.

Wittner L, Henze DA, Zaborszky L, Buzsaki G (2007), Three-dimensional reconstruction of the axon arbor of a CA3 pyramidal cell recorded and filled in vivo. Brain Struct Funct 212:75-83.

Woolf NJ (1991), Cholinergic systems in mammalian brain and spinal cord. Prog Neurobiol 37:475-524.

Wulff P, Ponomarenko AA, Bartos M, Korotkova TM, Fuchs EC, Bähner F, Both M, Tort ABL, et al. (2009), Hippocampal theta rhythm and its coupling with gamma oscillations require fast inhibition onto parvalbumin-positive interneurons. Proceedings of the National Academy of Sciences 106:3561.

Zemankovics R, Kali S, Paulsen O, Freund TF, Hajos N (2010), Differences in subthreshold resonance of hippocampal pyramidal cells and interneurons: the role of h-current and passive membrane characteristics. J Physiol 588:2109-2132.

CHAPTER 5 – SUMMARY

Biological neuronal networks are vastly complex and understanding or predicting the scientific principles that underlie the behavior and interactions of complex neural circuits is a monumental task. Despite the inherent challenges, neuroscientists have developed techniques to study neuronal functions from molecular to network level. Among the tools available to study neuroscience, engineering tools such as computational modeling are gaining popularity every day and are playing an important role. Computational modeling allows the investigation of hypotheses with large parameter variation at multiple levels of depth thus saving the considerable time and money that are inherently required for biological experimentation. Specific predictions made by the model can be tested with biological experiments to confirm the results. Models can be developed with different levels of abstraction depending on the function under study. Networks of neuronal modes can be constructed using realistic synaptic connections with short-term/ long-term plasticity if required to study biological processes and systems involving larger scale structures.

Here we have presented two studies that demonstrate the utility of modeling to address hypotheses in these unique systems at various levels of detail.

CHAPTER 2- In Chapter 2, we investigate the functioning of lower urinary tract (LUT) during filling/ voiding and also after spinal cord injury. LUT function is controlled by many involuntary reflexes and also have a neural control for voluntary voiding. Afferent nerves of LUT which carry sensory information across multiple levels of spinal cord are

responsible for several aspects of functioning in normal case. However, after spinal cord injury some of this information is not conveyed to higher order centers which is responsible for voluntary voiding and if this descending input is lost it leads to urinary incontinence. Studying the LUT circuit involves thorough testing of afferents, efferents and mediating neurons in the LUT circuit to get insights. The current model provides a framework at the cellular level for such a study and we investigate how guarding reflex and other parasympathetic and sympathetic reflexes work. We developed a cellular and network level biophysical model with rodent data and implemented closed loop calculation of pressure with efferent firing rate and volume and in-turn using the calculated pressure to estimate afferent firing rate which is then incorporated into the feedback loops appropriately.

Future work:

- There are variations in electrophysiological and functional properties of circuit elements between species, sex and across developmental changes. It is not feasible to make models for all species and this may not necessary. The long-term goal is to study dysfunctions in humans via stimulation or other intervention is the long-term goal, and it is believed that rodent and cat models may provide sufficient background to develop ideas for stimulation techniques that might be relevant for humans. We are currently working on a rodent model which should provide guidelines for further studies.
- Current model focusses primarily of functioning of LUT at spinal level with descending input from higher order center. However, there are complex computations that happen at these supraspinal stages and there are existing

networks that can be incorporated. At the other end there are models being developed of detrusor muscle also, if we can incorporate both to existing model this will increase the testing range of the model and gives a fully functioning model with several targets for interventions using electrical stimulation or chemical stimulation depending on dysfunction.

- Currently there is several gaps in the data related to dysfunctions of the circuit elements, e.g., after spinal cord injury. These gaps need to be filled in as data becomes available. But the nature of current model framework allows for testing part of the model where data is available.
- Finally, the present model is primarily at the cellular and network levels of the LUT. Molecular and genomic pathways are important elements of the overall problem, including in the various ganglia and in the bladder, and these levels are typically the targets of therapeutic interventions. Again, the modeling framework we propose can integrate these elements.

CHAPTER 3 - In chapter 3, we explore the interactions of intrinsic theta generators in rodent hippocampus. This work builds on a previously published work from our lab (Hummos et al., 2017). Previously we have shown that theta rhythm can be generated intrinsically to hippocampus identifying several generators. In current study we classify the intrinsic generators as resonators and synchronizing and show that for reliable rhythm generation we need at least one resonant and one synchronizing components. The model had Izhikevich models for principal cells in CA3 and the two abundant interneuron types basket cells (BCs) and oriens lacunosum-moleculare (OLM) interneurons, and the present

study incorporated realistic synapses among and between these interneurons. The network model also included synaptic currents such as AMPA, NMDA, GABA. Other aspects of the model include short-term synaptic plasticity, spatial connectivity patterns and known effects of acetylcholine.

Future work:

- To improve the model with more testable parameters and to add biological realism into the model, all single cell models will be tuned to match biological data using Hodgkin-Huxley formulation and model will be scaled to full rodent brain cell numbers.
- The current modeling framework can be easily adapted to study slow-gamma, fast-gamma and spontaneous gamma rhythms in hippocampus. Also, there is considerable interactions among theta and gamma rhythms. Future work will include reproduction of local field potential (LFP) data in addition to unit data which can help provide more reliable and experimentally validated predictions.

CHAPTER 4 - In chapter 4, we focus in-depth on model development process. We provide overview of the amygdala and its role in acquisition and expression of fear. We discuss how computational models can be used to investigate the fear circuit in mammals. We provide information on three popular biological based single cell model types such as integrate-and-fire, Izhikevich and biophysical model neuron. We then show step-by-step illustration of how we can go about developing the biophysical single cell models and the models developed are made publicly accessible. This chapter also

focusses on the challenges in modeling such models and how they can complement actual experimentation.

Future work:

- As more computational power becomes more accessible full-size networks can be modeled. Effective way to incorporate neuromodulation into the model need to be investigated. Many brain functions involve several brain regions and it is worth investing time to develop techniques to effectively these networks without the limitation of computational strain.

APPENDIX

Amygdala Models

INTRODUCTION

The mammalian amygdala has been the topic of intensive research, due largely to its prominent role in the acquisition, consolidation, and storage of memories associated with emotional events, including those related to reward (Baxter & Murray, 2002; Murray, 2007; Schulz, 2007) and aversive (LeDoux, 2008) memories. Emotional memory is viewed as an implicit or unconscious form of memory and contrasts with explicit or declarative memory mediated by the hippocampus. The amygdala has been shown to participate in a wide range of normal behavioral functions and psychiatric conditions (LeDoux 2002), and its structure and basic circuit connections and function seem to be conserved across species (Janak & Tye, 2015). However, despite two decades of intense research, we still do not understand the role of the various amygdalar microcircuits that involve their distinct nuclei (reviewed in Duvarci & Paré, 2014). It is been argued that biologically based computational models provide an important complement to experiments in studying distributed control of aversive behaviors by the amygdala (Nair, Paré, & Vicentic., 2016). Here we focus on such biologically based computational models.

This chapter is structured as follows. First, we provide a brief survey of computational models related to amygdala focusing on the nuclei involved in acquisition and expression of fear. We suggest how computational models can complement experimental investigations in reverse engineering the mammalian fear circuit. Second, we focus on a tutorial illustration of how biophysical models of the fear

circuit can be developed systematically starting with models for single cells, that is, provide a step-by-step introduction to creating biophysical models of amygdalar cells. We use the software package NEURON for this illustration. All the models are publicly accessible at the site http://engineering.missouri.edu/neuro/other-resources/ (click on "Single Neuron Models"). Finally, we highlight the need for integrating computational tools into neuroscience curricula and research, and to ensure meaningful interdisciplinary interactions among students from biological (biology, psychology) and physical (engineering, physics, mathematics, statistics) sciences. Such interactions are critical for tackling the important and exciting challenge of understanding the functioning of the fear as well as other circuits.

Computational Models of Amygdala

Computational models have been popular in physical sciences and engineering for a long time. Indeed, computational models are routinely included in undergraduate and graduate courses in these areas and form a critical element in the research enterprise. We briefly review computational models and then focus on how we might use such models in reverse engineering the mammalian fear circuit, including our own research with amygdala models (e.g., Fig.1; Kim et al., 2013a). Interestingly, the National Academy of Engineering has listed "reverse engineer the brain" as one of the 14 grand challenges in engineering for the 21st century, highlighting the fact that engineering tools including computational models have the potential to assist neuroscientists in probing nervous system function. This suggests an increase in the involvement of engineers in neuroscience research in the coming decades. Later in the section we provide a step-by-step introduction to the development of computational models of

single cells and networks, using a popular software package NEURON (Carnevale & Hines, 2006).

Levels of modeling

Simplified techniques to model neuronal cells include the popular connectionist, integrate-and-fire formulations (Dayan & Abbott, 2005). These have been enormously successful and have been used for various studies, particularly theoretical ones investigating stability and oscillations. Another promising modeling technique that uses the Izhikevich formulation (Izhikevich, 2004, 2007) to retain the key neurocomputational properties has also been used to develop large-scale models (Hummos, Franklin, & Nair, 2014; Izhikevich & Edelman, 2008). While these techniques continue to provide important insights, they do not directly model channel and synaptic neurophysiology, and so may not be suited for studies requiring more biological realism such as effects of manipulation of individual channel currents, and of neuromodulation. We focus here on biophysical models that incorporate channel and synaptic neurophysiology. Specifically, we first illustrate how such biophysical models have helped provide insights into the role of the various amygdalar nuclei in aversive learning, using data from the rodent literature.

From a modeling perspective, the nervous system can be viewed at several levels, including genetic, molecular, cellular, circuits, multiple circuits/region, and behavior levels. Although exciting experimental work at the genetic and molecular levels exists for the amygdala (e.g., Mahan and Ressler, 2012), modeling studies linking these to higher levels have been scarce, and so focus on cellular and higher levels here. Four of

these levels are depicted in Fig. 21.2—the single neuron level with its inputs and outputs shown in the figure; local brain region, which typically comprises homogeneous populations of neurons and such models provide "population level" output; and models of networks of such local regions. So, we start with the fundamental unit of a neuron. Different types of neurons are interconnected using connectivity data from biology to form networks representing local, regional, and whole brain anatomy. Indeed, in several ambitious brain modeling projects, leading researchers are incorporating neurophysiological data at multiple levels to develop very detailed and large-scale models of the mammalian brain (Eliasmith & Trujillo, 2014; Markram et al., 2015). It has been argued that two basic guidelines should be considered in developing large-scale models: the models should be linked to behavior, and they should have the capability of varying the level of simulated detail. We illustrate the modeling process at the cellular, circuit, and region levels using the amygdala and the mammalian fear circuit as the example case.

Fear learning and extinction depend on parallel computations in a vast distributed network (Pape & Paré, 2010; Sah, Faber, Lopez De Armentia, & Power, 2003). How has this circuit been modeled by researchers? To provide context to the discussion, we first adapt the general structure of Fig. 21.2 to the specific fear learning problem. The corresponding levels of focus for the fear learning problem are shown in Fig. 21.3. Fig. 21.3A shows the three types of tone responsive populations of pyramidal cells, with high (A), medium (B), and low (C) adapting types. Interneurons are of various types, with a typical fast spiking one shown in the panel. Fig. 21.3B shows both experimental (Repa et al., 2001) and model (Kim et al., 2013a) population responses (local circuit)

region of lateral amygdala (LA) cells after an auditory fear conditioning protocol. Panel 4C shows the challenge at the larger circuit level where numerous studies have implicated the hippocampus, amygdala, and the prefrontal cortex in regulating fear and extinction, but the details are presently unknown. This thus represents an exciting challenge presently for modeling researchers. After this level is understood, the next challenge will be connecting it to the behavioral level (Fig. 21.3D), which poses challenges too formidable to be tackled at the present time, and may require new tools and paradigms as mentioned in a later section.

Computational models of fear learning have typically used phenomenological (e.g., connectionist) or firing rate formalisms. One of the first computational models of the amygdala was an anatomically constrained connectionist model of the thalamo-cortico-amygdala regions for a fear conditioning application that associated tone inputs with a specific frequency (CS) with foot shock (US) (Armony, Servan-Schreiber, Cohen, & LeDoux, 1995). The model was trained using a modified Hebbian-type learning rule and was able to reproduce data related to frequency-specific changes of the receptive fields known to exist in the auditory thalamus and amygdala. A neural network connectionist model for emotional conditioning focusing on the amygdala and the orbitofrontal cortex and their interactions was proposed by Moren and Balkenius (2000). The amygdala was the locus of acquisition and the orbitofrontal cortex was the site for extinction learning. The model simulated basic phenomena related to emotional conditioning including acquisition, extinction, blocking, and habituation. A conceptual firing rate model of the amygdala that accounts for many aspects of delay and context conditioning was proposed by Krasne, Fanselow, and Zelikowsky (2011). Conditioning

and extinction are the result of neuromodulation-controlled long-term potentiation (LTP) at synapses of thalamic, cortical, and hippocampal afferents onto principal cells and inhibitory interneurons of the LA and basal amygdala (BA). The model included conditioning, secondary reinforcement, blocking, the immediate shock deficit, extinction, renewal, and a range of empirically valid effects of pre- and post training ablation or inactivation of hippocampus or amygdala nuclei, and provided several predictions related to contextual extinction. Another firing rate model (Ball, Hummos, & Nair, 2012) reported combinations of tone and shock densities that would provide experimental estimates of tone responsive and conditioned cell proportions after auditory Pavlovian fear conditioning (Repa et al., 2001). Furthermore, it provided several insights including how intrinsic connectivity might help distribute sensory inputs to produce conditioned responses in cells that do not directly receive both tone and shock inputs, and how a balance between potentiation of excitation and inhibition prevents stimulus generalization during fear learning. Vlachos, Herry, Luthi, Aertsen, and Kumar (2011) developed a network model using leaky integrate-and-fire neurons that reproduced the differential recruitment of two distinct subpopulations of BA neurons as seen in experiments. Plasticity was modeled using a calcium hypothesis. The model revealed that the two populations might encode contextual specificity of fear and extinction memories. A recent model focused on the poorly understood topic of contributions of the amygdala, prefrontal cortex, and hippocampus to fear conditioning, using a firing rate formulation (Moustafa et al., 2013). The authors propose that hippocampal input to both ventromedial prefrontal cortex (vmPFC) and basolateral amygdala is essential for contextual modulation of fear acquisition and extinction. The

model successfully reproduced data from several animal fear conditioning paradigms, including acquisition, extinction, reacquisition, and context specificity effects. Another class of computational models directly model channel and synaptic neurophysiology using the Hodgkin–Huxley modeling formulation that is the focus for the remainder of this chapter. This formulation is described next.

Biophysical models can assist with reverse engineering the mammalian fear circuit

A different class of models that has been reported previously for the mammalian fear circuit is the "biophysical" model, which uses a Hodgkin–Huxley formulation for membrane potential dynamics, and includes a more realistic neuronal morphology and incorporates individual current channels (e.g., sodium, potassium, calcium, etc.) and synapses such as N-methyl-D-aspartate (NMDA), α-amino-3-hydroxy-5-methyl-4-isoxazolepropionic acid (AMPA), and γ-aminobutyric acid (GABA). A biophysical model is thus able to utilize the rich neurophysiological data that are increasingly being generated (Nair, 2012). Such models have been used for a variety of applications including modeling the olfactory bulb, amygdala, perirhinal cortex, and dentate gyrus (Davison, Feng, & Brown, 2000; Feng, Samarth, Paré, & Nair, 2016; Kim et al., 2013a; Li, Nair, & Quirk, 2009; Samarth, Ball, Unal, Paré, & Nair, 2016; Schneider, Bezaire, & Soltesz, 2012). More details regarding such models, including how to develop them, are provided in a later section.

Biophysical models of Lateral amygdala (LA), basal amygdala (BA), intercalated cells of amygdala (ITC), central amygdala nucleus (Ce), and of the entire network constitute a promising approach to shed light on this question of how fear is learnt in the

mammalian brain. To illustrate how biophysical models incorporating channel and synaptic neurophysiology can further our understanding of fear learning, we describe the insights that emerged from one of our recent modeling studies (Kim et al., 2013b; Kim et al., 2015; Li et al., 2009). This model investigated whether the assignment of neurons to a fear memory trace involved a competitive synaptic process. Previously, it was observed that only a minority of LA neurons increase their responsiveness to the CS after fear conditioning (25%; Han et al., 2007; Repa et al., 2001; Rumpel, LeDoux, Zador, & Malinow, 2005) even though most cells receive the required inputs (Repa et al., 2001). Why might this be? Related to this observation, another study showed that LA cells expressing high levels of cAMP response element-binding protein (CREB) are preferentially recruited into the fear memory trace (cells with increased CS responsiveness after training or "plastic" cells (Han et al., 2007, 2009; Zhou et al., 2009). Moreover, when CREB was overexpressed or down-regulated in LA, the proportion of LA neurons in the memory trace remained constant, which led to the proposal that recruitment of LA neurons into the fear memory trace involves a competitive process (Han et al., 2007). Currently, the mechanisms underlying this competitive process remain unclear. To address these questions, a biophysical conductance-based model of LAd that includes 800 principal cells (PNs) and 200 interneurons (INs) was developed (Kim et al., 2013a), as an expanded version of our previous model (Li et al., 2009). Based on *in vitro* electrophysiological studies (Faber, Callister, & Sah, 2001), model neurons were endowed with various ionic conductances so that they could reproduce the electroresponsive properties of PNs and INs, as observed experimentally. For instance, to reproduce the continuum of spike frequency

adaptation seen in principal cells experimentally (Sah et al., 2003), the model featured three types of PNs, with high, intermediate, or low spike frequency adaptation, due to the differential expression of a Ca^{2+}-dependent K^+ current (gK_{Ca}). Afferents to these cells were constrained by previous tract-tracing and physiological studies, and included neuromodulatory inputs from dopaminergic and noradrenergic neurons. The model also included spatially heterogeneous connections between PNs and INs, based on an *in vitro* study (Samson & Paré, 2006).

Findings from the model

Because CREB decreases spike afterhyperpolarizations, we considered the possibility that a higher intrinsic excitability confers a competitive advantage to particular LA neurons. Consistent with this view, we observed that only 1% of model LA neurons with high spike frequency adaptation were plastic cells, compared to > 40% of the intrinsically more excitable neurons. However, if this factor (intrinsic excitability) acted independently, CREB overexpression would result in the recruitment of a higher number of LA cells to the memory trace. Yet, this is not what was seen experimentally or in the current model (CREB overexpression was simulated by converting less into more excitable cells). This suggested that one or more additional factors must be at play in the competitive process. Comparative analyses of the intrinsic connectivity of plastic vs. nonplastic cells revealed that a major substrate of this competition is the distribution of excitatory connections between principal cells and the amount of di-synaptic inhibition they generate in other projection cells. These two factors conspire to enhance the likelihood that some principal cells will fire more strongly to the CS at the expense of others. *Effectively, our modeling study provided a novel insight into a general*

principle of competition leading to memory formation: subsets of projection cells band together by virtue of their excitatory interconnections to suppress plasticity in other projection cells via the recruitment of local-circuit cells (Kim et al., 2013b).

In addition to the findings just cited, our prior models have revealed several insights: sustained firing properties of conditioned prelimbic mPFC neurons (Burgos-Robles, Vidal-Gonzalez, & Quirk, 2009) depended on monoamine modulation of PL-BLA (PL-prelimbic; BLA – Basolateral amygdala) microcircuits (Pendyam et al. 2013). Regarding extinction in the amygdala, an emerging debate pits LTP of inhibitory circuits against LTD (Long-term depression) of excitatory circuits (Kim et al., 2007). Our modeling indicated that both were required to achieve full extinction (Li et al., 2009). Another modeling study related to extinction showed how IL could overcome inter-ITC inhibition and reduce fear expression by decreasing the responsiveness of Ce neurons to BLA inputs (Li, Amano, Paré, & Nair, 2011). A very recent study showed how intrinsic mechanisms might stabilize encoding and retrieval circuits differentially in the hippocampus (Hummos et al., 2014).

How to Develop a Biologically Based Computational Model

The new area of computational neuroscience provides a tremendous opportunity for researchers from the quantitative disciplines of physics, mathematics, computer sciences, and engineering. This is because the process of developing a comprehensive computational model of various brain regions (including the amygdala), has only begun and much work remains. Neurophysiological data continue to be generated at increasing rates as we describe below, and so the time is ripe for the development of viable

computational models. As reviewed above, only a few computational models have been developed for the amygdala and these are either too simplistic or specific to certain nuclei. Indeed, we still lack information about amygdalar subcircuits and their involvement in different functions. So, on the experimental front, a key requirement is to clarify whether the amygdala is indeed involved in a particular function or disorder. In the case of such an involvement, the next step would be to design experiments to tease out the involvement and contributions of specific amygdalar subcircuits to the particular function or disorder. With a host of new tools such as optogenetics, this task is within reach presently, and we should have rich data to feed into computational models.

A computational model could be utilized in concert with experiments to investigate a host of "what if" scenarios, even if part of the neurophysiology data is presently unavailable. For this reason, computational models are beginning to be viewed as viable "tools" to complement *in vitro* and *in vivo* techniques, including using the novel experimental tools being developed. In this section, we present a detailed step-by-step approach of how to begin the process of developing biophysical computational models of the amygdala at the cellular and network levels, using the software package NEURON (Carnevale & Hines, 2006).

Three popular biologically based single-cell model types

The membrane potential of individual neurons exhibits unique dynamics that enable them, in very specific ways, to both be receptive to inputs from other neurons, and to themselves influence other neurons via their output spikes. These membrane potential

dynamics are termed “neurocomputational” properties, that is, the computational properties of the neuron that determine how its membrane potential changes (including spikes) in response to inputs. Izhikevich (2007) argues that a good neuron model should capture the relevant neurocomputational properties. A typical neuron in the human brain can have ~10,000 synapses (although only a small subset may be active in any state), and the presynaptic spikes that arrive via these connections constitute the “stimulus” received from other neurons. These inputs excite the neuron and the level of excitation is determined by the neurocomputational properties of the particular neuron.

We focus on three types of single-cell model types reported in the literature, the integrate-and-fire neuron, the Izhikevich neuron, and the biophysical model neuron. The interested reader is referred to an excellent comparative analysis of the properties of the various model types by Izhikevich (2004). After a description of the three model types and their mathematical representations, we illustrate how to develop all three models using a pyramidal neuron from the rodent LA as the example case. We also provide information that will enable readers to develop single-cell models of neurons on their own, via links to “canned” models that they can download and run.

Integrate-and-fire neuron

This is perhaps the simplest biologically based model of a neuron since it is linear and includes only the leak conductance and a spiking threshold. The implicit assumption is that voltage-gated conductances do not contribute to the initiation of the spike and activate instantaneously after the spiking threshold is crossed. With this logic, the spike itself can be neglected from the computations (and added artificially to the plot), and the

membrane potential reset to V_{rest} after the spike, as shown in Eq. 1.1,

$$C\frac{dV}{dt} = I - g_{leak}(V - E_{leak}); \text{ When } V > V_{thresh}, V = V_{rest} \quad \text{(Eq. 1.1)}$$

where g_{leak} and E_{leak} are the conductance and reversal potential, respectively, of the leak channel. This model can fire tonic spikes with constant frequency (i.e., is class 1 excitable) and it is an integrator (Izhikevich, 2007). The computation requires only four floating-point operations (additions, multiplications, etc.) plus one comparison with the threshold. Details about the integrate-and-fire formulation can be found in Dayan and Abbott (2005).

Izhikevich neuron

The model can exhibit firing patterns of all known types of cortical neurons with the choice of four parameters *a*, *b*, *c*, and *d* as shown in Eq. 1.2.

$$C\dot{V} = -k(v - v_r)(v - v_t) - u + I$$

(Eq. 1.2)

$$\dot{u} = a(b(v - v_r) - u)$$

$$\text{if } v \geq v_{peak}, \quad v = c, \text{ and } u = u + d$$

where v is the membrane potential, u is the recovery current, v_r is resting membrane potential, and v_t is the instantaneous threshold potential. The parameters k and b can be determined using the neuron's rheobase and input resistance. The variable u represents the sum of all slow currents with outward currents being positive. The sign of b determines whether the cell is an integrator ($b < 0$) or resonator ($b > 0$). The recovery time constant is a. The spike cut-off value is v_{peak}, and the voltage is reset to c after each

spike. Additional details related to the model can be found in Izhikevich (2002, 2007).

Biophysical model neuron

Biophysical conductance-based models of neurons, using the Hodgkin–Huxley formulation, are increasingly incorporating, to varying extents, the growing data characterizing neurophysiology, despite the absence of a systematic approach for the development of such models. Since biophysical models are the main focus of this chapter, we have provided a background and discuss issues related to such models in more detail.

Biological data used to constrain a biophysical neuronal model include morphology (Power Bocklisch, Curby, & Sah, 2011), known current channel types and their maximal conductance densities, passive properties of the cell (e.g., input resistance, time constant, resting potential), and responses to current injections (Bar-Ilan, Gidon, & Segev, 2012). It is also important to preserve synaptic integration characteristics, an area that is not well understood presently (Stuart, Spruston, & Hausser, 2008). These properties are determined from the literature for the particular neuron prior to developing the model equations using the formulation described next.

The equation for each compartment (soma or dendrite) followed the Hodgkin–Huxley formulation (Byrne & Roberts, 2009) in Eq. 1.3,

$$C_m dV_s/dt = -g_L(V_s - E_L) - g_c(V_s - V_d) - \sum I_{cur,s}^{int} - \sum I_{cur,s}^{syn} + I_{inj} \quad \text{(Eq. 1.3)}$$

where V_s/V_d are the somatic/dendritic membrane potential (mV), $I_{cur,s}^{int}$ and $I_{cur,s}^{syn}$ are the intrinsic and synaptic currents in the soma, I_{inj} is the electrode current applied to the

soma, C_m is the membrane capacitance, g_L is the conductance of leak channel, and g_c is the coupling conductance between the soma and the dendrite (similar terms added for other dendrites connected to the soma). The intrinsic current $I_{cur,s}^{int}$, was modeled as $I_{cur,s}^{int} = g_{cur} m^p h^q (V_s - E_{cur})$, where g_{cur} is its maximal conductance, *m* its activation variable (with exponent *p*), *h* its inactivation variable (with exponent *q*), and E_{cur} its reversal potential (a similar equation is used for the synaptic current $I_{cur,s}^{syn}$ but without *m* and *h*). The kinetic equation for each of the gating functions *x* (*m* or *h*) takes the form

$$\frac{dx}{dt} = \frac{x_\infty\left(V,[Ca^{2+}]_i\right) - x}{\tau_x(V,[Ca^{2+}]_i)} \quad \text{(Eq. 1.4)}$$

where x_∞ is the steady-state gating voltage- and/or Ca^{2+}-dependent gating variable and τ_x is the voltage- and/or Ca^{2+}-dependent time constant. The equation for the dendrite follows the same format with "*s*" and "*d*" switching positions in Eq. 1.3.

Developing the three types of computational models for a lateral amygdala (LA) neuron

How do the three single-cell model types compare as far as neurocomputational properties? A summary of the comparison is provided in Fig. 1.4 (adapted from Izhikevich, 2003). Usage of the integrate-and-fire model has been popular for applications involving very large network sizes and for studying stability issues (Dayan & Abbott, 2005). The Izhikevich formulation may be a better choice for applications that require improved cellular characteristics, in addition to network features. For applications that require manipulation at the individual current and synaptic levels, the

biophysical model formulation may be more appropriate.

We next illustrate the development of all three types of single-cell models in a tutorial mode using an example case of a principal cell in the rodent LA (Faber et al., 2001). For this, as a first step, the reader can download instructions, together with codes for developing such models themselves from the site http://engineering.missouri.edu/neuro/other-resources/ (click on "Single Neuron Models"). The instructions explain in detail how to model each type of cell, and then provide an example of how to develop these for an LA neuron. The reader can utilize the procedure and modify the codes to develop single-cell models of their own choice. Briefly, the procedure to develop a model neuron is as follows: (1) select the model formulation from the three types above; (2) determine all the neuronal characteristics to be modeled (e.g., resting potential, membrane time constant, frequency–current responses); and (3) follow the step-by-step procedure outlined in the instructions. The model codes for the three formulations are provided in separate folders. The "hands-on" tutorial will provide the reader with an understanding of how to model single-cell types using any of the three formulations. Fig. 1.5 shows the responses of the four different LA single-cell types (pyramidal cells of types A, B, and C, and a fast-spiking inhibitory interneuron), using the three methods. Note that although the single-cell models are developed using the NEURON software package, the procedure is general and the user can develop the model using other software of their preference such as GENESIS (http://genesis-sim.org/), and NEST (http://www.nest-simulator.org/), all of which are described at the Organization for Computational Neurosciences site (http://www.cnsorg.org/software). Once this is accomplished, the next step will be to

model networks of neurons using the single-cell models.

Moving to the computational model of a local circuit region

In a local network (level 2 in Fig. 1.2), collections of neurons, largely homogenous, interact with each other via excitatory or inhibitory connections. *In vitro* and *in vivo* studies have focused on such local regions (e.g., amygdala, hippocampus) and reliable biological data about single-cell properties, and connectivity is available for some of these brain regions. If the inputs to such local networks can be characterized effectively, viable models with predictive capability can be developed for such local networks, for example, the LA network model described above (Kim et al., 2013a; Li et al., 2009), which was successful in replicating the experimentally reported formation of two different tone responsive populations in rodents after Pavlovian conditioning (Repa et al., 2001). A flowchart illustrating the modeling process for this network case is shown in Fig. 21.6. The reader is referred to our prior publication for details related to the development of the model itself (Kim et al., 2013a); the model is available for download from the public database https://senselab.med.yale.edu/modeldb/.

Next Steps in Modeling the Amygdala and the Fear Circuit

The challenges facing the computational neuroscience community at the cellular and systems/network levels stem largely from our present lack of information about the microcircuitry and neurophysiological mechanisms relevant for the particular function studied.

Single-cell modeling—some challenges

Single-cell modeling is perhaps the most well understood aspect of neurocomputational models, and key computations performed by single neurons in the context of their role in networks have been characterized extensively (Brunel, Hakim, & Richardson, 2014; Herz, Gollisch, Machens, & Jaeger, 2006). However, some issues remain, which we highlight below.

Morphology

How many compartments should one select when developing a single-cell model? Better understanding of dendritic function will help address this question. Although dendrites have been shown to have active channels, the role of these channels in dendritic information processing are only beginning to be understood (Stuart et al., 2008). We provide a brief review of the literature to highlight the issue, and the reader is referred to the cited references for guidance on the selection of appropriate numbers of compartments in single-cell models.

Active channels in dendrites are more easily recruited by synaptic input than by retrograde input from the soma (Spruston, 2008). Dendritic spike propagation to the soma is extremely limited, and single action potentials propagate through dendrites better than spike trains, with a frequency-dependent decrease in spike amplitudes observed in spike trains (Johnston, Magee, Colbert, & Cristie, 1996). A uniform distribution of Na^+ channels in dendrites with some decrease in density and in threshold in distal apical dendrites has been shown to facilitate back-propagating action potentials (BPAPs) from soma (Johnston et al., 1996). In CA1 pyramidal neurons, the A-type K^+ channels increase in density toward the distal dendrites and this is hypothesized to

attenuate BPAPs. Both CA1 and layer V neurons show a similar somatodendritic gradient of HCN channels, presumably to reduce IPSP amplitude and decrease distance dependence of EPSP temporal summation in the soma (Spruston, 2008). Ca^{2+} channels are present in dendrites and they can be opened by BPAPs, local dendritic spikes, and also by synaptic potentials (Johnston et al., 1996). AMPA conductance shows a gradient, with conductance decreasing distally along a dendrite. Since distal dendrites have higher input resistance, a lower current is needed to achieve the same membrane voltage difference (Katz et al., 2009).

While Na^{+}, NMDA and Ca^{2+} spikes are reported in pyramidal neurons (Major, Larkum, & Schiller, 2013), their functional role is not fully understood. Na^{+} spikes are thought to assist BPAPs (Johnston et al., 1996). NMDA spikes are predominant in distal dendritic branches and in basal dendrites. NMDA spikes travel longer distances than EPSPs and may be required in long dendritic branches for more reliable communication. The distal junction of the apical trunk has been shown to produce Ca^{2+} spikes, presumably integrating inputs from more distal dendrites. It is observed experimentally that the threshold of Ca^{2+} spike is lowered if it is preceded by an AP that back-propagates (Larkum, Zhu, & Sakmann, 1999). The role of these emerging dendritic mechanisms in single-cell computations, and, importantly, in plasticity in network models remains to be unraveled.

The principal cells in the amygdala are largely of the pyramidal type with both apical and basal dendrites. Better understanding of the issues discussed in this section will suggest appropriate improvements in both morphology and dynamics for the compartmental models of pyramidal neurons of the amygdala described above.

Neuromodulation

How do we model the effect of neuromodulators and neuropeptides on neurons? Neuromodulators such as dopamine and norepinephrine are known to alter the functioning of neurons and circuits by changing both current channels and synaptic properties, for example, see review in Marder, O'Leary, T., and Shruti (2015). Modeling the effect of neuromodulators is dependent on information about the distribution of neuromodulator receptors on the cells, and on the level of neuromodulators (low, medium, high) depending on whether the region has neuromodulator terminals. Although information about these mechanisms is scarce presently, the hope is that, as with other "gaps" in knowledge, this one will also be filled in the next decade. As an example of how neuromodulator effects can be incorporated into a model, the reader is referred to the LA model in Kim et al. (2013a). These authors survey how neuromodulators have long been implicated in fear and anxiety, and focus on how they regulate Pavlovian fear learning and synaptic plasticity in LA.

Challenges in moving from cellular to network and to behavior levels

The transition in modeling from a single-cell to local or regional network levels and then to larger networks and to the whole brain is the goal of computational neuroscience. Again, lack of information about the relevant microcircuitry and functional connectivity at all these levels during various "states" of behavior (e.g., fear, pleasure) limits the development and fidelity of such models presently. Nevertheless,

researchers have been attempting to develop large-scale models, focusing on specific behaviors (Izhikevich & Edelman, 2008; Markram, 2012). With the rich complexity of brain processes leading to an equally complex set of behaviors, decisions about the "right" model, at both single-cell and network levels, to replicate the behavior of interest promise to provide challenges to both biological and computational neuroscientists. We describe next some of these challenges for the mammalian fear circuit.

There is evidence that fear conditioning induces widespread synaptic plasticity in several brain areas (Pape & Paré, 2010). In addition to the amygdala, prefrontal cortex and hippocampus regions discussed above, thalamic (Weinberger, 2011) and cortical (Letzkus et al., 2011) regions have also been implicated, and more information on these fronts will surely emerge. Several studies (reviewed in Ji & Maren, 2007) have revealed that the ventral hippocampus (VH) and infralimbic (IL) sector of mPFC modulate the amygdala during the acquisition and recall of extinction. Recent inactivation studies suggest the simultaneous involvement of VH, BA, and mPFC in two possible "loops" (Orsini, Kim, Knapska, & Maren, 2011).

A goal of future research will be to generalize the model of the amygdala to reward learning, and by adding other relevant nuclei (e.g., basomedial amygdala), taking into account the different functional roles of particular nuclei and their connections (Janak & Tye, 2015). Accomplishing the goal outlined above of creating a comprehensive model of the entire amygdala and of the larger fear (and other brain) circuits will require interdisciplinary expertise and interactions, including usage of the "tool" of computational neuroscience. Wang and Krystal, (2014) characterize the challenges

faced in understanding the important application of amygdala-centric psychiatric disorders as follows: “It is our belief that these challenges cannot be overcome without theory and computational modeling. To advance the field, we need new infrastructure, resources, and training of cross-disciplinary young talents who are well versed both in mathematical modeling and experimentation.” Reverse engineering the fear circuit is perhaps one of the important challenges in clinical neuroscience, and promises to provide exciting opportunities for interdisciplinary collaborations including among neuroscientists and computational researchers. Indeed, numerous universities are developing curricula incorporating computational approaches in biology and neuroscience, and this bodes well for future students and researchers interested in the exciting area of reverse engineering brain circuits.

FIGURES

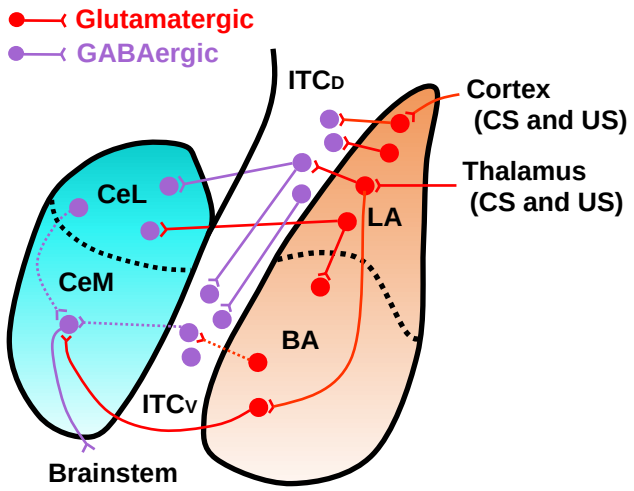

Figure 1.1 Amygdalar nuclei relevant to auditory fear and extinction. Pyramidal neurons and their projections are in red. Inhibitory interneurons and their projections are in blue. Inputs from prelimbic and infralimbic cortices, and from ventral hippocampus are not shown. Amygdalar pathways relevant to auditory fear. Tone and shock information arrive at LA via thalamic and cortical routes. LA projects to BA, ITC_D and CeL. BA fear neurons project to CeM and BA extinction neurons project to ITC_V (fear recall circuit in bold and extinction recall in dashed line type). Ce represents the amygdalar output which projects to the brainstem and other regions eliciting fear. ITC: inter-calated cells (subscripts D - dorsal, V-ventral); CeL/CeM: lateral/medial part of the central nucleus of the amygdala.

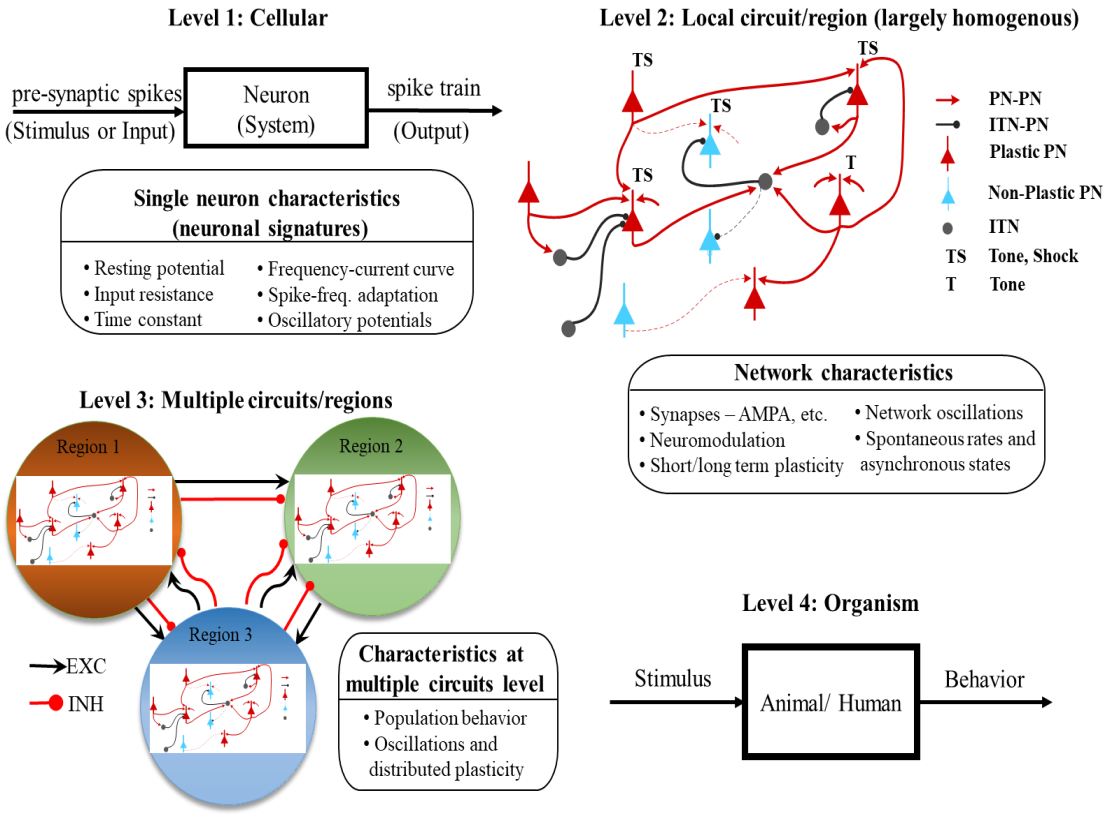

Figure 1.2. Four levels of computational modeling in neuroscience.

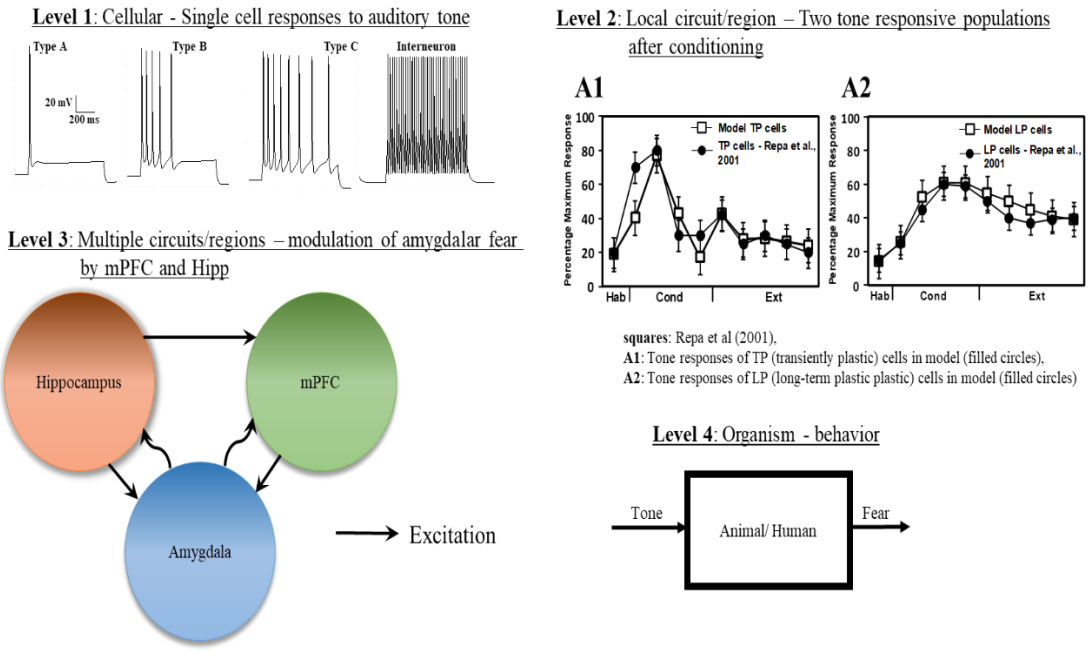

Figure 1.3. Illustration of the four levels of modeling using the mammalian fear circuit.

Models	Biophysically meaningful	tonic spiking	phasic spiking	tonic bursting	phasic bursting	mixed mode	spike frequency adaptation	class 1 excitable	class 2 excitable	spike latency	subthreshold oscillations	resonator	integrator	rebound spike	rebound burst	threshold variability	bistability	DAP	accommodation	Inhibition-induced spiking	Inhibition-induced bursting	chaos
Integrate and Fire	-	+	-	-	-	-	-	+	-	-	-	-	+	-	-	-	-	-	-	-	-	-
Izhikevich	-	+	+	+	+	+	+	+	+	+	+	+	+	+	+	+	+	+	+	+	+	+
Hodgkin-Huxley	+	+	+	+			+	+	+	+	+	+	+	+	+	+	+	+	+		+	

Figure 1.4. Attributes of various single cell model types; adapted from Izhikevich (2004).

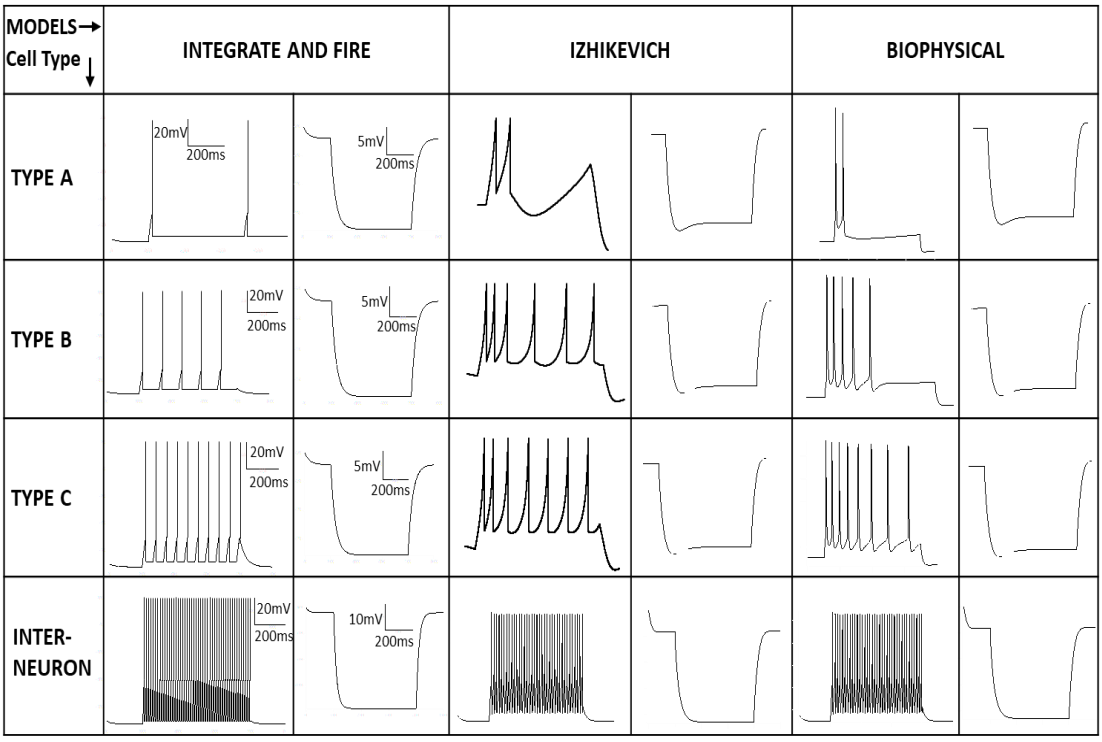

Figure 1.5. Membrane potential responses to current injections for the three LA cell types, using three model formulations. The scale bar for x-axis for all panels is 200 ms; the scale bar for the y-axis is 20 mV for all depolarizing injections, and 5 mV for all hyperpolarizing injections, unless stated otherwise. See text for other details.

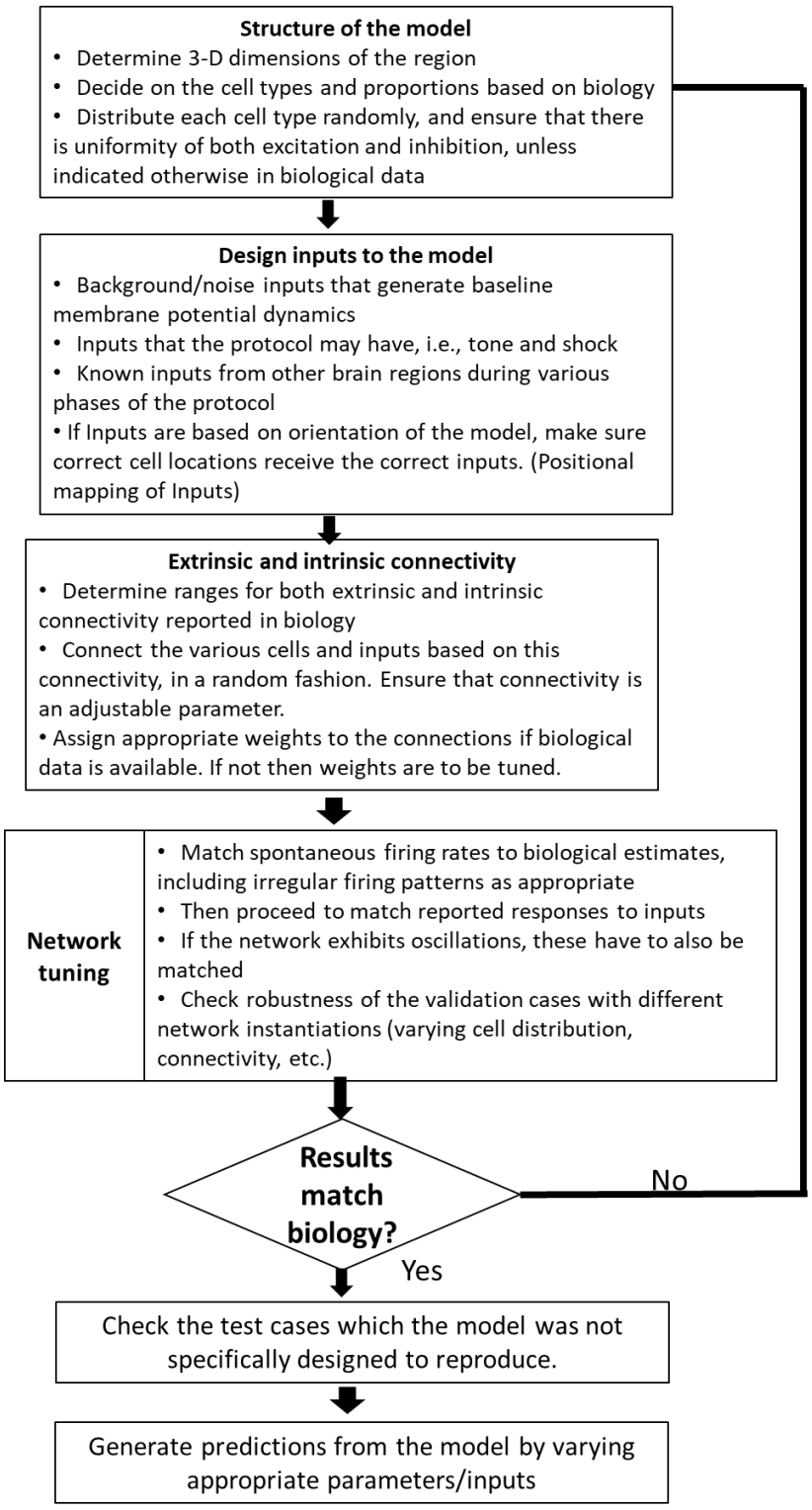

Figure 1.6. Flowchart illustrating procedure to create a neuronal network model of a local region.

REFERENCES

Armony, J. L., Servan-Schreiber, D., Cohen, J. D., & LeDoux, J. E. (1995). An anatomically constrained neural network model of fear conditioning. *Behavioral Neuroscience, 109*(2), 246–257.

Ball, J. M., Hummos, A. M., & Nair, S. S. (2012). Role of sensory input distribution and intrinsic connectivity in lateral amygdala during auditory fear conditioning: A computational study. *Neuroscience, 224*, 249–267.

Bar-Ilan, L., Gidon, A., & Segev, I. (2012). The role of dendritic inhibition in shaping the plasticity of excitatory synapses. *Front Neural Circuits, 6*, 118.

Baxter, M. G., & Murray, E. A. (2002). The amygdala and reward. *Nature Reviews: Neuroscience, 3*(7), 563–573.

Brunel, N., Hakim, V., & Richardson, M. J. E. (2014). Single neuron dynamics and computation. *Current Opinion in Neurobiology, 25*(0), 149–155.

Burgos-Robles, A., Vidal-Gonzalez, I., & Quirk, G. J. (2009). Sustained conditioned responses in prelimbic prefrontal neurons are correlated with fear expression and extinction failure. *Journal of Neuroscience, 29*(26), 8474–8482.

Byrne, J. H., & Roberts, J. L. (2009). *From molecules to networks,: An introduction to cellular and molecular neuroscience* (2nd edn). Academic Press, San Diego CA.

Carnevale, N., & Hines, M. (2006). *The NEURON book*. Cambridge: Cambridge University Press.

Davison, A. P., Feng, J., & Brown, D. (2000). A reduced compartmental model of the mitral cell for use in network models of the olfactory bulb. *Brain Research Bulletin, 51*(5), 393–399.

Dayan, P., & Abbott, L. F. (2005). *Theoretical neuroscience: Computational and mathematical modeling of neural systems*. Cambridge, MA: MIT Press.

Duvarci, S., & Paré, D. (2014). Amygdala microcircuits controlling learned fear. *Neuron, 82*(5), 966–980.

Eliasmith, C., & Trujillo, O. (2014). The use and abuse of large-scale brain models. *Current Opinion in Neurobiology, 25*, 1–6.

Faber, E. S., Callister, R. J., & Sah, P. (2001). Morphological and electrophysiological properties of principal neurons in the rat lateral amygdala in vitro. *Journal of Neurophysiology, 85*(2), 714–723.

Feng, F., Samarth, P., Paré, D., & Nair, S. S. (2016). Mechanisms underlying the formation of the amygdalar fear memory trace: A computational perspective. *Neuroscience, 322*, 370–376.

Han, J. H., Kushner, S. A., Yiu, A. P., Cole, C. J., Matynia, A., Brown, R. A., … & Josselyn, S. A. (2007). Neuronal competition and selection during memory formation. *Science, 316*(5823), 457–460.

Han, J. H., Kushner, S. A., Yiu, A. P., Hsiang, H. L., Buch, T., Waisman, A., … Josselyn, S. A. (2009). Selective erasure of a fear memory. *Science, 323*(5920), 1492–1496.

Herz, A. V., Gollisch, T., Machens, C. K., & Jaeger, D. (2006). Modeling single-neuron dynamics and computations: A balance of detail and abstraction. *Science, 314*(5796), 80–85.

Hummos, A., Franklin, C. C., & Nair, S. S. (2014). Intrinsic mechanisms stabilize encoding and retrieval circuits differentially in a hippocampal network model. *Hippocampus, 24*(12), 1430-1448.

Izhikevich, E. M. (2003). Simple model of spiking neurons. *IEEE Transactions on Neural Networks, 14*(6), 1569–1572.

Izhikevich, E. M. (2004). Which model to use for cortical spiking neurons? *Neural Networks, IEEE Transactions on Neural Networks, 15*(5), 1063–1070.

Izhikevich, E. M. (2007). Dynamical systems in neuroscience: the geometry of excitability and bursting. *Computational neuroscience.* MIT Press, Cambridge MA.

Izhikevich, E. M., & Edelman, G. M. (2008). Large-scale model of mammalian thalamocortical systems. *Proceedings of the National Academy of Sciences of the United States of America, 105*(9), 3593–3598.

Janak, P. H., & Tye, K. M. (2015). From circuits to behaviour in the amygdala. *Nature, 517*(7534), 284–292.

Ji, J., & Maren, S. (2007). Hippocampal involvement in contextual modulation of fear extinction. *Hippocampus, 17*(9), 749–758.

Johnston, D., Magee, J. C., Colbert, C. M., & Cristie, B. R. (1996). Active properties of neuronal dendrites. *Annual Review of Neuroscience, 19*, 165–186.

Katz, Y., Menon, V., Nicholson, D. A., Geinisman, Y., Kath, W. L., & Spruston, N. (2009). Synapse distribution suggests a two-stage model of dendritic integration in CA1 pyramidal neurons. *Neuron, 63*(2), 171–177.

Kim, D., Paré, D., & Nair, S. S. (2013a). Mechanisms contributing to the induction and storage of Pavlovian fear memories in the lateral amygdala. *Learning & Memory, 20*(8), 421–430.

Kim, D., Paré, D., & Nair, S. S. (2013b). Assignment of model amygdala neurons to the fear memory trace depends on competitive synaptic interactions. *Journal of Neuroscience, 33*(36), 14354–14358.

Kim, D., Samarth, P., Feng, F., Paré, D., & Nair, S. S. (2016). Synaptic competition in the lateral amygdala and the stimulus specificity of conditioned fear: A biophysical modeling study. *Brain Structure and Function, 221*(2163-2182).

Kim, J., Lee, S., Park, K., Hong, I., Song, B., Son, G., … & Choi, S. (2007). Amygdala depotentiation and fear extinction. *Proceedings of the National Academy of Science of the United States of America, 104*(52), 20955–20960.

Krasne, F. B., Fanselow, M. S., & Zelikowsky, M. (2011). Design of a neurally plausible model of fear learning. *Frontiers in Behavioral Neuroscience, 5*, 41.

Larkum, M. E., Zhu, J. J., & Sakmann, B. (1999). A new cellular mechanism for coupling inputs arriving at different cortical layers. *Nature, 398*(6725), 338–341.

LeDoux, J. (2008). Amygdala. *Scholarpedia, 3*(4), 2698.

Letzkus, J. J., Wolff, S. B., Meyer, E. M., Tovote, P., Courtin, J., Herry, C., & Luthi, A. (2011). A disinhibitory microcircuit for associative fear learning in the auditory cortex. *Nature, 480*(7377), 331–335.

Li, G., Amano, T., Paré, D., & Nair, S. S. (2011). Impact of infralimbic inputs on intercalated amygdala neurons: A biophysical modeling study. *Learning & Memory, 18*(4), 226–240.

Li, G., Nair, S. S., & Quirk, G. J. (2009). A biologically realistic network model of acquisition and extinction of conditioned fear associations in lateral amygdala neurons. *Journal of Neurophysiology, 101*(3), 1629–1646.

Mahan, A.L., Ressler, K.J. (2012) Fear conditioning, synaptic plasticity and the amygdala: implications for posttraumatic stress disorder. *Trends in Neuroscience, 35*, 24–35.

Major, G., Larkum, M. E., & Schiller, J. (2013). Active properties of neocortical pyramidal neuron dendrites. *Annual Review of Neuroscience, 36*, 1–24.

Marder, E., O'Leary, T., & Shruti, S. (2015). Neuromodulation of circuits with variable parameters: single neurons and small circuits reveal principles of state-dependent and robust neuromodulation. *Annual Review of Neuroscience, 37*, 329–346.

Markram, H. (2012). The Human Brain Project. *Scientific American, June*, 50–55.

Markram, H., Muller, E., Ramaswamy, S. Reimann, M. W., Abdellah, M., Aguado Sanchez, C. Ailamaki, A., … & Muñoz-Céspedes, A. (2015). Reconstruction and simulation of neocortical microcircuitry. *Cell, 163*(2), 456–492.

Moren J, Balkenius J (2000) A computational model of emotional learning in the amygdala: from animals to animals. *In: Sixth international conference on the simulation of adaptive behavior*. MIT Press, Cambridge, pp 383–391.

Moustafa, A. A., Gilbertson, M. W., Orr, S. P., Herzallah, M. M., Servatius, R. J., & Myers, C. E. (2013). A model of amygdala-hippocampal-prefrontal interaction in fear conditioning and extinction in animals. *Brain and Cognition, 81*(1), 29-43.

Murray, E. A. (2007). The amygdala, reward and emotion. *Trends in Cognitive Sciences, 11*(11), 489–497.

Nair, S. S. (2012). Auditory fear circuits in the amygdala—insights from computational models. In B. Ferry (Ed.), *The amygdala—a discrete multitasking manager (*pp. 141-170). InTech Publishing.

Nair, S. S., Paré, D., & Vicentic, A. (2016). Biologically-basd neural circuit modeling for the study of fear learning and extinction. *NPJ Science of Learning*, 1:16015.

Orsini, C. A., Kim, J. H., Knapska, E., & Maren, S. (2011). Hippocampal and prefrontal projections to the basal amygdala mediate contextual regulation of fear after extinction. *Journal of Neuroscience, 31*(47), 17269–17277.

Pape, H. C., & Paré, D. (2010). Plastic synaptic networks of the amygdala for the acquisition, expression, and extinction of conditioned fear. *Physiological Reviews, 90*(2), 419–463.

Power, J. M., Bocklisch, C., Curby, P., & Sah, P. (2011). Location and function of the slow afterhyperpolarization channels in the basolateral amygdala. *Journal of Neuroscience, 31*(2), 526–537.

Repa, J. C., Muller, J., Apergis, J., Desrochers, T. M., Zhou, Y., & LeDoux, J. E. (2001). Two different lateral amygdala cell populations contribute to the initiation and storage of memory. *Nature Neuroscience, 4*(7), 724–731.

Rumpel, S., LeDoux, J., Zador, A., & Malinow, R. (2005). Postsynaptic receptor trafficking underlying a form of associative learning. *Science, 308*(5718), 83–88.

Sah, P., Faber, E. S., Lopez De Armentia, M., & Power, J. (2003). The amygdaloid complex: Anatomy and physiology. *Physiological Reviews, 83*(3), 803–834.

Samarth, P., Ball, J. M., Unal, G., Paré, D., & Nair, S. S. (2017). Mechanisms of memory storage in a model perirhinal network. *Brain Structure and Function, 222*(1), 183-200.

Samson, R. D., & Paré, D. (2006). A spatially structured network of inhibitory and excitatory connections directs impulse traffic within the lateral amygdala. *Neuroscience, 141*(3), 1599–1609.

Schneider, C. J., Bezaire, M., & Soltesz, I. (2012). Toward a full-scale computational model of the rat dentate gyrus. *Front Neural Circuits, 6*, 83.

Schulz, W. (2007). Reward. *Scholarpedia, 2*(3), 1652.

Spruston, N. (2008). Pyramidal neurons: Dendritic structure and synaptic integration. *Nature Reviews: Neuroscience, 9*(3), 206–221.

Stuart, G., Spruston, N., & Hausser, M. (2008). *Dendrites*. Oxford, New York: Oxford University Press.

Vlachos, I., Herry, C., Luthi, A., Aertsen, A., & Kumar, A. (2011). Context-dependent encoding of fear and extinction memories in a large-scale network model of the basal amygdala. *PLoS Computational Biology, 7*(3), e1001104.

Wang, X.-J., & Krystal, J. H. (2014). Computational psychiatry. *Neuron, 84*(3), 638–654.

Weinberger, N. M. (2011). The medial geniculate, not the amygdala, as the root of auditory fear conditioning. *Hearing Research, 274*(1–2), 61–74.

Zhou, Y., Won, J., Karlsson, M. G., Zhou, M., Rogerson, T., Balaji, J., … & Silva, A. J. (2009). CREB regulates excitability and the allocation of memory to subsets of neurons in the amygdala. *Nature Neuroscience, 12*(11), 1438–1443.

PUBLICATIONS, CONFERENCES AND OTHER PRESENTATIONS

Refereed Journals

Guntu V, Latimer B, Shappell E, Schulz DJ, Nair SS (2020) Modeling the neural circuit of lower urinary tract *(In preparation)*

Guntu V, Banks T, Hummos A, Hummos A, Nair SS (2020) Interplay of resonant and synchronizing generators in a hippocampal theta model. *(In preparation)*

Guntu V, Franklin CC, Hummos A, Nair SS (2020) Cellular and synaptic correlates of pattern formation in a hippocampal model. *(Resubmitting)*

Latimer B, Bergin DA, **Guntu V**, Schulz DJ, Nair SS (2018), Integrating Model-Based Approaches into a Neuroscience Curriculum--An Interdisciplinary Neuroscience Course in Engineering. IEEE Transactions on Education:1-9.

Latimer B, Bergin DA, **Guntu V**, Schulz DJ, Nair SS (2018), Open Source Software Tools for Teaching Neuroscience. Journal of undergraduate neuroscience education : JUNE : a publication of FUN, Faculty for Undergraduate Neuroscience 16:A197-A202.

Alturki A, Feng F, Nair A, **Guntu V**, Nair SS (2016) Distinct current modules shape cellular dynamics in model neurons. *Neuroscience* 334:309-331.

Book Chapters

Guntu V, Latimer B, Shappell E, Schulz DJ, Nair SS (2020) Challenges in modeling the neural control of LUT, Chapter in *Urinary Bladder Physiology: Computational Insights. (In Review)*

Guntu V, Feng F, Alturki A, Nair A, Samarth PS, Nair SS (2017) Amygdala Models, Chapter in *Computational Models of Brain and Behavior*, John Wiley and Sons.

Conference Papers and Abstracts

Guntu V, Hummos A, Nair S.S (2018). Interplay of resonant and synchronizing generators in the hippocampal theta model. *Society for Neuroscience Poster*, San Diego, CA

Gahl M, **Guntu V**, Latimer B, Schulz D.J Nair S.S (2018). Modeling the neural circuit of rodent urinary tract. *Society for Neuroscience Poster*, San Diego, CA

Guntu V, C Sinks, KM Lett, DJ Schulz and SS Nair (2017) Modeling the dynamics of bladder control networks after spinal cord injury. *Society for Neuroscience Poster*, Washington, DC

Alturki A, Nair A, **Guntu V**, Nair SS (2015) Single Neuron Models for Network Simulations. *Indian Control Conference.*

Alturki A, Feng F, Nair A, **Guntu V**, Nair SS (2015) Single neuron model with multiple biological characteristics. *Society for Neuroscience Poster*, Chicago , IL

Franklin CC, **Guntu V**, Nair SS (2014) Development of neuronal single cell models for network simulations. *Society for Neuroscience Poster*, Washington, DC

Sinks C, **Guntu V**, Blasius C, Lett KM, Schulz DJ, Nair SS (2014) Modeling of Neural Micturition Control Circuits. *Society for Neuroscience Poster*, Washington, DC

Alturki A, Nair A, **Guntu V**, Nair SS (2014) Comparison of single cell models for neuronal network simulations. *Society for Neuroscience Poster*, Washington, DC

Franklin CC, Yankang C, **Guntu V**, Nair SS (2012) Reduced Order Modeling Of Biological Neurons For Network Simulations. *5th Annual Dynamic Systems and Control Conference.*

Franklin CC, Hummos A, **Guntu V**, Nair SS (2012) A Biologically Realistic Computational Model of The Hippocampus. *Society for Neuroscience Poster*, New Orleans, LA

VITA

Vinay Sandeep Kumar Guntu was born March 5th, 1988, in Andhra Pradesh, India. He received his B.Tech in Electronics and Communications Engineering from Jawaharlal Nehru Technological University in Hyderabad, India. During his undergraduate, he focused on the research of satellite communications and robotics. Vinay entered a maters program in Mizzou fall of 2010 and graduate with ME from department of Electrical and Computer Engineering. He entered Ph.D. program under Satish Nair in 2012 to study computational neuroscience. Since then, he has authored or co-authored six journal publications (3 in preparation), two conference articles, two book chapters and presented eight posters to the annual Society for Neuroscience conference. During his time in University of Missouri he served as graduate teaching assistant for computational neuroscience (4 semesters), programmable logic controller (3 semesters) and feedback controls (1 semester). Managerial role as program manager for Mizzou Neuro NSF REU (4 years). Club/ ORG activities include founder and coach of Mizzou Badminton Club (4 years) and general secretary for Cultural Association of India (1year).